

Fine Guidance Sensor Instrument Handbook for Cycle 32



FGS Instrument Handbook	3
List of Figures	5
List of Tables	7
Acknowledgments	8
Chapter 1: Introduction	9
1.1 Purpose	10
1.2 Instrument Handbook Layout	11
1.3 The FGS as a Science Instrument	12
1.4 Technical Overview	13
1.5 Planning and Analyzing FGS Observations	19
1.6 FGS Replacement in SM4	20
Chapter 2: FGS Instrument Design	21
2.1 The Optical Train	22
2.2 FGS Detectors	27
2.3 HST's Spherical Aberration	28
2.4 The FGS Interferometric Response	29
2.5 The FGS1r Articulated Mirror Assembly	34
2.6 FGS Aperture and Filter	38
2.7 FGS Calibrations	42
Chapter 3: FGS Science Guide	43
3.1 The Unique Capabilities of the FGS	44
3.2 Position Mode Precision Astrometry	45
3.3 Transfer Mode Binary Stars and Extended Objects	46
3.4 Combining FGS Modes Determining Stellar Masses	51
3.5 Angular Diameters	53
3.6 Relative Photometry	55
3.7 Moving Target Observations	58
3.8 Summary of FGS Performance	59
3.9 Special Topics Bibliography	60
Chapter 4: Observing with the FGS	62
4.1 Position Mode Overview	63
4.2 Planning Position Mode Observations	64
4.3 Position Mode Observing Strategies	71
4.4 Transfer Mode Overview	74
4.5 Planning a Transfer Mode Observation	77
4.6 Transfer Mode Observing Strategies	83
Chapter 5: FGS Calibration Program	87
5.1 Position Mode Calibrations and Error Sources	88
5.2 Transfer Mode Calibrations and Error Sources	98
5.3 Linking Transfer and Position Mode Observations	104
5.4 Cycle 21 Calibration and Monitoring Program	105
5.5 Special Calibrations	106
Chapter 6: Writing a Phase II Proposal	107
6.1 Phase II Proposals: Introduction	108
6.2 Instrument Configuration	109
6.3 Special Requirements	114
6.4 Overheads	116
6.5 Proposal Logsheet Examples	118
Chapter 7: FGS Astrometry Data Processing	132
7.1 Data Processing Overview	133
7.2 Exposure-Level Processing	134
7.3 Visit-Level Processing	136
7.4 Epoch-Level Processing	139

Appendix A: Target Acquisition and Tracking	144
A.1 FGS Control	145
A.2 Target Acquisition and Position Mode Tracking	146
A.3 Transfer Mode Acquisition and Scanning	152
A.4 Visit Level Control	153
Appendix B: FGS1r Performance Summary	154
B.1 FGS1r's First Three Years in Orbit	155
B.2 Angular Resolution Test	160
B.3 FGS1r's Angular Resolution: Conclusions	164
B.4 FGS1r: Second AMA Adjustment	165
B.5 FGS1r: Third AMA Adjustment	166
Glossary of Terms	167

FGS Instrument Handbook

Version 28.0 – January 2021

[PDF version](#)

Fine Guidance Sensor Instrument Handbook for Cycle 32

User Support

- Please contact the HST Help Desk for assistance. We encourage users to access the new web portal where you can submit your questions directly to the appropriate team of experts.
 - **Website:** <http://hsthhelp.stsci.edu>
 - **E-mail:** help@stsci.edu

Additional Resources

Information and other resources are available from the STScI website:

- <http://www.stsci.edu/hst/instrumentation/fgs>

FGS Instrument Contact

Name	Title	Phone	e-mail
Ed Nelan	Instrument Scientist	(410) 338-4992	nelan@stsci.edu

Revision History

Version	Date	Editor
28.0	January 2021	E. P. Nelan
27.0	December 2019	E. P. Nelan
26.0	January 2019	E. P. Nelan
25.0	May 2018	E. P. Nelan
24.0	January 2017	E. P. Nelan
23.0	January 2016	E. P. Nelan
22.0	January 2015	E. P. Nelan
21.0	January 2014	E. P. Nelan
20.0	December 2012	E. P. Nelan

19.0	December 2011	E. P. Nelan
18.0	December 2010	E. P. Nelan
17.0	January 2010	E. P. Nelan
16.0	December 2007	E. P. Nelan
15.0	October 2006	E. P. Nelan
14.0	October 2005	E. P. Nelan
13.0	October 2004	E. P. Nelan
12.0	October 2003	E. P. Nelan and J. Younger
11.0	October 2002	E. P. Nelan and R. B. Makidon
10.0	June 2001	E. P. Nelan and R. B. Makidon
9.0	June 2000	E. P. Nelan and R. B. Makidon
8.0	June 1999	E. P. Nelan and R. B. Makidon
7.0	June 1998	O. L. Lupie & E. P. Nelan
6.0	June 1996	S. T. Holfeltz
5.0	June 1995	S. T. Holfeltz, E. P. Nelan, L. G. Taff, and M. G. Lattanzi
1.0	October 1985	Alain Fresneau

Citation

In publications, refer to this document as:

- Nelan, E., et al., 2021, “Fine Guidance Sensor Instrument Handbook”, Version 28.0, (Baltimore: STScI)

List of Figures

Figure 1.1: FGS Interferometric Response (the “S-Curve”)
Figure 1.2: FGSs in the HST Focal Plane (Projected onto the Sky)
Figure 1.3: FGS Star Selector Geometry
Figure 2.1: FGS1r Optical Train Schematic
Figure 2.2: Light Path from Koesters Prisms to the PMTs
Figure 2.3: The Koesters Prism: Constructive and Destructive Interference.
Figure 2.4: Full Aperture S-Curves of the Original FGSs
Figure 2.5: Improved S-Curves for Original FGSs when Pupil is in Place
Figure 2.6: FGS1r S-Curves in Full Aperture Across the Pickle
Figure 2.7: FGS1r S-curves
Figure 2.8: FGS1r S-curves 2005
Figure 2.9: Shows the changes in the FGS1r S-curves resulting from the January 2009 AMA adjustment.
Figure 2.10: FGS Proposal System and Detector Coordinate Frames
Figure 2.11: FGS1r Filter Transmission
Figure 2.12: PMT Efficiency
Figure 3.1: Comparison: PC Observation v. FGS Observation
Figure 3.2: Simulated PC Observations v. FGS Observations of a 70mas Binary
Figure 3.3: Comparison of FGS1r and FGS3 Transfer Mode Performance
Figure 3.4: Relative Orbit of the Low-Mass Binary System Wolf 1062 AB
Figure 3.5: Mira-type variable with a resolved circumstellar disk
Figure 3.6: Flare Outburst of Proxima Centauri as Observed with FGS3
Figure 3.7: Triton Occultation of the Star TR180 as Observed by FGS 3
Figure 4.1: Default FESTIME as a Function of V Magnitude for F583W FGS1r: NEA as a Function of Magnitude and FESTIME
Figure 4.2: A Sample Visit Geometry
Figure 4.3: Binary S-Curves Generated from FGS1r X-Axis Data
Figure 4.4: FGS1r (F583W) S-Curves: Single and Co-Added
Figure 4.5: Evolution of S-curve morphology along the FGS1r Y-axis
Figure 5.1: Overlay of the pointings used for the FGS3 OFAD calibration
Figure 5.2: Overlay of pointings used for the FGS1r OFAD calibration
Figure 5.3: FGS2 Guide Star Motion at the Onset of a Day/Night Transition
Figure 5.4: Effects of jitter on an FGS1r S-Curve (single scan)
Figure 5.5: Temporal Stability: FGS3 v. FGS1r
Figure 6.1: Example 1: Field of View at Special Orientation
Figure 6.2: Example 2: Field of View at Special Orientation
Figure 6.3: Example 3: Trans + Pos Mode Visits
Figure 6.4: Example 4: Trans + Pos Mode Exposures
Figure 7.1: CALFGSA Common Processing Tasks

Figure 7.2: CALFGSA Transfer Mode Processing Tasks

Figure 7.3: CALFGSB Position Mode Processing

Figure A.1: Location of IFOV as FGS Acquires a Target

Figure A.2: Offset of True Null from $S_y=0$

Figure A.3: X,Y Position in Detector Space of FGS 3's IFOV
During WalkDown to FineLock and Subsequent Tracking
of a Star in FineLock

Figure B.1: FGS1r S-Curves: Before and After AMA Adjustment

Figure B.2: FGS1r S-Curves: First Six Months After
AMA Adjustment

Figure B.3: FGS1r S-Curves: Second Six Months After
AMA Adjustment

Figure B.4: Optimized FGS1r S-Curves Used in Angular
Resolution Test

Figure B.5: FGS1r Transfer Function: Change in Angular
Separation of a Binary

Figure B.6: FGS1r Transfer Function Amplitude w/ Binary
Separation

List of Tables

Table 2.1: FGS1r Dark Counts

Table 2.2: FGS1r Dead Times

Table 2.3: Approximate Reference Positions of each FGS
in the HST Focal Plane

Table 2.4: Available Filters

Table 3.1: FGS1r TRANSFER Mode Performance: Binary Star

Table 4.1: Filters for which FGS1r will be Calibrated

Table 4.2: Default FES Times

Table 4.3: F-factor Transmission Estimator for Combination
of Filter and Color

Table 4.4: FGS1r: Dark Counts

Table 4.5: Recommended FGS1r Exposure Times

Table 4.6: FGS1r Transfer Mode Filters to be Calibrated
During Cycle 8

Table 4.7: Suggested Minimum Number of Scans
for Separations < 15 mas

Table 5.1: FGS1r Position Mode Calibration and Error
Source Summary

Table 5.2: FGS1r Transfer Mode Calibrations
and Error-Source Summary

Table 5.3: Library of cycle 10 calibration point source S-curves

Table 6.1: FGS Instrument Parameters

Table 6.2: Summary of Calibrated Mode and Filter Combination

Table 6.3: Pos Mode Optional Parameters

Table 6.4: Trans Mode Optional Parameters

Table 6.5: Pos Mode Overheads

Table 6.6: Pos Mode Overheads and Exposure Time vs. -Magnitude

Table 6.7: Trans Mode Observing Overheads

Table 6.8: Target and Exposure Input for Example 1

Table 6.9: Target and Exposure Input for Example 3

Table 6.10: Reference/Check Star Pattern

Table 6.11: Target and Exposure Input for Example 4

Table B.1: FGS1r Angular Resolution Test: Effective
Signal-to-Noise Ratios

Table B.2: FGS1r Angular Resolution Test: Binary Star Analysis

Acknowledgments

The contact person for the STScI FGS Program is Ed Nelan (nelan@stsci.edu).

Many dedicated colleagues have contributed time and expertise to the STScI FGS Astrometry Program over so many years. (and in fact, were the FGS Astrometry Program). We wish to express our sincerest gratitude for their essential support of this program (in the hope it continues through many more years): Linda Abramowicz-Reed and Kevin Chisolm at BFGoodrich, the members of the Space Telescope Astrometry Team, especially Otto Franz and Larry Wasserman at Lowell Observatory, Fritz Benedict and Barbara McArthur with the University of Texas at Austin, and Denise Taylor at STScI.

STScI would like to thank BFGoodrich, in particular Kevin Chisholm and Linda Abramowicz-Reed for their invaluable assistance during the adjustment of the Articulating Mirror Assembly (AMA) to re-optimize FGS1r (on three occasions), FGS2r, and FGS2r2. And not least, we would like to acknowledge that Chris Ftaclas originated and developed the conceptual basis of the AMA, which has enabled the FGS1r to fulfill its potential as a science instrument.

We would also like to thank Susan Rose and Steve Hulbert at STScI for their invaluable help with the preparation and publication of this Instrument Handbook. Without their patience and guidance, this Handbook could not have come together.

We thank Alain Fresneau for establishing the astrometry program at STScI.

Chapter 1: Introduction

Chapter Contents

- [1.1 Purpose](#)
- [1.2 Instrument Handbook Layout](#)
- [1.3 The FGS as a Science Instrument](#)
- [1.4 Technical Overview](#)
- [1.5 Planning and Analyzing FGS Observations](#)
- [1.6 FGS Replacement in SM4](#)

The precision pointing required of the *Hubble Space Telescope* (HST) motivated the design of the *Fine Guidance Sensors* (FGS). These large field of view (FOV) white light interferometers are able to track the positions of luminous point source objects with ~ 1 millisecond of arc (mas) precision. In addition, the FGS can scan an object to obtain its interferogram with sub-mas sampling. These capabilities enable the FGS to perform as a high-precision astrometer and a high angular resolution science instrument which can be applied to a variety of objectives, including:

- relative astrometry with an accuracy approaching 0.2 mas for targets with $V < 16.8$;
- detection of close binary systems down to ~ 8 mas, and characterization of visual orbits for systems with separations as small as 12 mas;
- measuring the angular size of extended objects
- 40 Hz relative photometry (e.g., flares, occultations, transits) with milli-magnitude accuracy.

The purpose of this Handbook is to provide information needed to propose for HST/FGS observations (Phase I), to design Phase II programs for accepted FGS proposals (in conjunction with the Phase II Proposal Instructions), and to describe the FGS in detail.

1.1 Purpose

The FGS Instrument Handbook is the basic reference manual for observing with the FGS. It describes the FGS design, properties, performance, operation, and calibration. The Handbook is maintained by the Observatory Support Group at STScI, who designed this document to serve three purposes:

- To help potential FGS users decide whether the instrument is suitable for their goals, and to provide instrument-specific information for preparing Phase I observing proposals with the FGS.
- To provide instrument-specific information and observing strategies relevant to the design of Phase II FGS proposals (in conjunction with the [Phase II Proposal Instructions](#)).
- To provide technical information about the FGS and FGS observations.

The [FGS Data Handbook](#) provides complementary information about the analysis and reduction of FGS data, and should be used in conjunction with this Instrument Handbook. In addition, we recommend visiting the FGS World Wide Web pages for frequent updates on performance, calibration results, and methods of data reduction and analysis. These pages can be found at:

<http://www.stsci.edu/hst/instrumentation/fgs>

1.2 Instrument Handbook Layout

To guide the proposer through the FGS's capabilities and help optimize the scientific use of the instrument, we have produced the *FGS Instrument Handbook*, the layout of which is as follows:

- [Chapter 1](#): Introduction, describes the layout of the *FGS Instrument Handbook* and gives a brief overview of the instrument and its capabilities as a science instrument.
- [Chapter 2](#): FGS Instrument Design, details the design of the FGS. Specific attention is given to the optical path and the effect of optical misalignments on FGS observations. The interferometric Transfer Function is described in detail, along with effects which degrade Transfer Function morphology. Descriptions of apertures and filters are also presented here.
- [Chapter 3](#): FGS Science Guide, serves as a guide to the scientific programs which most effectively exploit FGS capabilities. The advantages offered by the FGS are described together with suitable strategies to achieve necessary scientific objectives. A representative list of publications utilizing the FGS for scientific observations is included for reference.
- [Chapter 4](#): Observing with the FGS, describes the detailed characteristics of the two FGS observing modes - Position mode and Transfer mode - as well as the observational configurations and calibration requirements which maximize the science return for each mode.
- [Chapter 5](#): FGS Calibration Program, describes sources of FGS errors, associated calibrations, and residual errors for Position and Transfer mode observations. A discussion of calibration plans for the upcoming Cycle is also included.
- [Chapter 6](#): Writing a Phase II Proposal, serves as a practical guide to the preparation of Phase II proposals, and as such is relevant to those researchers who have been allocated HST observing time.
- [Chapter 7](#): FGS Astrometry Data Processing, briefly describes the FGS astrometry data processing pipeline and analysis tools. The various corrections for both Position and Transfer mode observations are described along with the sequence in which they are applied.

In addition to the above chapters, we also provide two appendices:

- [Appendix A: Target Acquisition and Tracking](#): Target Acquisition and Tracking, describes the acquisition of targets in both Position and Transfer modes. The target acquisition scenario may have implications for observations of moving targets or targets in crowded fields.
- [Appendix B: FGS1r Performance Summary](#): FGS1r Performance Summary, describes the evolution of FGS1r during its first three years in orbit and the adjustment of the AMA to improve performance in this instrument.

1.3 The FGS as a Science Instrument

The FGS has two modes of operation: Position mode and Transfer mode. In Position mode the FGS locks onto and tracks a star's interferometric fringes to precisely determine its location in the FGS FOV. By sequentially observing other stars in a similar fashion, the relative angular positions of luminous objects are measured with a per-observation precision of about 1 mas over a magnitude range of $3.0 < V < 16.8$. This mode is used for relative astrometry, i.e., for measuring parallax, proper motion, and reflex motion. Multi-epoch programs have achieved accuracies of 0.2 mas or better (1-sigma).

In Transfer mode an object is scanned to obtain its interferogram with sub-mas sampling. Using the fringes of a point source as a reference, the composite fringe pattern of a non-point source is deconvolved to determine the angular separation, position angle, and relative brightness of the components of multiple-star systems or the angular diameters of resolved targets (Mira variables, asteroids, etc.).

As a science instrument, the FGS is a sub-milliarcsecond astrometer and a high angular resolution interferometer. Some of the investigations well suited for the FGS are listed here and discussed in detail in [Chapter 3](#):

- **Relative astrometry** (position, parallax, proper motion, reflex motion) with -single-measurement accuracies of about 1 milliarcsecond (mas). Multi-epoch observing programs have determine parallaxes with accuracies of 0.2 mas and better.
- **High-angular resolution observing:**
 - detect duplicity or structure down to 8 mas
 - derive visual orbits for binaries as close as 12 mas.
- **Absolute masses and luminosities:**
 - The absolute masses and luminosities of the components of a multiple-star system can be determined by measuring the system's parallax while deriving visual orbits and the brightnesses of the stars.
- **Measurement of the angular diameters** of non-point source objects down to about 8 mas.
- **40Hz 1-2% long-term relative photometry:**
 - Long-term studies or detection of variable stars.
- **40Hz milli-magnitude relative photometry over orbital timescales.**
 - Light curves for stellar occultations, flare stars, etc.

1.4 Technical Overview

1.4.1 The Instrument
1.4.2 Spectral Response
1.4.3 The S-Curve: The FGS's Interferogram
1.4.4 FGS1r and the AMA
1.4.5 Field of View
1.4.6 Modes of Operation
Table of Contents

1.4.1 The Instrument

The FGS is a white-light shearing interferometer. It differs from the long-baseline Michelson Stellar Interferometer in that the angle of the incoming beam with respect to the *HST*'s optical axis is measured from the tilt of the collimated wavefront presented to the “Koesters prism” rather than from the difference in the path length of two individual beams gathered by separate apertures. Thus, the FGS is a *single aperture* (single telescope) interferometer, well suited for operations aboard *HST*. *In addition*, the FGS is a two dimensional interferometer; it scans or tracks an object's fringes in two orthogonal directions simultaneously. As a science instrument, the FGS can observe targets as bright as $V=3$ and as faint as $V=17.0$ (dark counts dominate for $V>17$ targets).

1.4.2 Spectral Response

The FGS employs photomultiplier tubes (PMTs) for detectors. The PMTs—four per FGS—are an end-illuminated 13-stage venetian blind dynode design with an S-20 photocathode. The PMT sensitivity is effectively monotonic over a bandpass from 4000 to 7000Å, with an ~18% efficiency at the blue end which diminishes to ~2% at the red end.

Each FGS contains a filter wheel fitted with 5 slots. FGS1r contains three wide-band filters, F550W, F583W (sometimes called CLEAR), F605W, a 5-magnitude Neutral Density attenuator (F5ND), and a 2/3 pupil stop, referred to as the PUPIL. Only the F583W and the F5ND are supported by standard calibrations for science observations. The PUPIL is calibrated for guide duty. Transmission curves of the filters and recommendations for observing modes are given in [Chapter 2](#) and [Chapter 4](#) respectively.

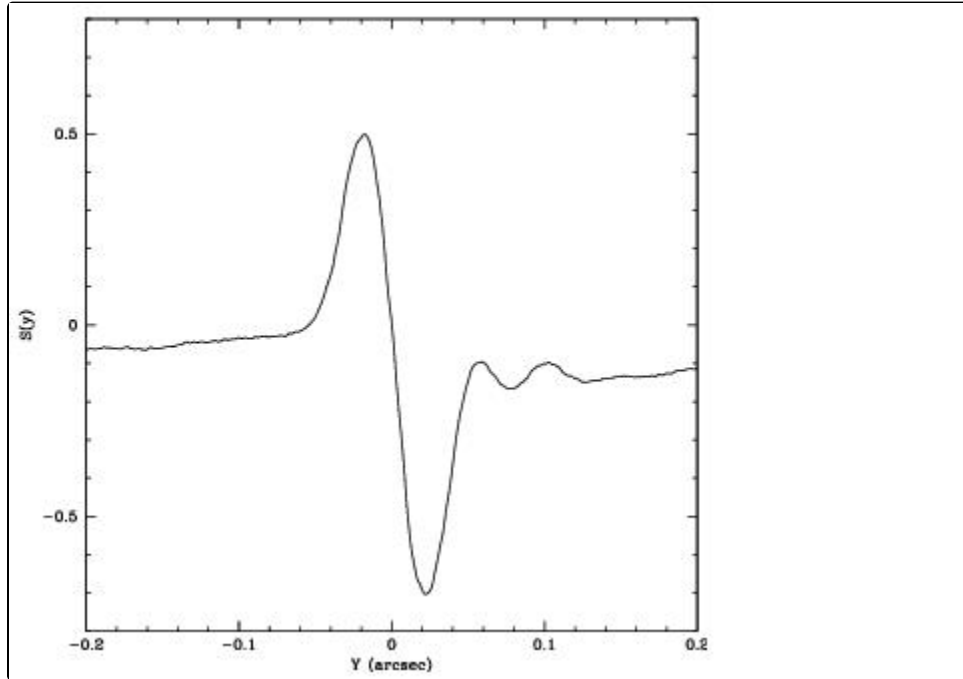
1.4.3 The S-Curve: The FGS's Interferogram

The FGS interferometer consists of a polarizing orthogonal beam splitter and two Koesters prisms. The Koesters prism, discussed in [Chapter 2](#), is sensitive to the tilt of the incoming wavefront. Two beams emerge from each prism with relative intensities correlated to the *tilt* of the input wavefront. The relation between the input beam tilt and the normalized difference of the intensities of the emergent beams, measured by pairs of photomultiplier tubes, defines the fringe visibility function, referred to as the “S-Curve”. [Figure 1](#) shows the e from a point source. To sense the tilt in two dimensions, each FGS contains two Koesters prisms oriented orthogonally with respect to one another. A more detailed discussion is given in [Chapter 2](#).

1.4.4 FGS1r and the AMA

During the Second Servicing Mission in March 1997 the original FGS1 was replaced by FGS1r. This new instrument was improved over the original design by the re-mounting of a flat mirror onto a mechanism capable of tip/tilt articulation. This mechanism, referred to as the *Articulated Mirror Assembly*, or AMA, allows for precise in-flight alignment of the interferometer with respect to *HST*'s OTA. This assured optimal performance from FGS1r since the degrading effects of *HST*'s spherically aberrated primary mirror would be minimized (the COSTAR did not correct the aberration for the FGSs). This topic is discussed in detail in [Chapter 2](#).

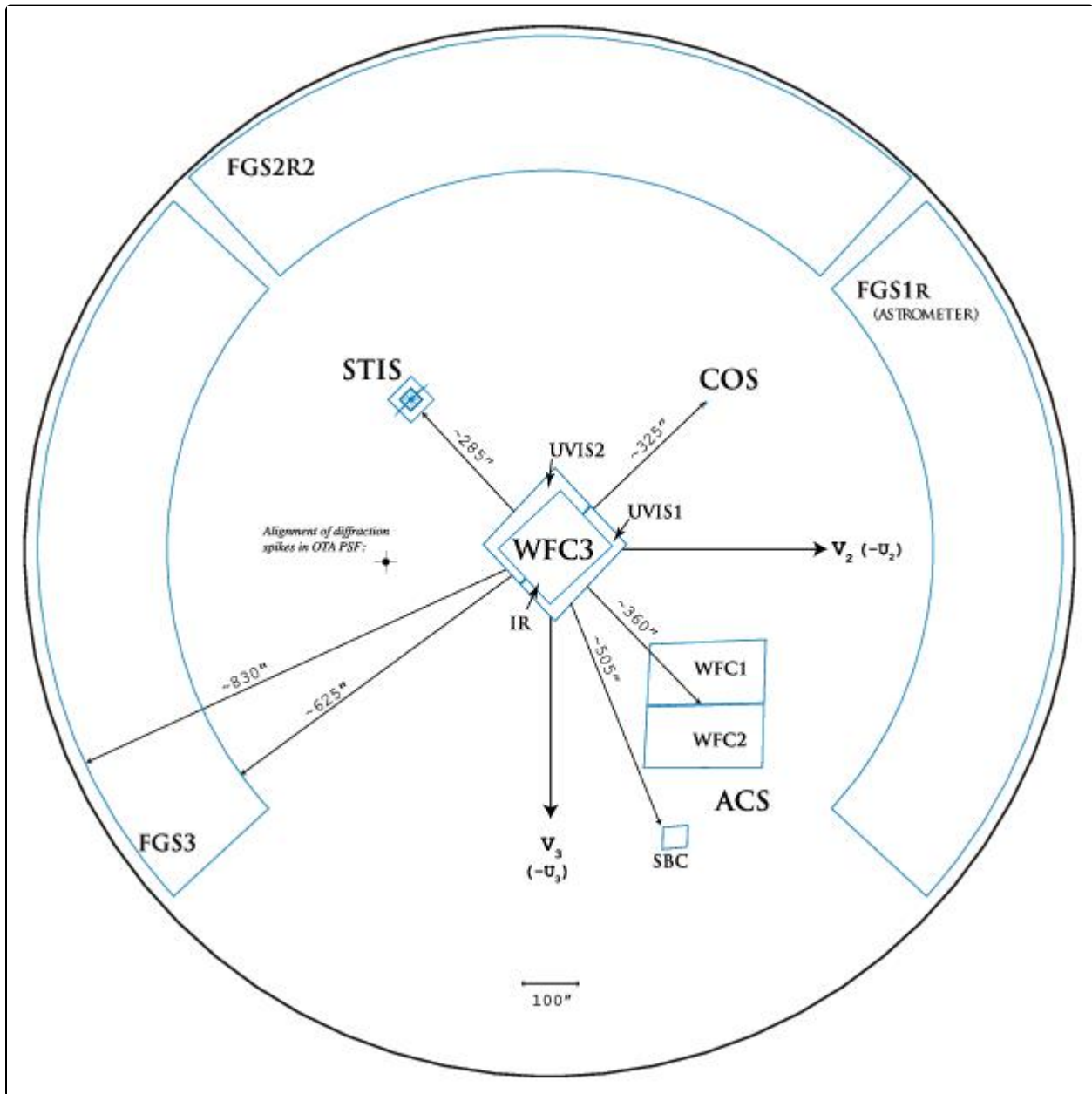
Figure 1.1: FGS Interferometric Response (the “S-Curve”)



1.4.5 Field of View

The total *field of view* (FOV) of an FGS is a quarter annulus at the outer perimeter of the *HST* focal plane with inner and outer radii of 10 and 14 arcmin respectively. The total area (on the sky) subtended by the FOV is ~ 69 square arcminutes. The entire FOV is accessible to the interferometer, but only a 5×5 arcsec aperture, called the *Instantaneous Field of View* (IFOV), samples the sky at any one time. A dual component Star Selector Servo system (called SSA and SSB) in each FGS moves the IFOV to a desired position in the FOV. The action of the Star Selectors is described in detail in [Chapter 2](#), along with a more detailed technical description of the instrument. [Figure 1.2](#) shows a schematic representation of the FGSs relative to the *HST* focal plane after Servicing Mission 4.

Figure 1.2: FGSs in the *HST* Focal Plane (Projected onto the Sky)



1.4.6 Modes of Operation

The FGS has two modes of operation: Position mode and Transfer mode.

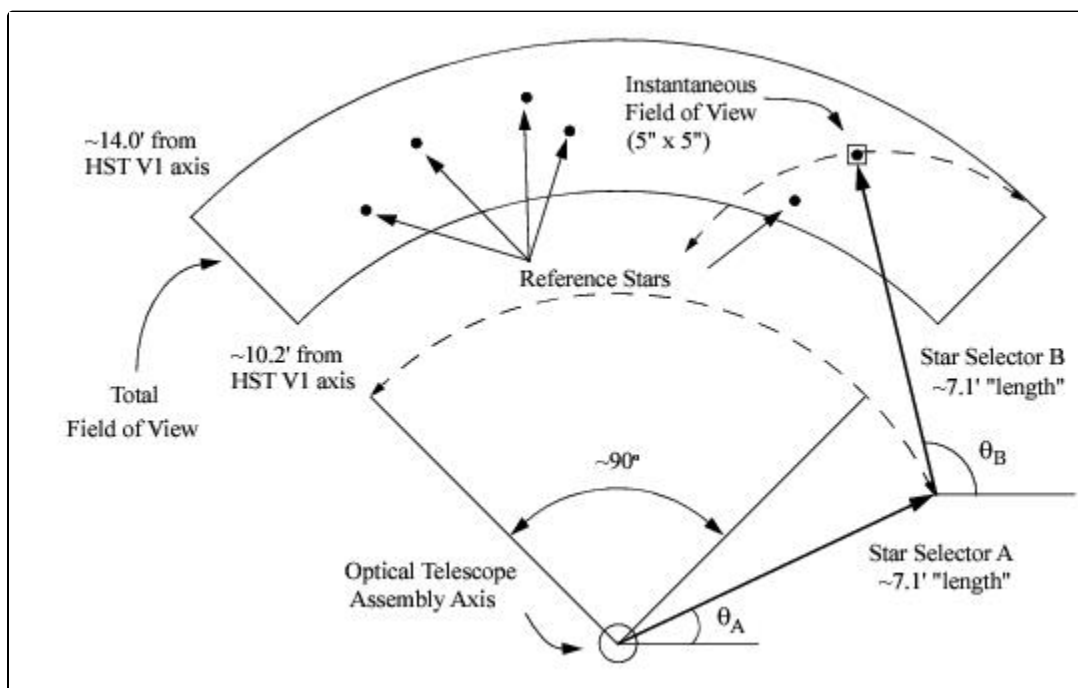
Position Mode

The FGS Position mode is used for relative astrometry, i.e. parallax, proper motion, reflex motion and position studies. In Position mode, the *HST* pointing is held fixed while selected FGS targets are sequentially observed (fringes are acquired and tracked, see [Appendix A: Target Acquisition and Tracking](#)) for a period of time ($2 < t < 120$ sec, selected by the observer) to measure their relative positions in the FOV. Two-dimensional positional and photometric data are continuously recorded every 25 msec (40 Hz). The raw data are composed of a Star Selector encoder angles (which are converted to FGS X and Y detector coordinates during ground processing) and photomultiplier (PMT) counts. [Figure 1.3](#) is a schematic of the FGS FOV and IFOV. The figure shows how Star Selectors A and B uniquely position the IFOV anywhere in the FGS FOV.

Transfer Mode

In Transfer mode, the FGS obtains an object's interferograms in two orthogonal directions by scanning the Instantaneous Field of View (IFOV) across the target (typically in 1" scan lengths). Transfer mode observing is conceptually equivalent to imaging an object with sub-milliarcsecond pixels. This allows the FGS to detect and resolve structure on scales smaller than *HST*'s diffraction limit, making it ideal for detecting binary systems with separations as small as 8 mas with ~ 1 mas precision.

Figure 1.3: FGS Star Selector Geometry



1.5 Planning and Analyzing FGS Observations

[1.5.1 Writing an FGS Proposal](#)

[1.5.2 Data Reduction](#)

[Table of Contents](#)

1.5.1 Writing an FGS Proposal

[Chapter 3](#) and [6](#) are of particular use in designing and implementing an FGS proposal. [Chapter 3](#) provides information on a variety of scientific programs which exploit the unique astrometric capabilities of the FGS. [Chapter 6](#) provides guidelines on how to design the Phase II proposal. In [Chapter 6](#) we provide examples of observing strategies and identify special situations where further discussions with STScI are recommended.

1.5.2 Data Reduction

The *FGS Data Handbook* provides a detailed description of the FGS data and related data reduction. Chapters [5](#) and [7](#) in this Instrument Handbook contain useful summaries of that information. [Chapter 5](#) provides a discussion of the accuracies and sources of errors associated with FGS data in addition to a detailed description of the calibration program planned for the upcoming Cycle. [Chapter 7](#) describes the set of software tools which are available to observers to reduce, analyze and interpret FGS data. Please check the [FGS Web pages](#) for details on these tools.

1.6 FGS Replacement in SM4

A total of four FGS units were built, an “engineering test unit” (ETU) and three for installation on *HST*. Prior to the second servicing mission the mechanical health of both FGS1 and FGS2 had degraded to the point that the reliability of each unit became questionable. Moreover, it was recognized that the deleterious affect of *HST*’s spherical aberration, to which the FGSs are still subject, could be partially mitigated by replacing the fixed mounted “fold-flat mirror #3” with an articulating mirror assembly (AMA) that can be commanded from the ground to provide the means to align the FGS interferometric elements with *HST*’s optical axis. Therefore the ETU was refurbished with the AMA and made flight-ready for insertion into HST in Servicing Mission 2 (SM2).

FGS2 had been showing chronic trends of mechanical wear, more so than FGS1, and thus had been slated for replacement in SM2. However, a few months before SM2, FGS1 displayed acute mechanical failure symptoms and appeared to be at greater risk than FGS2. Therefore, the refurbished ETU replaced FGS1, and has since been referred to as FGS1r. With the advantage of the AMA, FGS1r has proved itself superior to FGS3 as an astrometric instrument, and has been used as such since 1999.

Meanwhile, the original FGS1, which was returned to Earth at the completion of SM2, was refurbished with new mechanical components and an AMA. Designated FGS2r, it was installed in *HST* during SM3A. The original FGS2 was returned to Earth and refurbished with the expectation that it would replace the venerable FGS3 in a future servicing mission. However, since mid 2006 FGS2r has been showing problems with the LED on one of its star selector servos. With a failing LED, which is sensed by the FGS firmware to provide closed-loop control of the instrument, FGS2r experienced an increased guide star acquisition failure rate. Therefore, it was replaced in SM4 with the refurbished unit (the original FGS2).

The refurbished FGS installed in SM4 is referred to as FGS2r2. Unlike FGS1r and FGS2r, its optics had been realigned using the specially developed full field of view test set. This enabled the Goodrich optical engineers to eliminate “beam walk”, an effect that causes the interferometer’s relative alignment with the HST optical axis to change as the star selectors assembly is rotated to observe stars across the FGS FOV. This beam walk degrades the benefit of the AMA for mitigating *HST*’s spherical aberration. (The AMA can be used to optimize the FGS performance at any one place, but only one place, in the FOV.) The commissioning of FGS2r2 in June 2009, after the AMA adjustment, resulted in near optimal interferometric performance across its entire FOV. Nonetheless, because FGS1r is well calibrated for scientific observations, and has demonstrated superb performance as a science instrument, it continues to be designated as the *HST* science FGS.

Chapter 2: FGS Instrument Design

Chapter Contents

- [2.1 The Optical Train](#)
- [2.2 FGS Detectors](#)
- [2.3 HST's Spherical Aberration](#)
- [2.4 The FGS Interferometric Response](#)
- [2.5 The FGS1r Articulated Mirror Assembly](#)
- [2.6 FGS Aperture and Filter](#)
- [2.7 FGS Calibrations](#)


2.1 The Optical Train

- 1. [2.1.1 The Star Selectors](#)
- 2. [2.1.2 The Interferometer](#)
- 3. [Table of Contents](#)

Each FGS comprises two orthogonal white-light, shearing interferometers, their associated optical and mechanical elements, and four S-20 photo-multiplier tubes (PMTs). For clarity, we divide the FGS optical train into two sections: [Section 2.1.1](#) and [Section 2.1.2](#).

1. 2.1.1 The Star Selectors

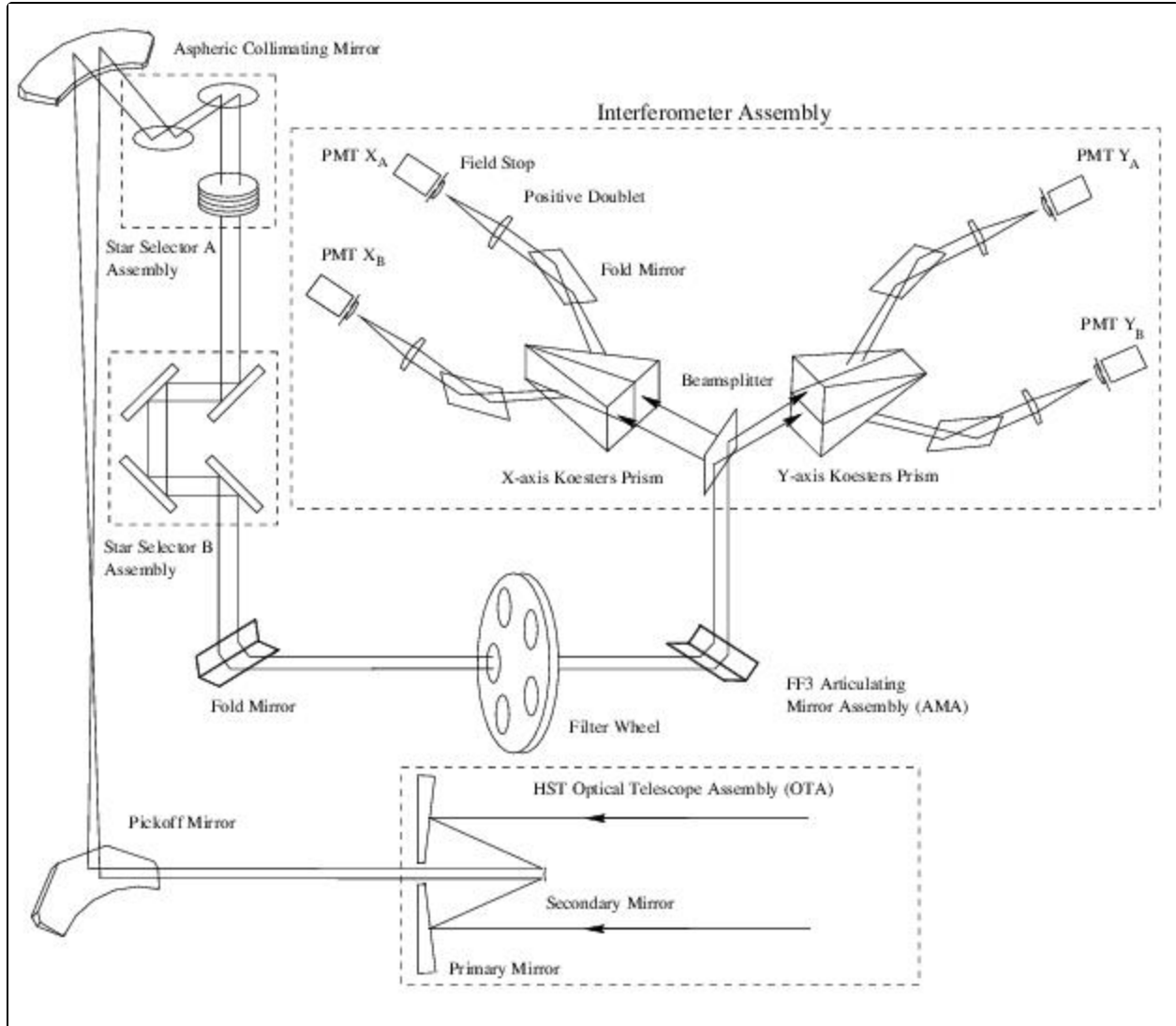
A schematic view of the FGS optical train is shown in [Figure 2.1](#). Light from the *HST* Optical Telescope Assembly (OTA) is intercepted by a plane pickoff mirror in front of the HST focal plane and directed into the FGS. The beam is collimated and compressed (by a factor of ~ 60) by an *aspheric collimating mirror*, and guided to the optical elements of the Star Selector A (SSA) servo assembly. This assembly of two mirrors and a five element refractive corrector group can be commanded to rotate about the telescope's optical axis. The corrector group compensates for designed optical aberrations induced by both the asphere and the HST Optical Telescope Assembly (OTA). The asphere contributes astigmatism, spherical aberration and coma to the incident beam. Aberrations from the OTA's Ritchey-Chretien design include astigmatism and field curvature.

 **The FGS design does not correct for the unexpected spherical aberration from the telescope's misfigured primary mirror.**

After the SSA assembly, the beam passes through a field stop (not shown) to minimize scattered light and narrow the field of view. The four mirrors of the Star Selector B (SSB) assembly intercept and redirect the beam to a fold flat mirror and through the filter wheel assembly. From there, the Articulating Mirror Assembly (AMA) reflects the beam onto the Polarizing Beam Splitter. Like the SSA, the SSB assembly rotates about a vector parallel to the telescope's optical axis. Together the SSA and SSB assemblies allow for the transmission to the polarizing beam splitter only those photons originating from a narrow region in the total FGS field of view. This area, called the *Instantaneous Field of View* (IFOV), is a 5×5 arcsec patch of sky, the position of which is uniquely determined by the rotation angles of both the SSA and SSB. The IFOV can be brought to any location in the full FOV and its position can be determined with sub-milliarcsecond precision (see [Figure 1.3](#)).

The AMA is an enhancement to the original FGS design. It allows for in-flight alignment of the collimated beam onto the polarizing beam splitter and therefore the Koesters prisms. Given *HST*'s spherically aberrated OTA, this is an important capability, the benefits of which will be discussed in subsequent chapters.

Figure 2.1: FGS1r Optical Train Schematic



2. 2.1.2 The Interferometer

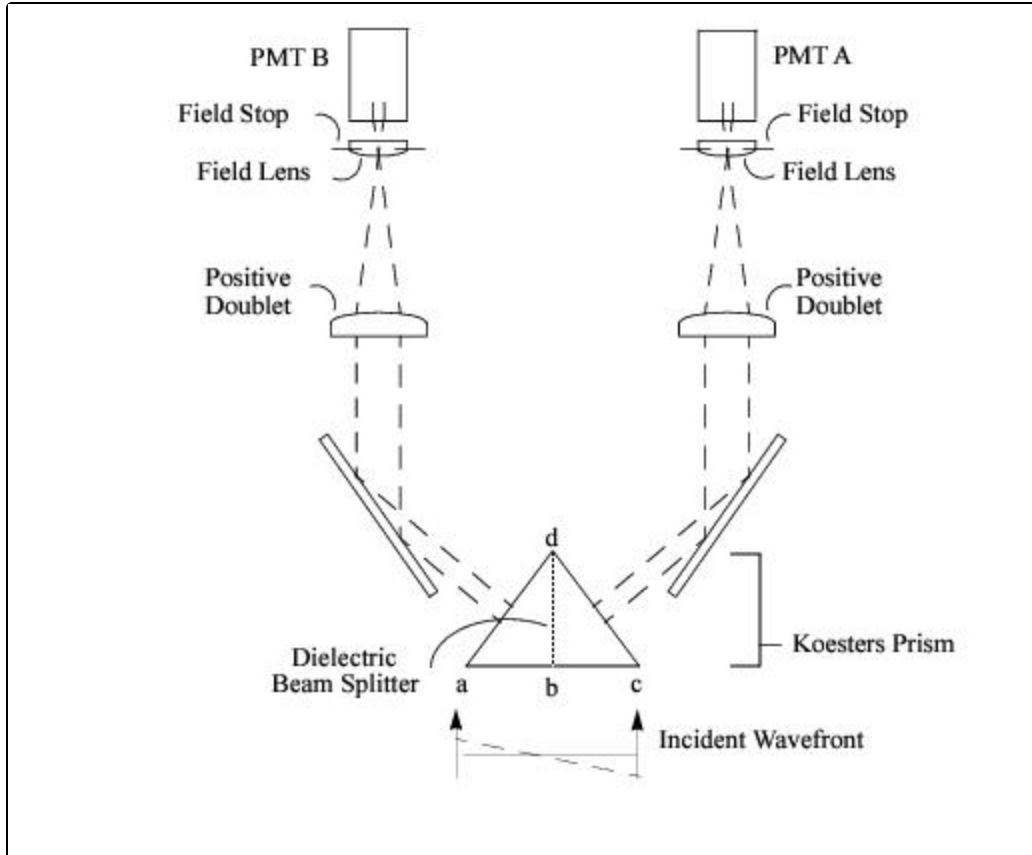
The interferometer consists of a polarizing beam splitter followed by two Koesters prisms. The polarizing beam splitter divides the incoming unpolarized light into two plane polarized beams with orthogonal polarizations, each having roughly half the incident intensity. The splitter then directs each beam to a Koesters prism and its associated optics, field stops, and photomultiplier tubes. [Figure 2.2](#) illustrates the light path between the Koesters prism and the PMTs.

The Koesters prisms are constructed of two halves of fused silica joined together along a coated surface which acts as a dielectric beam splitter. The dielectric layer performs an equal intensity division of the beam, reflecting half and transmitting half, imparting a 90 degree phase lag in the transmitted beam. This division and phase shift gives the Koesters prism its interferometric properties: the beam reflected from one side of the prism interferes constructively or destructively with the beam transmitted from the other side. The degree of interference between the two beams is directly related to the angle, or tilt, between the incoming wavefront's propagation vector and the plane of the dielectric surface.

Each Koesters prism emits two exit beams whose relative intensities depend on the tilt of the incident wavefront. Each beam is focussed by a positive doublet onto a field stop assembly (which narrows the IFOV to 5×5 arcsec). The focussed beams are recollimated by field lenses (after the field stop) and illuminate the photomultiplier tubes (PMT). The PMT electronics integrate the photon counts over 25 millisecond intervals.

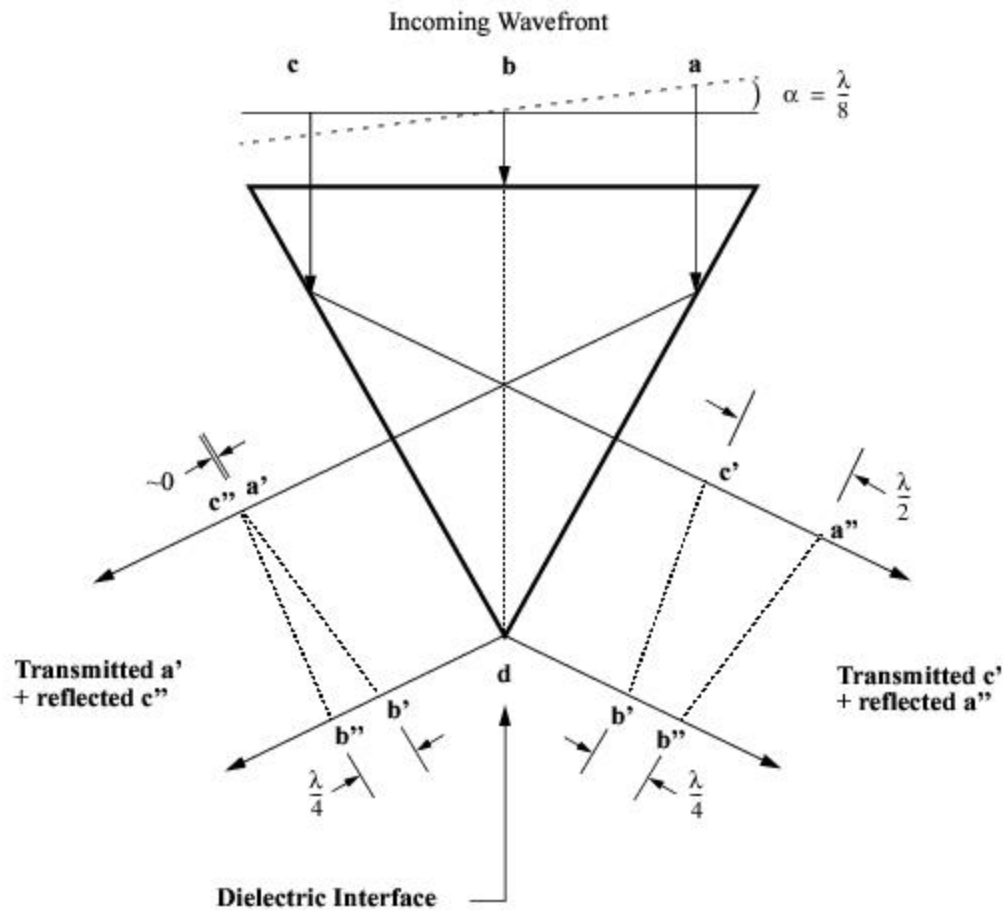
The Koesters prism is sensitive to the angle of the incoming wavefront as *projected* onto its dielectric surface. To measure the *true* (non-projected) direction of the source, each FGS has two Koesters prisms oriented perpendicular to one another (and therefore a total of 4 PMTs).

Figure 2.2: Light Path from Koesters Prisms to the PMTs



Small rotations of the star selector A and B assemblies alter the direction of the target's collimated beam, and hence the tilt of the incident wavefront with respect to the Koesters prisms. [Figure 2.3](#) is a simplified illustration of Koesters prism interferometry. As the wavefront rotates about point b, the relative phase of the transmitted and reflected beams change as a function of angle α . When the wavefront's propagation vector is parallel to the plane of the dielectric surface (b-d) a condition of *interferometric null* results, and the relative intensities of the two emergent beams will ideally be equal. When α is not zero, the intensities of the left and right output beams will be unequal and the PMTs will record different photon counts.

Figure 2.3: The Koesters Prism: Constructive and Destructive Interference.



This case shows the interference within the Koesters Prism for a wavefront with a tilt α such that the ray entering the prism at point a is advanced by $\lambda/4$ with respect to the ray entering at point c . The rays a' and c' are transmitted through the dielectric surface and are retarded by $\lambda/4$ in the process. Rays c'' and a'' are reflected by the dielectric and suffer no change in phase. Rays c' and a'' are interferometrically recombined and exit the prism on the right hand side. Similarly, rays a' and c'' are recombined and exit to the left. The intensity of each exit ray depends upon the phase difference of recombined reflected and transmitted rays.

The rays exiting the prism at its apex will always consist of components with 90 degree phase difference (because the reflected and transmitted components initially had zero phase difference, but the dielectric retarded the transmitted wave by $\lambda/4$). Therefore, at the apex, constructive and destructive interference occur at the same rate and the two exit rays have equal intensity. In the example shown here, the intensity of the rays exiting the left face of the prism increases as one moves along the face, away from the apex, in the direction of increasing constructive interference (the recombined beams a' and c'' have zero phase difference). On the right face of the prism, destructive interference increases away from the apex (a' and c' are out of phase by 180 deg), so the intensity of these rays diminishes along the face. Therefore the intensity of the left hand beam is greater than that of the right hand beam. The tilt α in this example corresponds to a peak of the S-curve. Rotating the wavefront about point b by 2α in a clockwise direction would produce the other peak of the S-curve.

2.2 FGS Detectors

The FGS photomultiplier tubes (PMTs, four per FGS) are end-illuminated, 13 stage venetian blind dynode S-20 photon-counting detectors with an effective photocathode area of about 4 mm. The A and B channels for each FGS interferometric axis operate independently. The PMTs are sensitive over a bandpass of 4000-7000Å, with an efficiency of ~ 18% at the blue and diminishing linearly to about 2% at the red end. Each PMT has a characteristic dark count rate, as well as a “dead time” during which time it is unable to record the arrival of a new photon while it is still processing a previously arrived photon. The FGS1r PMT dead times were measured on orbit using two stars of very similar spectral type (HD 209458 and PO41C) that differ by 4.34 magnitudes.

The FGS1r dark counts for each channel are given in [Table 2.1](#). The FGS1r dead times, in seconds, are given in [Table 2.2](#).

Table 2.1: FGS1r Dark Counts

PMT	counts/second ¹	stdev
AX	174.6	±2
BX	84.4	±2
AY	164.0	±2
BY	252.0	±2

¹ Values based on an average of 40Hz PMT counts and associated standard deviations.

Table 2.2: FGS1r Dead Times

Ax	2.0759×10^{-7}
Bx	2.3018×10^{-7}
Ay	2.1074×10^{-7}
By	2.2297×10^{-7}

2.3 HST's Spherical Aberration

The interferometric response of the Koesters prism arises from the difference in optical path lengths of photons entering one side of the prism to those entering the other side (and therefore to the tilt of the wavefront). A photon transmitted by the dielectric surface within the prism is re-combined with one which has been reflected by the surface. Both of these photons were incident on the prism's entrance face at points equidistant from, but on opposite sides of, the dielectric surface. The degree to which they constructively or destructively interfere depends solely on their difference in phase, which by design, should depend only upon the wavefront tilt. Any optical aberration in the incident beam that does not alter the phase difference of the recombining beams will not affect the interferometric performance of the FGS. Such aberrations are considered to be *symmetric*.

No correction for the *HST's* spherical aberration is incorporated in the original or refurbished FGSs. Though the Koesters prisms are not sensitive to symmetric aberrations (e.g., spherical aberration), small misalignments in the internal FGS optical train shift the location of the beam's axis of tilt ("b" in [Figure 2.2](#) and in [Figure 2.3](#)) effectively breaking the symmetry of the spherical aberration. This introduces an error in the phase difference of the re-combining photons and degrades the interferometric response.

With *HST's* 0.23 microns of spherical aberration, a decentering of the wavefront by only 0.25 mm will decrease the modulation of the S-Curve to 75% of its perfectly aligned value. If the telescope were not spherically aberrated (i.e., if the wavefront were planar) misalignments up to five times this size would hardly be noticeable. The impact of *HST* spherical aberration and the improved performance of FGS1r are discussed in the next sections.

2.4 The FGS Interferometric Response

[2.4.1 The Ideal S-Curve](#)

[2.4.2 Actual S-Curves](#)

[Table of Contents](#)

FGS interferometry relates the wavefront tilt to the normalized difference of intensity between the two beams emerging from the Koesters prism (see [Figure 2.3](#)). As the tilt varies over small angles (as when the IFOV scans the target), this normalized intensity difference defines the interferogram, or “S-Curve”, given by the relation,

$$S_x = (A_x - B_x) / (A_x + B_x),$$

where A_x and B_x are the photon counts from PMTXA and PMTXB respectively, accumulated over 25 milliseconds intervals when the IFOV is at location x . The Y-axis S-Curve is defined in an analogous manner. [Figure 1.1](#), FGS Interferometric Response (the “S-Curve”) shows an S-Curve resulting from several co-added scans of a point source.

Because the FGS is a white light, broad bandpass interferometer, its S-Curve is essentially a single fringe interferogram. The spectral incoherence of white light causes the higher order fringes to be strongly damped. Because the S-Curve is a normalized function, its amplitude is not sensitive to the target’s magnitude provided the background and dark contributions to the input beam are relatively small. However, as fainter targets are observed (i.e., $V \geq 14.5$), the S-Curve’s amplitude will be reduced (background and dark counts contributions are not coherent with light from the target). Usually the effect of dark + background is easily calibrated and therefore does not compromise the instrument’s scientific performance in either Position or Transfer mode. In a similar fashion the PMT deadtimes, if not accounted for, will reduce the amplitude of the observed fringes for stars brighter than $V \sim 9$ when observed with the F583W element. This effect is easily removed during calibration.

2.4.1 The Ideal S-Curve

The intensity of each beam exiting the Koesters prism is the integral of the intensity of each ray along the entire half-face of the prism. When the IFOV is more than 100 milliarcseconds (mas) from the location of the interferometric null, the PMTs of a given channel record nearly equal intensities since the re-combining beams are essentially incoherent over such large optical path differences (the photons constructively and destructively interfere at approximately the same rate). Closer to the interferometric null (at about ± 40 mas from the null), a signal emerges as the Koesters prism produces exit beams of different relative intensities.

Maximum fringe visibility of the ideal S-Curve min/max extremes is 0.7, occurring at about -20 and $+20$ mas for the positive and negative fringe maxima, respectively. Thus the “peak-to-peak” amplitude is 1.4. An ideal S-curve is inverse symmetric about the central “zero point crossing”. This crossing occurs when the wavefront’s propagation vector is normal to the Koesters prism entrance face, a condition referred to as interferometric null (jargon derived from guide star tracking or Position mode observing for when a star’s fine error signal has been nulled out).

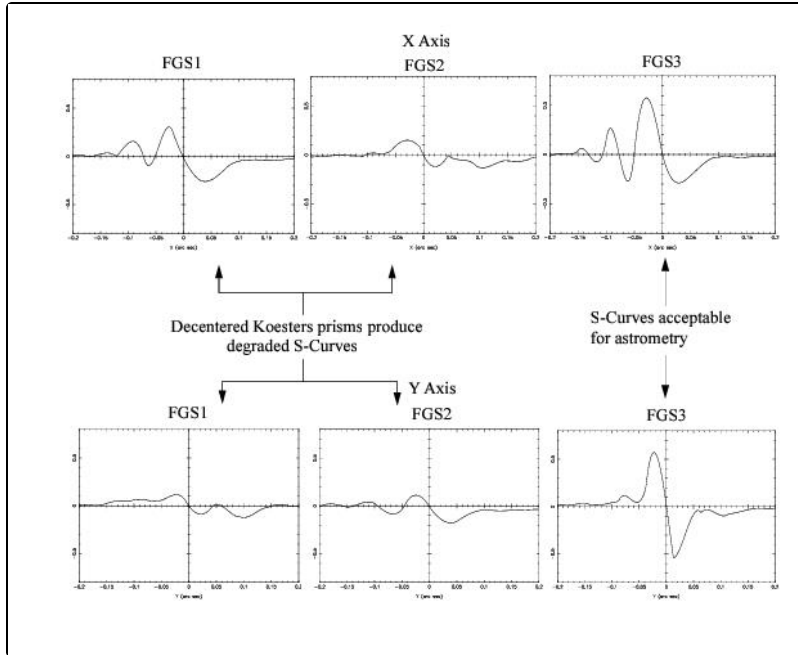
2.4.2 Actual S-Curves

HST's Spherical Aberration

The characteristics of real S-Curves depend on several factors: the quality and fabrication of the internal optics, the relative sensitivity of the PMTs, the alignment of the internal optics, the filter in use, the color of the target, and the effect of the spherically aberrated HST primary mirror. Some of the effects can be removed during processing and calibration, while others limit the performance of the instrument.

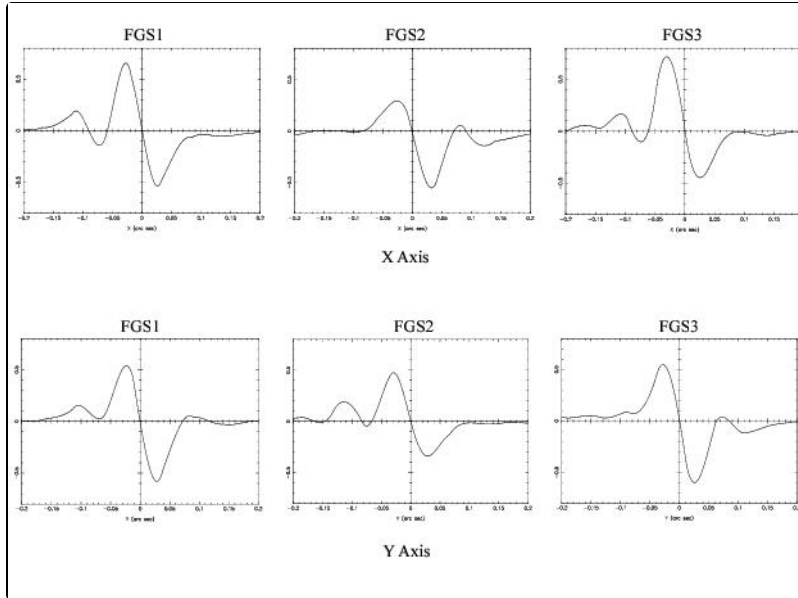
Referring back to [Figure 2.3](#), if the tilt axis of the incident beam is not at point 'b,' the beam is said to be *decentered* with respect to the Koesters prism. Given the presence of spherical aberration from the *HST's* misfigured primary mirror, the wavefront presented to the Koesters prism is not flat but has curvature. This greatly amplifies the effects of misalignments in the FGS optical train. A decentered spherically aberrated beam introduces a phase error between the re-combining transmitted and reflected beams, resulting in degraded S-Curve characteristics. The interferometric response (in filter F583W) of the 3 original FGSs are shown in [Figure 2.4](#). Decenter emerges as morphological deformations and reduced modulation of the fringes. Of the original three FGSs, FGS3 was the only instrument with sufficient fringe visibility to perform as an astrometric science instrument.

Figure 2.4: Full Aperture S-Curves of the Original FGSs



The degrading effects due to the misalignment of an FGS with the spherically aberrated OTA can be reduced by masking out the outer perimeter of the HST primary mirror. This eliminates the photons with the largest phase error. The 2/3 PUPIL stop accomplishes this and restores the S-Curves to a level which allows the FGS to track guide stars anywhere in the FOV. Unfortunately, it also blocks 50% of the target's photons, so nearly a magnitude of the *HST* Guide Star Catalog is lost. [Figure 2.5](#) shows the improvement of the S-Curve signature with the 2/3 PUPIL in place relative to the full aperture for the three FGSs. The PUPIL has been used for *HST* guiding since launch.

Figure 2.5: Improved S-Curves for Original FGSs when Pupil is in Place



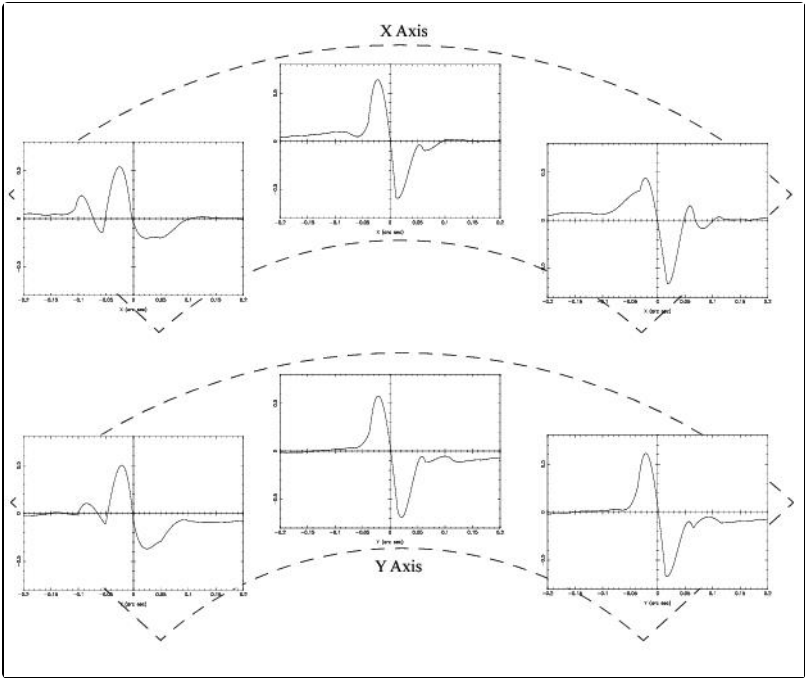
Field Dependence and Temporal Stability of the S-Curves

The Star Selectors center the beam on the face of the Koesters prisms while varying the tilt of the wavefront. Errors in the alignment of either the SSA or SSB with respect to the Koesters prisms will decenter the beam on the face of the prisms. Since the servos rotate over large sky angles to bring the IFOV to different positions in the Field of View, misalignments of these elements result in field-dependent S-curves. For this reason, Transfer mode observations should be restricted to the center of the FGS FOV, the only location supported by observatory calibrations.

The S-Curve measurements in the original three FGSs indicated large decenters of the Koesters prisms in FGS1 and FGS2 and field dependency in FGS3. FGS1r also shows field dependence, as can be seen for three positions across the FGS1r FOV in [Figure 2.6](#) (however, note that its x,y fringes are near ideal at the FOV center).

Temporal stability of S-Curves is also a concern. Monitoring of the FGS3 S-Curves along the X-axis showed the instrument suffered from variability of such amplitude that it could not be used to reliably resolve binary systems with projected X-axis separations less than ~ 20 mas. Conversely, FGS1r is far more stable. Its interferometric fringes show much less temporal variation, allowing the observer to confidently distinguish the difference between a point-source and a binary star system with a separation of 8 mas. This, in part, prompted the switch to FGS1r as the Astrometer for Cycle 8 and beyond.

Figure 2.6: FGS1r S-Curves in Full Aperture Across the Pickle



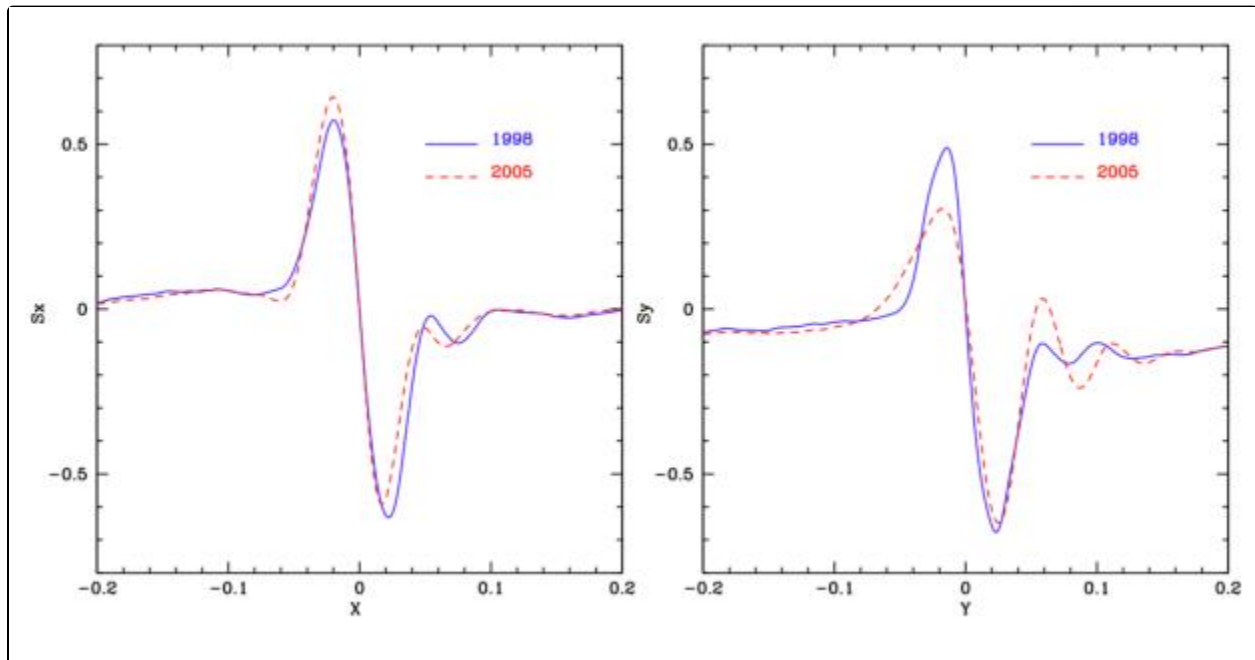
2.5 The FGS1r Articulated Mirror Assembly

FGS1r has been improved over the original FGS design by the insertion of the articulating mirror assembly (AMA) designed and built by Raytheon (formerly Hughes Danbury Optical Systems, currently BFGoodrich Space Flight Systems). A static fold flat mirror (FF3 in [Figure 2.1](#)) in FGS1r was mounted on a mechanism capable of tip/tilt articulation. This Articulating Mirror Assembly (AMA) allows for in-orbit re-alignment of the wavefront at the face of the Koesters prism. An adjustable AMA has proven to be an important capability since, given HST's spherical aberration, even a small misalignment degrades the interferometric performance of the FGS. On orbit testing and adjustment of the AMA were completed during FGS1r's first year in orbit. A high angular resolution performance test executed in May 1998 demonstrated the superiority of FGS1r over FGS3 as a science instrument. Therefore, FGS1r has been designated the Astrometer and has replaced FGS3 in this capacity. Information on the FGS1r calibration program can be found in [Chapter 5](#).

The AMA has been adjusted to yield near-perfect S-Curves at the center of the FGS1r FOV, and an optimum compromise results for the remainder of the FOV. The variation of S-Curve characteristics across the FOV arises from "beam walk" at the Koesters prisms as the star selectors rotate to bring the IFOV to different locations in the FGS FOV. This field dependence does not necessarily impair FGS1r's performance as a science instrument, but it does restrict Transfer mode observations to the center of the FOV since it is the only location calibrated for that mode (Position mode is calibrated for the entire FOV).

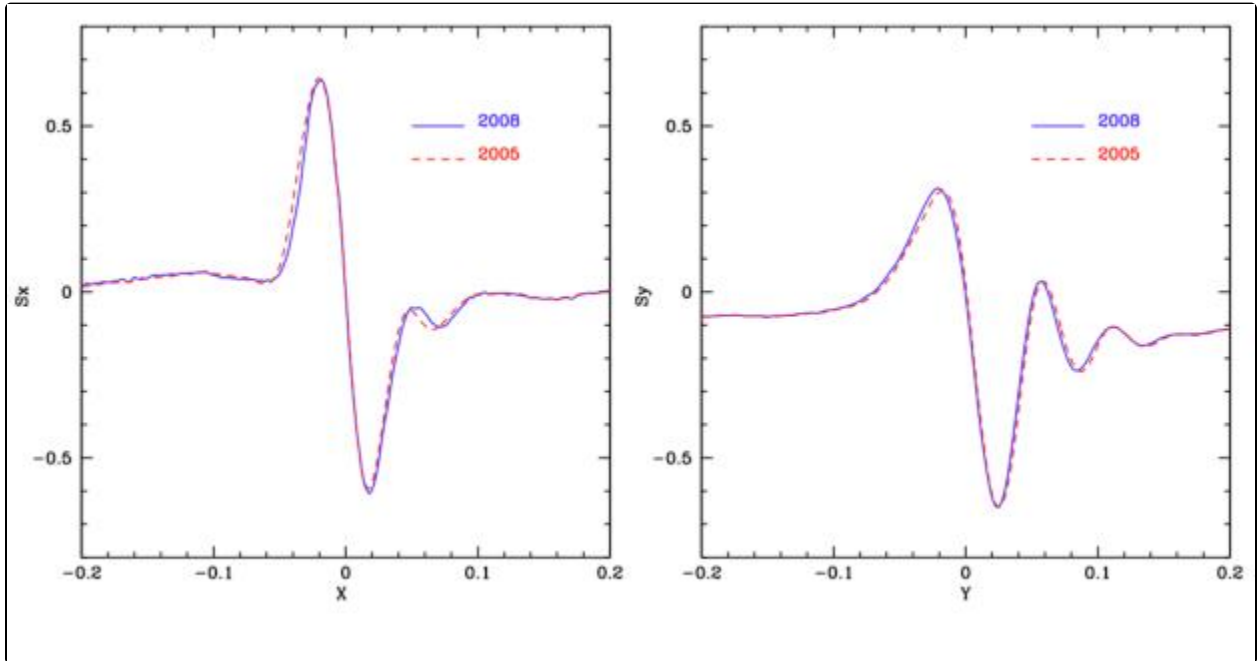
The FGS1r S-curves were seen to degrade over time between 1998 and 2005, particularly along the Y-axis, as shown in [Figure 2.7](#).

Figure 2.7: FGS1r S-curves



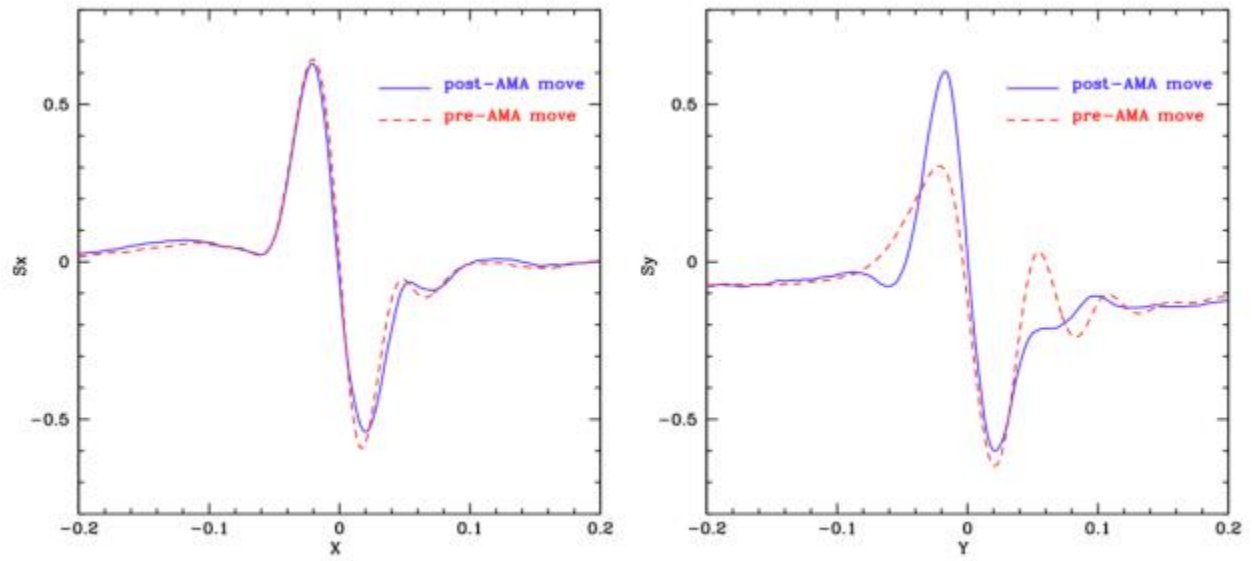
However, since 2005 the S-curves changes were insignificant, as shown in [Figure 2.8](#)

Figure 2.8:FGS1r S-curves 2005



Therefore, with the FGS1r demonstrating long term stability, the AMA was adjusted once again on January 22, 2009 to restore the instrument's S-curves at the center of its FOV. It is important to note that Transfer mode science observations obtained (before) after January 22, 2009 should use calibration data obtained (before) after that date for the scientific analysis of that data.

Figure 2.9: Shows the changes in the FGS1r S-curves resulting from the January 2009 AMA adjustment.



2.6 FGS Aperture and Filter

2.6.1 FOV and Detector Coordinates

2.6.2 Filters and Spectral Coverage

2.6.1 FOV and Detector Coordinates

Figure 1.2 shows the HST focal plane positions of the FGSs as projected onto the sky. Figure 2.10 is similar, but includes the addition of two sets of axes: the FGS detector coordinate axes, and the POSTARG coordinate axes (used in the Phase II proposal instructions to express target offsets).

⚠ The detector reference frame and the POS TARG reference frames differ from each other and from the Vehicle Coordinates V2,V3 (or U2,U3).

Each FGS FOV covers approximately 69 square arcmin, extending radially from 10 arcmin to 14 arcmin from the *HST*'s boresight and axially 83.3 degrees on the inner arc and 85 on its outer arc. The IFOV determined by the star selector assemblies and field stops is far smaller, covering only 5×5 arcsec. Its location within the pickle depends upon the Star Selector A and B rotation angles. To observe stars, the star selector assemblies must be rotated to bring the IFOV to the target. This procedure is called slewing the IFOV.

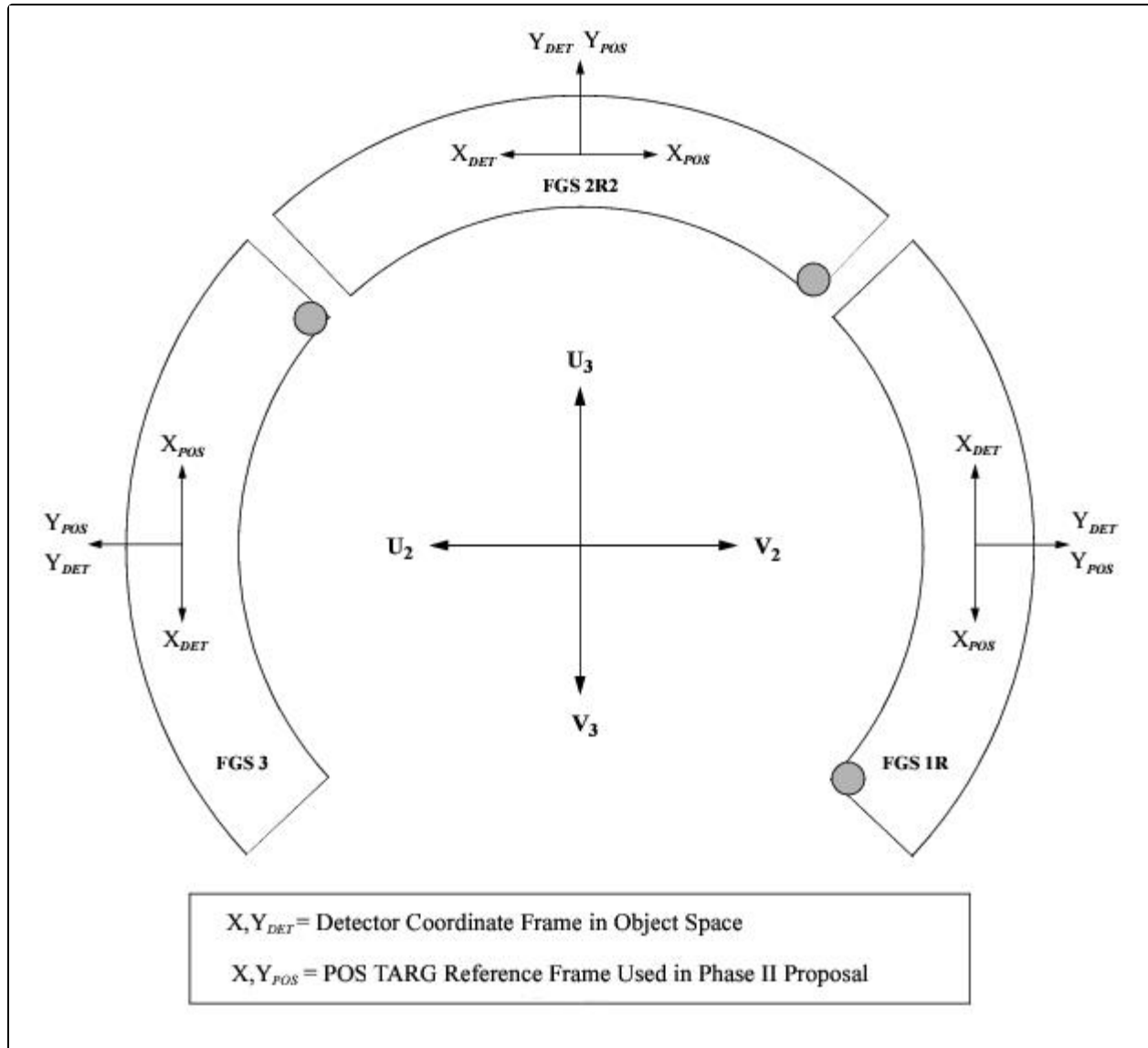
The (X,Y) location of the IFOV in the pickle is calculated from the Star Selector Encoder Angles using calibrated transformation coefficients. Each FGS has its own detector space coordinate system, the (X,Y)DET axes, as shown in Figure 2.10. FGS2 and FGS3 are nominally oriented at 90 and 180 degrees with respect to FGS1r, but small angular deviations are present (accounted for in flight software control and data reduction processing). The FGS detector reference frame is used throughout the pipeline processing. The POS TARG coordinate axes, $^{(X,Y)}_{POS}$, should be used to express offsets to target positions in the Phase II proposal (Special Requirements column). See 6.2.2 Target Orientation Visit-level Special Requirements.

The *approximate* U2,U3 coordinates for the aperture reference position (default placement of a target) for each FGS and the angle from the $+Y_{DET}$ and $+Y_{POS}$ Axis are given in Table 2.3. The angles are measured from $+U3$ to $+Y$ in the direction of $+U2$ (or counterclockwise in Figure 2.10). Note that the FGS internal detector coordinate reference frame and the POS TARG reference frame have opposite parities along their respective X-axes.

Table 2.3: Approximate Reference Positions of each FGS in the HST Focal Plane

Aperture	U2 (arcsec)	U3 (arcsec)	Angle (from +U3 axis)
FGS1r	-723	+10	~270
FGS2r2	0	+729	~0
FGS3	+726	+6	~90

Figure 2.10: FGS Proposal System and Detector Coordinate Frames



2.6.2 Filters and Spectral Coverage

Filter Bandpasses

The filter wheel preceding the dielectric beam splitter in each FGS contains five 42mm diameter slots. Four of these slots house filters—F550W, F583W, F605W and F5ND—while the fifth slot houses the PUPIL stop. This stop helps restore the S-Curve morphology throughout the FOV of each FGS by blocking out the outer 1/3 perimeter of the spherically aberrated primary mirror. The filter selection for each FGS, their central wavelengths, and widths are listed in [Table 2.4](#). The transmission curves (filters and PUPIL) are given in [Figure 2.11](#). The PMT efficiency is given in [Figure 2.12](#).

Figure 2.11: FGS1r Filter Transmission

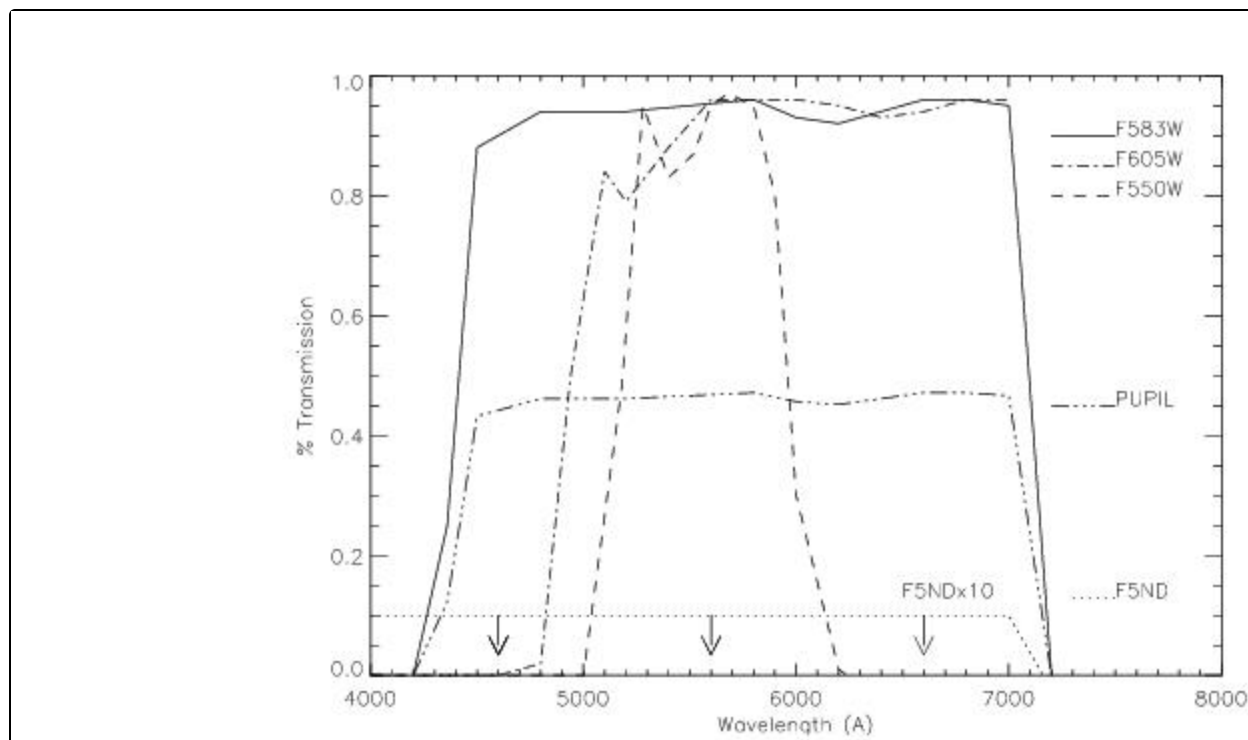
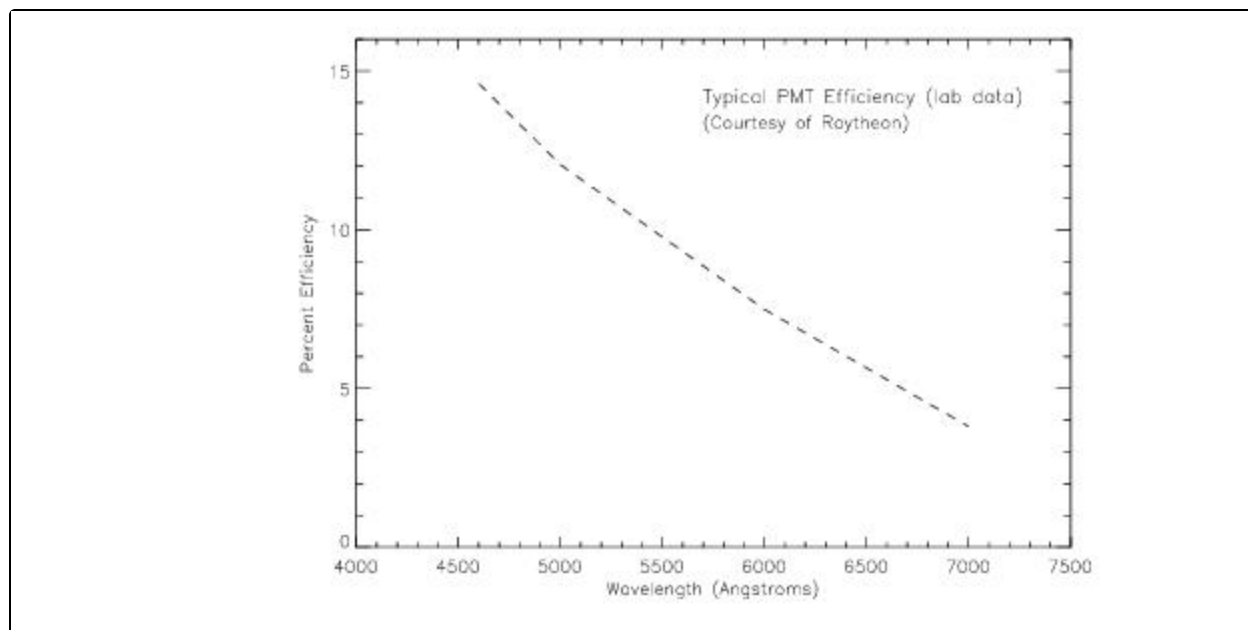


Table 2.4: Available Filters

Filter	Central Wavelength Å	Spectral Range Å	FWHM Å	FGS
F583W	5830	4600–7000	2340	1,1R,2,3
F605W	6050	4800–7000	1900	1,1R,2
PUPIL	5830	4600–7000	2340	1,1R,2,3
F550W	5500	5100–5875	750	1,1R,2,3
F650W	6500	6200–6900	750	3
F5ND	5830	4600–7000	2340	1,1R,2,3


Figure 2.12: PMT Efficiency



2.7 FGS Calibrations

For the most part, the calibration requirements of the current Cycle's GO science programs will be supported by STScI. For Position mode observations, this includes the optical field angle distortion (OFAD) calibration, cross-filter effects, lateral color effects, and the routine monitoring of the changes in distortion and scale across the FOV.

For Transfer mode, STScI will calibrate the interferograms (S-Curves) as a function of a star's spectral color. In addition, the S-Curves will be monitored for temporal stability.

 ***Only the center of the FGS1r FOV will be calibrated for Transfer mode observations.***

Chapter 3: FGS Science Guide

Chapter Contents

- [3.1 The Unique Capabilities of the FGS](#)
- [3.2 Position Mode Precision Astrometry](#)
- [3.3 Transfer Mode Binary Stars and Extended Objects](#)
- [3.4 Combining FGS Modes Determining Stellar Masses](#)
- [3.5 Angular Diameters](#)
- [3.6 Relative Photometry](#)
- [3.7 Moving Target Observations](#)
- [3.8 Summary of FGS Performance](#)
- [3.9 Special Topics Bibliography](#)

3.1 The Unique Capabilities of the FGS

As a science instrument the FGS offers unique capabilities not presently available by other means in space or on the ground. Its unique design and ability to sample large areas of the sky with milliarcsecond (mas) accuracy or better gives the FGS advantages over all current or planned interferometers.

The FGS has two observing modes, Position and Transfer mode. In Position mode the FGS measures the relative positions of luminous objects within its Field of View (FOV) with a per-observation accuracy of ~ 1 mas for targets with $3.0 < V < 16.8$. Multi-epoch programs can achieve relative astrometric measurements with accuracies approaching to 0.2 mas.

In Transfer mode the FGS is used as a high angular resolution observer, able to detect structure on scales as small as 8 mas. It can measure the separation (with ~ 1 mas accuracy), position angle, and the relative brightness of the components of a binary system down to ~ 10 mas for cases where $\Delta V < 1.5$. For systems with a component magnitude difference of $2.0 < \Delta m < 4.0$, the resolution is limited to 20 mas.

By using a “combined mode” observing strategy, employing both Position mode (for parallax, proper motion, and reflex motion) and Transfer mode (for determination of a binary’s visual orbit and relative brightnesses of the components), it is possible to derive the total and fractional masses of a binary system, and thus the mass-luminosity relationship for the components.

Alternatively, if a double lined spectroscopic system is resolvable by the FGS, then the combination of radial velocity data with Transfer mode observations can yield the system’s parallax and therefore the physical size of the orbit, along with the absolute mass and luminosity of each component.

In this chapter, we offer a brief discussion of some of the science topics most conducive to investigation with the FGS.

3.2 Position Mode Precision Astrometry

A Position mode visit consists of sequentially measuring the positions of stars in the FGS FOV while maintaining a fixed HST pointing. This is accomplished by slewing the FGS Instantaneous Field of View (IFOV, see [Figure 1.3](#)) from star to star in the reference field, acquiring each in FineLock (fringe tracking) for a short time (2 to 100 sec.). This yields the relative positions of the observed stars to a precision of ~ 1 milli-arcsecond (mas).

With only three epochs of observations at times of maximum parallax factor (a total of six HST orbits), the FGS can measure an object's relative parallax and proper motion with an accuracy of about 0.5 mas. Several multi-epoch observing programs have resulted in measurements accurate to ~ 0.2 mas. Unlike techniques which rely upon photometric centroids, the accuracy of FGS measurements are not degraded when observing variable stars or binary systems. And techniques which must accumulate data over several parallactic epochs would have greater difficulty detecting comparably high frequency reflex motions (if present).

3.3 Transfer Mode Binary Stars and Extended Objects

3.3.1 Observing Binaries: The FGS vs. HST's Cameras

3.3.2 Transfer Mode Performance

In Transfer mode, the FGS scans its IFOV across a target to generate a time-tagged (40 Hz) mapping between the position of the IFOV (in both X and Y) and counts in the four PMTs. These data are used to construct the interferogram, or transfer function, of the target via the relation

$$S_x = (A_x - B_x) / (A_x + B_x)$$

as described in [Chapter 2](#). The data from multiple scans are cross correlated and co-added to obtain a high SNR transfer function.

In essence, Transfer mode observing is conceptually equivalent to sampling an object's PSF with milliarcsecond pixels. This enables the FGS to resolve structure on scales finer than *HST*'s diffraction limit, making it ideal for studying close binary systems and/or extended objects.

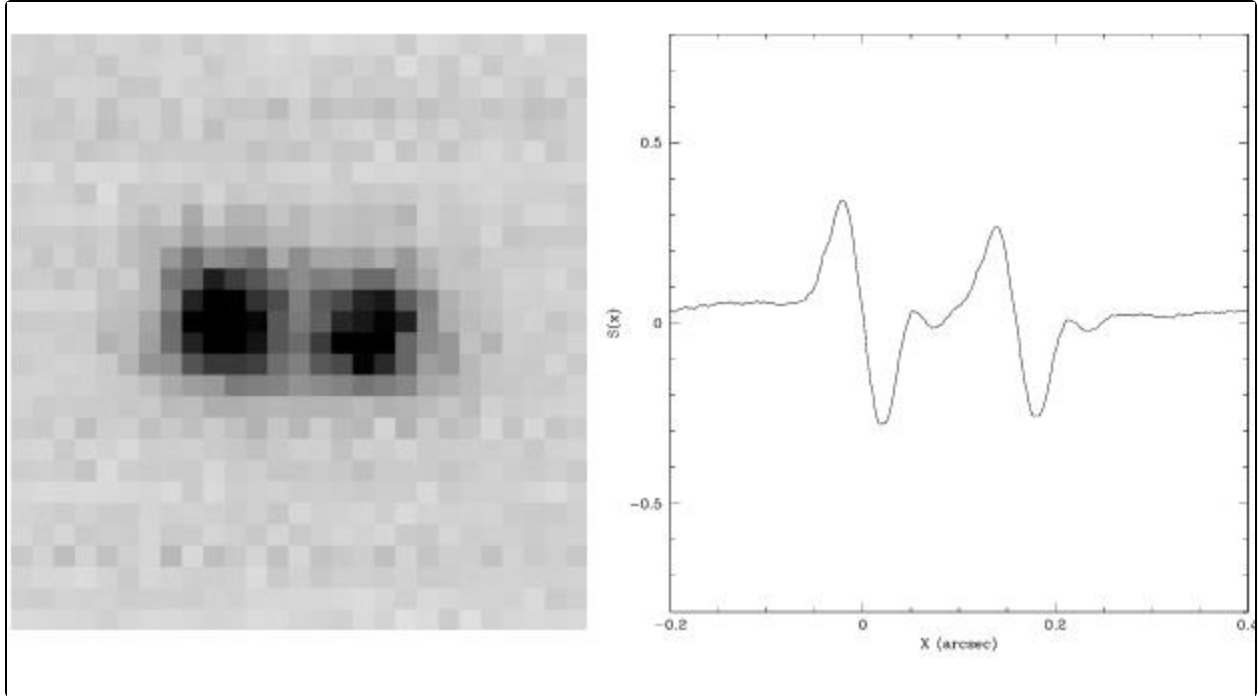
The transfer function of a multiple star system is a normalized linear superposition of the S-Curves of the individual stars, with each S-curve scaled and shifted by the relative brightness and angular separation of the components. If the components are widely separated ($> \sim 60$ mas), two S-Curves are clearly observed in the transfer function, as illustrated in the left panel of [Figure 3.1](#). Smaller separations result in merged S-Curves with modulation and morphology differing significantly from that of a single star. [Figure 4.3](#) illustrates these points.

By using point source S-curves from the calibration library one can deconvolve the composite observed transfer function of a binary star into component S-Curves (done by either Fourier Transforms or semi-automated model fitting) to determine the separation, position angle, and relative brightness of the components. If enough epochs of data are available, the time-tagged position angles and angular separations can be used to construct the apparent relative orbit, from which one can derive the parameters P , a , i , ω and Ω which define the true relative orbit. Note that the semi-major axis is an angular quantity; to convert it to a physical length, one must know the object's distance (which can be obtained from parallax measurements).

3.3.1 Observing Binaries: The FGS vs. HST's Cameras

The FGS, while capable of very-high angular resolution observations, is not an "imaging" instrument like *HST*'s cameras. However, the ability to sample the S-curve with milli-arcsecond resolution allows the FGS to resolve structure on scales too fine for the cameras. To illustrate, we present a comparison between binary observations with *HST*'s Planetary Camera (PC) and with FGS1r in [Figure 3.1](#). The image at left is a PC snapshot image of the Wolf-Rayet + OB binary WR 146 (Niemela et al. 1998). To the right is a simulated FGS1r "image" of this binary shown at the same scale. With the 0.042" pixels of the PC, the binary pair is clearly resolved. Based on point-spread function (PSF) photometry, Niemela et al. publish a separation of 168^{+31} mas for this pair. In comparison, an analysis of the FGS "observation" of the binary yields a separation of 168^{+1} mas, a far more accurate result.

Figure 3.1: Comparison: PC Observation v. FGS Observation

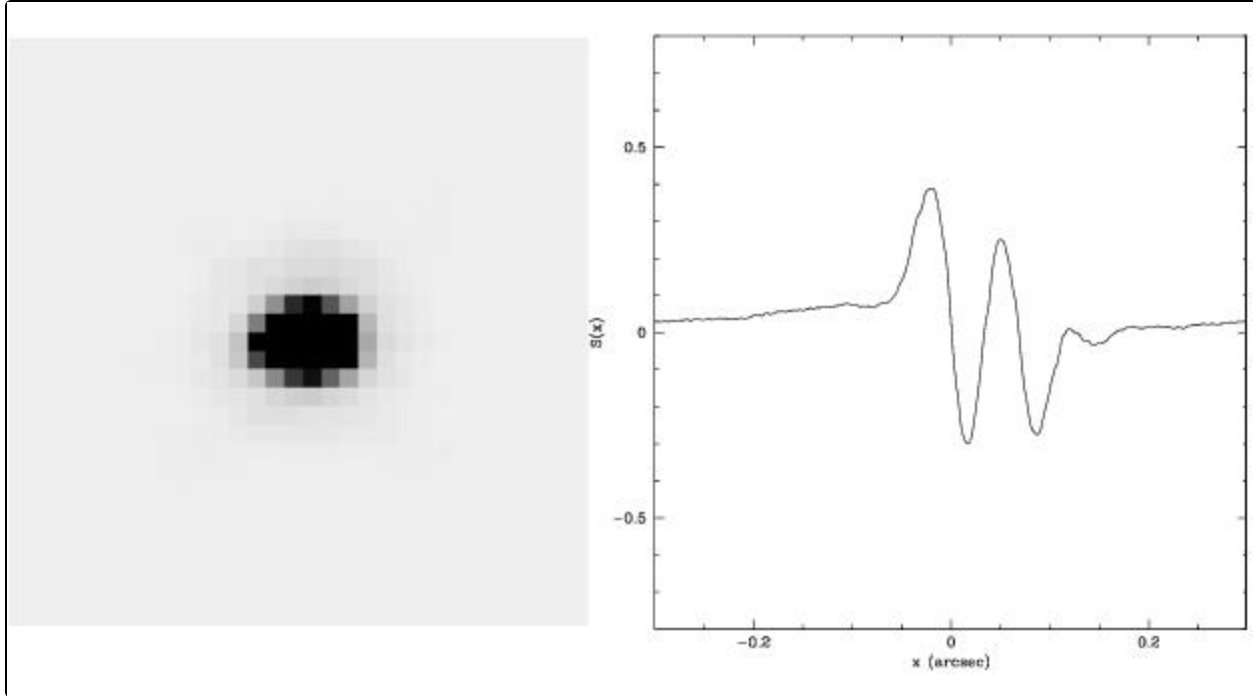


The figure on the left is from an observation by Niemela et al. (1998) of the WR+OB binary WR 146. They measure an angular separation of 168^{+31} mas. The figure on the right is a simulation of an FGS1r observation of the same object. The separation of the stars could be measured to better than 1 mas.

Though a vigorous WFC3 (ACS/HRC would be a more capable contender, but it is unfortunately no longer available) observing strategy involving multiple exposures and image recombination techniques (i.e., “drizzling”) might improve the resolution of the binary, the accuracy of the measured separation would not match that achievable with the FGS. Most importantly, the FGS can *just as easily detect the components and accurately measure their separations for binaries as close as 12 mas*, a feat not possible with *HST*’s cameras regardless of the observing strategy, (for example refer to Nelan et al., 2004 AJ 128, Nelan, 2667 AJ 134).

In [Figure 3.2](#), we show a TinyTIM simulation of a PC image (as a stand-in for WFC3) of a 70 mas binary and an FGS observation of the same simulated pair. Note the PC image suggests—by its shape—that the observed binary is not a point source. However, it would be difficult to determine an accurate component separation or brightness ratio from this image. This is not a problem for the FGS, where both components are easily resolved, and an accurate separation and mass ratio can be determined.

Figure 3.2: Simulated PC Observations v. FGS Observations of a 70mas Binary



The figure on the left is a TinyTIM simulation of a PC image of a 70 mas binary composed of stars of nearly equal brightness (no dithering). The figure to the right is an FGS simulation of the same observation. Note that the binary structure is far more obvious in the FGS fringes. The FGS can just as easily resolve binary systems down to 12 mas.

3.3.2 Transfer Mode Performance

The most relevant way to express the FGS Transfer mode performance is through its ability to detect and to resolve components of a multiple component system. [Figure 3.3](#) is a plot of the *predicted* parameter space defined by the separation in milli-arcseconds and the relative brightness of the components of a binary system. The shaded areas are the domains of success in resolving binary systems for both FGS3 and FGS1r. The extension of FGS1r into the smaller separation parameter space is attributed to an optimized S-Curve achieved by proper adjustment of the articulating mirror assembly (see [Chapter 2](#) for more details), and to the fact that its fringes are highly stable in time. (FGS3, by comparison, suffers a persistent random variability of its x-axis fringe which precludes it from reliably studying binary systems with separations less than about 20 mas.) These data originate from simulations and are supported by a special assessment test run aboard the spacecraft in May 1998 as well as GO science data (see [Appendix B](#) for more details).

Figure 3.3: Comparison of FGS1r and FGS3 Transfer Mode Performance

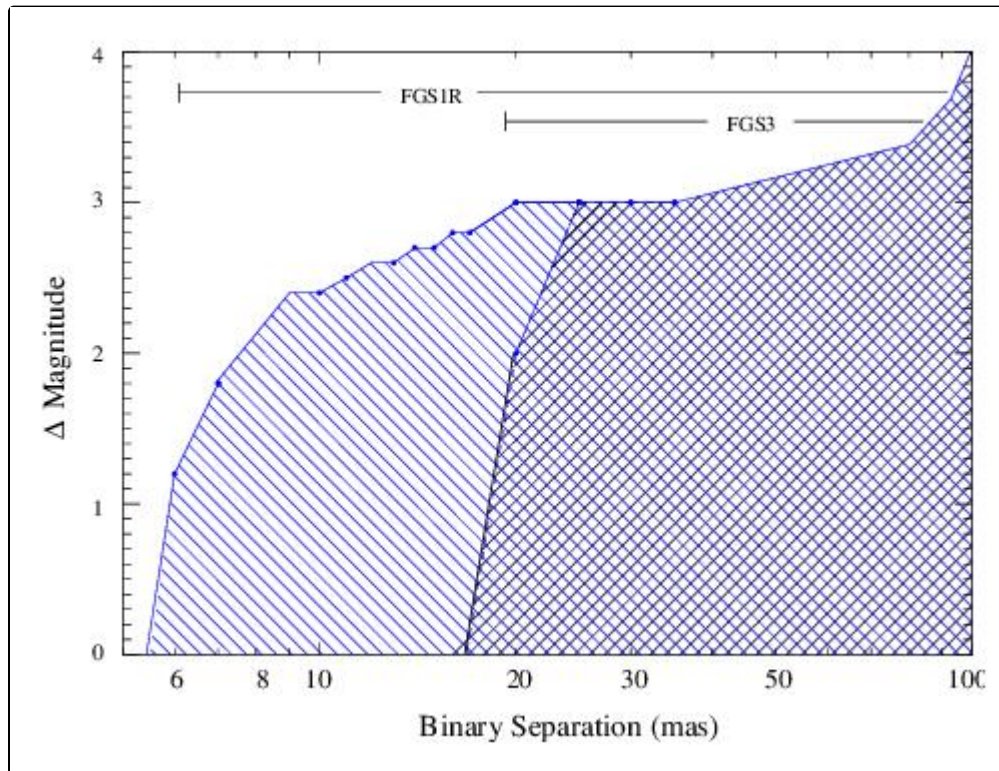


Table 3.1 contains the expected resolution limits for FGS1r. Columns 1 and 2 show the separation and accuracy for a single measurement, column 3 details the relative brightness limit needed to achieve that precision, and the last column is the apparent magnitude of the system. For example, a separation of 10 mas is detectable if the system is ~14 magnitudes or brighter and the magnitude difference of the components (Δm) is less than 1.0. Likewise, the separation of the components of a $V=16.6$ binary is measurable to an accuracy of about 2 mas if their separation is greater than ~15 mas and their magnitudes differ by less than 2.

Table 3.1: FGS1r TRANSFER Mode Performance: Binary Star

Minimum Separation (mas)	Estimated Accuracy (mas)	Maximum Δ Mag	Maximum V
7 ¹	-	1.0	14.0
10a	-	1.0	15.0
15	2	2.0	16.6
20	1	2.5	16.2
20	2	3.0	16.2
50	1	3.5	15.5

¹ This represents detection of non-singularity under ideal conditions. Reliable measurements of the angular separation might not be achievable.

3.4 Combining FGS Modes Determining Stellar Masses

Stellar mass determination is essential for many astronomical studies: star formation, stellar evolution, calibrating the mass/luminosity function, determining the incidence of stellar duplicity, and the identification of the low-mass end of the main sequence, for example.

The *combination* of Position mode *and* Transfer mode observations is an effective means to derive a full orbital solution of a binary system. Wide-angle astrometry from a multi-epoch Position mode program can be used to measure the parallax, proper motion and reflex motion of a binary system. High angular resolution Transfer mode observations can be used to determine the relative orbit and differential photometry of the components. [Figure 3.4](#) illustrates the benefit of this technique as applied to the low mass binary system Wolf 1062 (Benedict et al. 2001). The small inner orbit of the primary star was determined from Position mode measurements of the primary's position relative to reference field stars. The large orbit of the secondary low mass companion was derived from Transfer mode observations of the binary, which at each epoch yields the system separation and position angle. Combining these data allows one to locate the system barycenter and thereby compute the relative mass of each component. And with the parallax known (from the Position mode data), the total system mass, and hence the mass of each component, can be determined.

Figure 3.4: Relative Orbit of the Low-Mass Binary System Wolf 1062 AB

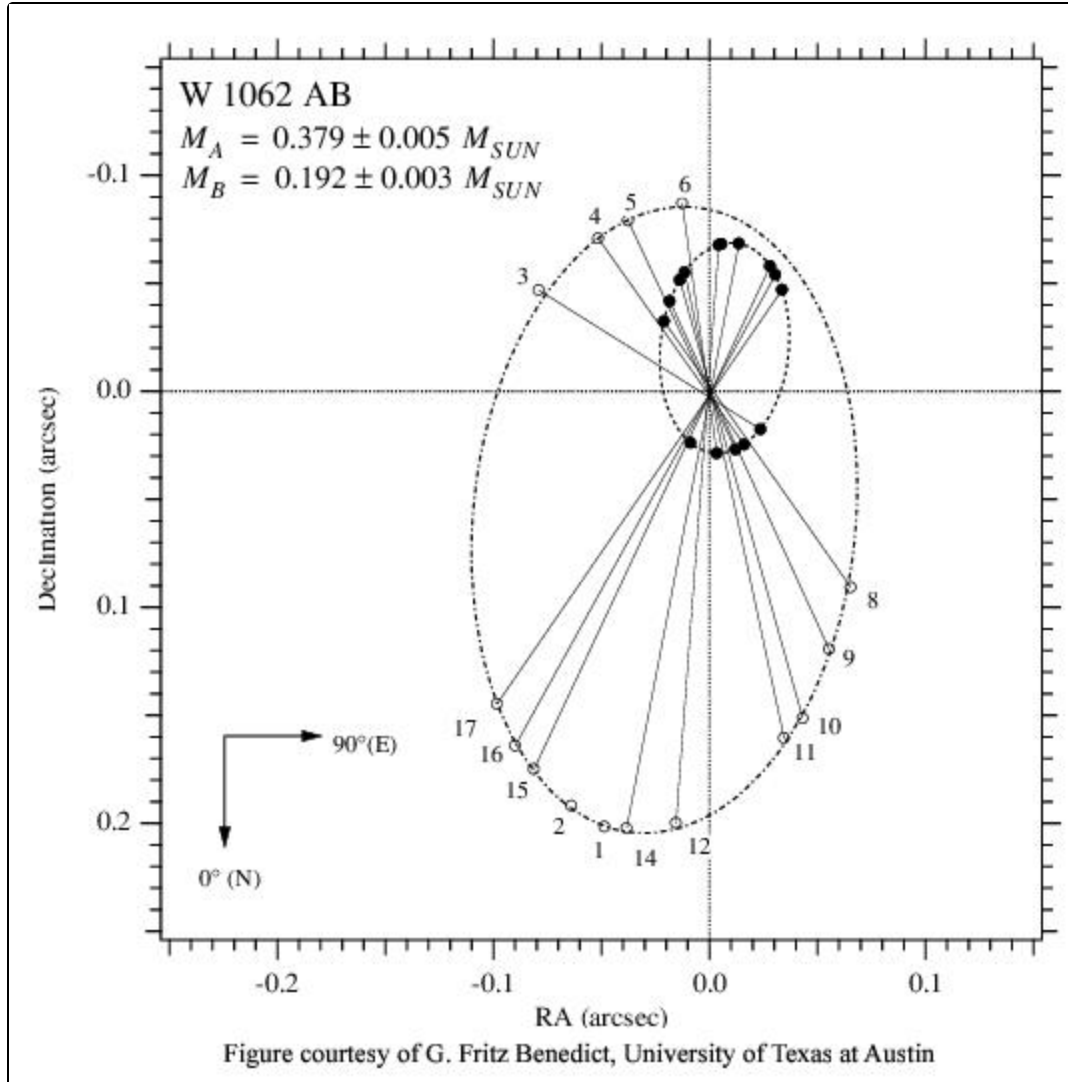
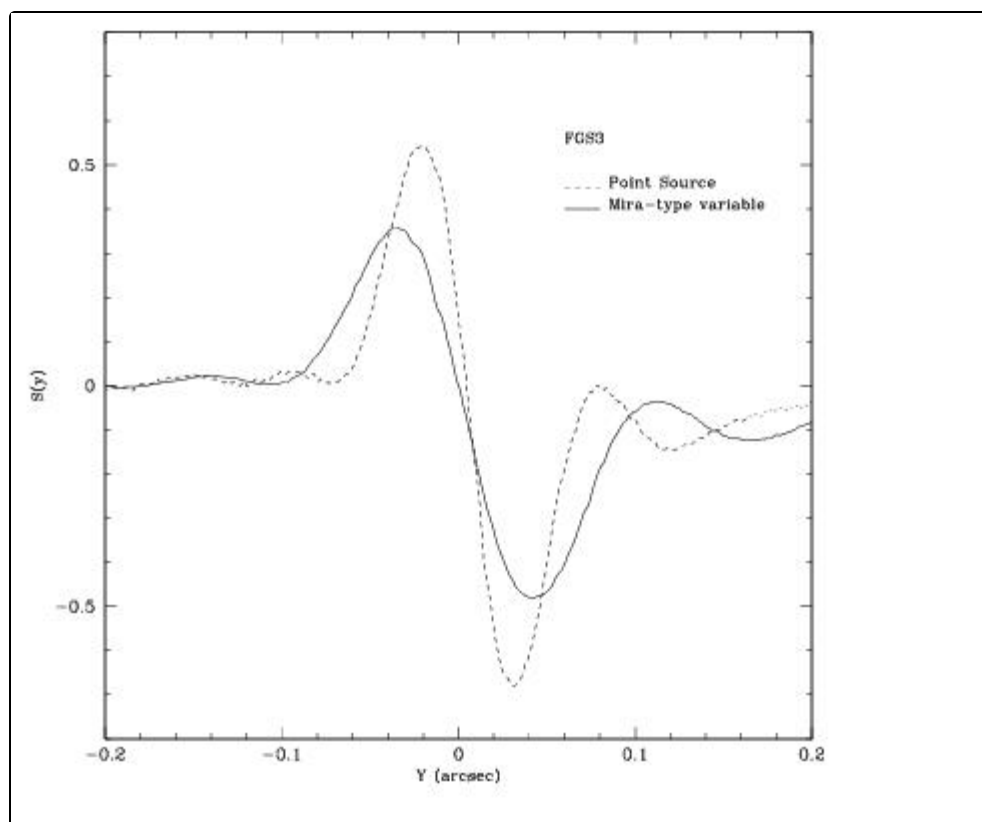


Figure 3.4 shows the orbits of the components of Wolf 1062 about the system's barycenter. This has been determined from both Transfer mode observations, which yield the relative orbit, and Position mode observations, which map the orbit of the primary relative to reference stars distributed about the FGS FOV (in effect establishing the inertial reference frame). Note that the Position mode data also yield the system's parallax and proper motion.

3.5 Angular Diameters

The FGS has been used (Lattanzi et al. 1997) to determine the angular diameters of non-point sources. The example given in [Figure 3.5](#) shows the Transfer Function of a Mira-type variable superposed on the S-Curve of a point source (both observed with FGS3). The extended source - a disk of 78 ± 2 mas - is clearly distinguishable from a point source. In addition to stellar discs, other objects which might be (or have been) resolved by the FGS include galactic nuclei, asteroids, and planetary moons.

Figure 3.5: Mira-type variable with a resolved circumstellar disk



3.6 Relative Photometry

While observing in Position mode, FGS3 serendipitously observed the outburst of a flare on the nearby star Proxima Centauri ([Figure 3.6](#), see Benedict et al. 1998). The FGS has also been used to measure the relative flux of a star during an occultation of that star by the Neptunian moon Triton ([Figure 3.7](#)), and the data were subsequently used to examine the thermal structure of Triton's atmosphere (see Elliot et al. 1998 and Elliot et al. 2000).

The absolute FGS photometric response of FGS 3 has been stable at the 2% level over the past eight years (L. Reed, BFGoodrich). FGS1r is expected to be as stable or better. For relative photometry on time scales of orbits, the FGS has been shown to be stable at the 1 milli-magnitude level, thus affording an opportunity for 0.1–0.2% time series photometry.

Figure 3.6: Flare Outburst of Proxima Centauri as Observed with FGS3

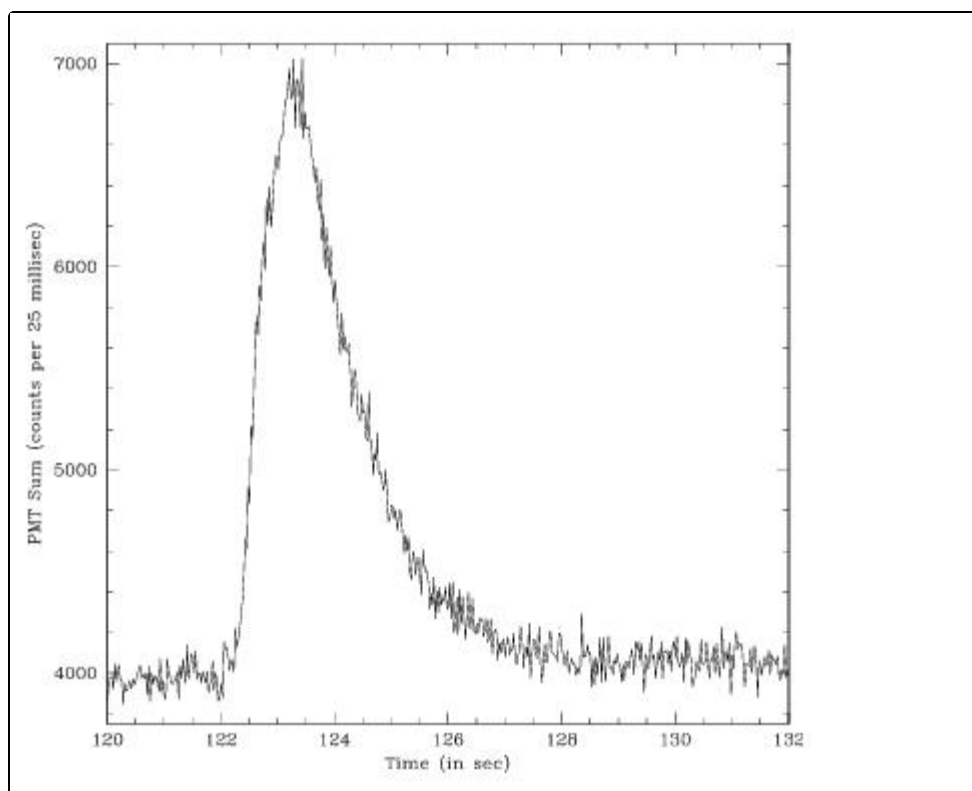
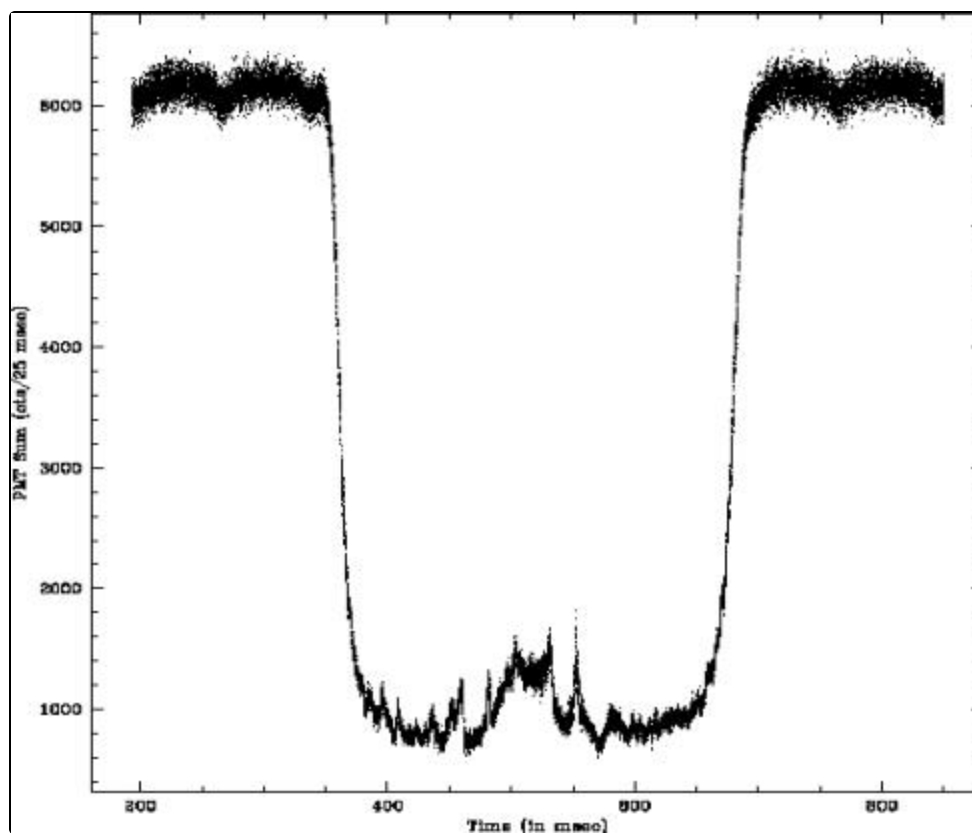


Figure 3.7: Triton Occultation of the Star TR180 as Observed by FGS 3



3.7 Moving Target Observations

The FGS is suitable for the observation of solar system objects in both Position and Transfer modes. The technique to acquire the data is not as straightforward as standard *HST* moving target observations, but in cases where the target is not moving too rapidly, the observation is certainly feasible. We note that the FGS has been used in previous Cycles to observe Main Belt asteroids, both in Position mode and in Transfer mode. More detail on moving target observations can be found in [Chapter 4](#).

3.8 Summary of FGS Performance

In Position mode, the FGS offers capabilities not achievable by other HST instrument or by the current generation of ground-based interferometers. These capabilities include:

- a large field of view (69 arcmin^2).
- large dynamic range.
- a *per-observation* precision of $\sim 1 \text{ mas}$ for $V < 16.8$.
- multi-epoch astrometry accurate to $\sim 0.2 \text{ mas}$.

Similarly, the FGS Transfer mode offers:

- 7 to 10 mas resolution down to $V = 14.5$, with wider separations observable to $V = 16.8$.
- the ability to determine relative separation and position angle of a binary system's components, and hence the apparent relative orbit of the system.

Additionally, mixed-mode observations - employing both Position mode and Transfer mode - allow the user to combine parallax, proper motion, and relative orbit information to derive the true orbit of a multiple-star system and a determination of stellar masses.

The FGS's two observing modes make it possible for the instrument to resolve structure in objects too faint for other interferometers and on scales too small for any imaging device, while simultaneously measuring the distance to that object. It is anticipated the FGS will be the sole occupant of this niche until the arrival of the long baseline interferometer in space, such as the Space Interferometry Mission (SIM), expected to launch in 2009.

3.9 Special Topics Bibliography

- [3.9.1 STScI General Publications](#)
- [3.9.2 Position Mode Observations](#)
- [3.9.3 Transfer Mode Observations](#)
- [3.9.4 Miscellaneous Observations](#)
- [3.9.5 Web Resources](#)

3.9.1 STScI General Publications

- [Hubble Space Telescope Phase II Proposal Instructions](#),
- [HST Data Handbook](#).

3.9.2 Position Mode Observations

- Benedict, G. F. et al., "Interferometric Astrometry of the Detached White Dwarf - M Dwarf Binary Feige 24 Using HST Fine Guidance Sensor 3: White Dwarf Radius and Component Mass Estimates", 2000, *AJ*, 119, 2382.
- McArthur, B. E. et al., "Astrometry with Hubble Space Telescope Fine Guidance Sensor 3: The Parallax of the Cataclysmic Variable RW Triangulum", 1999, *ApJ*, 520, L59.
- Harrison, Thomas E. et al., "Hubble Space Telescope Fine Guidance Sensor Astrometric Parallaxes for Three Dwarf Novae: SS Aurigae, SS Cygni, and U Geminorum", 1999, *ApJ*, 515, L93.

3.9.3 Transfer Mode Observations

- Benedict, G.F. et al., "Precise Masses for Wolf 1062 AB from Hubble Space Telescope Interferometric Astrometry and McDonald Observatory Radial Velocities", 2001, *AJ*, 121.1607.
- Henry, T. J. et al., "The Luminosity Relation at the End of the Main Sequence (0.08 - 0.20 M_{solar})", 1999, *ApJ*, 512, 864.
- Gies, D. R. et al., "The O-type Binary 15 Monocerotis Nears Periastron," 1997, *ApJ*, 475, L49.
- Lattanzi, M.G., et al., "Interferometric Angular Diameters of Mira Variables with the Hubble Space Telescope", 1997, *ApJ*, 485, 328.
- Nelan, E.P., "Resolving LB11146 with HST's Fine Guidance Sensor 2007, *AJ* 134, 193N.
- Nelan, E.P. "Resolving DB Stars in the Carina Nebula with HST's Fine Guidance Sensor, 2004, *AJ* 128, 323N.
- Simon, M., S.T. Holfeltz, and L.G. Taff, "Measurement of T Tauri Binaries Using the Hubble Space Telescope Fine Guidance Sensors", 1996, *ApJ*, 469, 980.

3.9.4 Miscellaneous Observations

- Elliot, J. L. et al., "Global Warming on Triton," *Nature*, 393, 765, 1998.

3.9.5 Web Resources

Many additional documents, including Instrument Science Reports and ST Analysis Newsletters are available through the FGS Web page:

<http://www.stsci.edu/hst/instrumentation/fgs>

Chapter 4: Observing with the FGS

Chapter Contents

- [4.1 Position Mode Overview](#)
- [4.2 Planning Position Mode Observations](#)
- [4.3 Position Mode Observing Strategies](#)
- [4.4 Transfer Mode Overview](#)
- [4.5 Planning a Transfer Mode Observation](#)
- [4.6 Transfer Mode Observing Strategies](#)

4.1 Position Mode Overview

4.1.1 The Position Mode Visit

4.1.2 The Position Mode Exposure

4.1.1 The Position Mode Visit

A Position mode visit yields measurements of the location of objects in the FGS's total field of view (FOV), and hence their relative angular positions. The objects are observed sequentially according to the sequence of exposure lines in the proposal. The target list of a typical Position mode visit consists of the science object(s) and reference stars used to define the local reference frame. A subset of the targets, referred to as check stars, should be observed several times during the course of the visit to track any spurious motion of the FGS's FOV on the plane of the sky (e.g., thermally induced drift or OTA focus changes). The changes in the positions of the check stars are used to model the drift as a function of time so that its contaminating effect can be eliminated from the astrometry.

An FGS astrometry visit begins when the HST computer - the 486 - commands the Star Selector Servos to place the IFOV at the predicted location of the first star specified in the visit (as per Phase II proposal). Control is transferred to the Fine Guidance Electronics (FGE) microprocessor, which commands the FGS to acquire and track the target (Search, CoarseTrack, and FineLock). Later, at a specific spacecraft clock time, after the exposure time + overhead has expired, the 486 resumes control of the FGS, terminates the FineLock tracking of the object and slews the IFOV to the expected location of the next star in the sequence. This process repeats until the FGS has completed all exposures in the visit. The spacecraft's pointing is held fixed on the sky under the control of the guiding FGSs for the entire visit unless otherwise instructed by the Phase II proposal. The status flags, photometry and instantaneous location of the IFOV is recorded every 25 msec (40 Hz).

4.1.2 The Position Mode Exposure

During a Position mode exposure the object is tracked in FineLock (see [Appendix A: Target Acquisition and Tracking](#)). After the target is acquired by the Search and CoarseTrack procedures, FineLock begins with a WalkDown, a series of steps of the IFOV toward the CoarseTrack photocenter. At each step, the IFOV is held fixed for a period defined by FESTIME (Fine Error Signal averaging time) while the PMT data are integrated to compute the Fine Error Signal (FES, the instantaneous value of the S-Curve) on each axis. Once the FES on both axes have exceeded a pre-set threshold, FineLock tracking begins. The star selectors are continuously adjusted after every FESTIME to re-position the IFOV in an attempt to zero out the FES during the next integration period. The objective is to present the Koesters prism a wavefront with zero tilt.

The defining parameters of an exposure are the target magnitude, the filter, the FESTIME and the exposure time. These topics are discussed in the following sections.

4.2 Planning Position Mode Observations

- 4.2.1 Target Selection Criteria
- 4.2.2 Filters
- 4.2.3 Background
- 4.2.4 Position Mode Exposure Time Calculations
- 4.2.5 Exposure Strategies for Special Cases
- 4.2.6 Sources Against a Bright Background
- 4.2.7 Crowded Field Sources

4.2.1 Target Selection Criteria

When targets are selected for FGS Position mode observations, several options and requirements should be considered. These options are described below.

Brightness

The bright limit for FGS1r is $V = 8.0$ without the neutral density filter in place. With the F5ND filter, objects of $V = 3.0$ or fainter can be observed. The faint limit is $V \sim 17.0$.

Near Neighbors

FGS target acquisition in Position mode will be unreliable if the target has a neighbor of comparable or greater brightness within a radius of 10 arcseconds. In essence, the FGS's IFOV—a $5'' \times 5''$ box—expects to encounter the target star within the search radius. Companions of similar brightness within this search radius may be mistakenly acquired instead of the target. However, for magnitude differences $\Delta m > 1$, companions within $\sim 6''$ will not affect the acquisition of the brighter target. Note that binary stars with component separations less than about $0.5''$ can be successfully acquired in Position mode, regardless of the Δm . Refer to the discussion under [Section 4.2.5](#) for further details regarding the acquisition of binary systems in Position mode.

Target Field

The target field consists of the science target and reference stars. Observations of the reference stars will be used to define the local reference frame for relative astrometry. Since the optical field angle distortions are calibrated most accurately in the central region of the FOV, the pointing of the spacecraft (via POS_TARG commands—[Chapter 6](#) for more details) should be specified to place the target field (as much as possible) in this area.

If the visit also includes Transfer mode observations of an object, the spacecraft pointing should be chosen to place the object at the FOV center, as this is the only location calibrated for Transfer mode. If the target field geometry requires the Transfer mode observations be executed at other locations in the FOV, special calibrations will be needed. Proposers should consult STScI's Help Desk for assistance.

Reference Stars

Ideally, reference stars should have the following characteristics:

- Have magnitudes in the range $8 < V < 15$ to avoid the need for an F5ND cross-filter calibration and to minimize exposure times.
- Be geometrically distributed around the target.
- Have at least 10 arcsec distance between one another and from the science target to avoid acquisition of the wrong object.
- Should fall within the FOV for all HST orientations specified in the proposal.

Check Stars

Check stars, which are a subset of the target list, are observed several times over the course of an orbit (visit). Two or more check stars, distributed across the field, provide the information needed to characterize the drift of the FGS's FOV on the sky (which is typically about 4 mas over the course of the visit). Each check star should be observed at least three times. The best check stars are brighter than 14th magnitude to minimize exposure time, and should include the science object for the highest accuracy astrometry.

4.2.2 Filters

Table 4.1 is a listing of the FGS1r filters, their calibration status and applicable brightness restrictions. (Refer back to Figure 2.11 for the filter transmissions as a function of wavelength.)

Table 4.1: Filters for which FGS1r will be Calibrated

Filter	Calibration Status	Comments	Target Brightness Restrictions
F583W	Full	“Clear” filter; OFAD calibration filter; Position Mode Stability Monitor	
F5ND	Limited	Pos Mode Cross Filter calibration with F583W; limited to selected locations within the FOV.	Required for targets w/ $3.0 < V < 8.0$;
PUPIL	No	Not calibrated	$V > 7.5$
F605W	No	Not calibrated	$V > 8.0$
F550W	No	Not calibrated	$V > 7.5$



Only the F583W filter will be calibrated for Position mode for the full FGS FOV. Filter F5ND will be calibrated only at selected locations within the FOV

PUPIL Not Recommended for Position Mode

Occupying the fifth slot on the wheel is the PUPIL. It is not a filter but rather a 2/3 pupil stop. Use of the PUPIL significantly reduces the degrading effect of spherical aberration (which does not necessarily improve Position mode performance) but collaterally alters the field dependence of the distortions. Consequently, the OFAD calibration for the F583W filter cannot be applied to PUPIL observations. In addition, PUPIL observing attenuates the object's apparent brightness by nearly a full magnitude, which sets the faint limiting magnitude at about $V=16$ while making observations of stars fainter than $V = 14.5$ excessively time consuming.

FESTIME and Signal-to-Noise

Photon statistics dominates the noise in the measured position of stars fainter than $V \sim 13.0$. To track fainter objects, the Fine Error Signal must be integrated for longer periods. [Table 4.1](#) lists the default FESTIMES for various target magnitudes. The default FESTIMES, determined from the Phase II target magnitude, are appropriate for most observations, and are set to ensure that photon noise, when converted into the Noise Equivalent Angle (NEA), does not exceed a predefined angular error threshold. The NEA is given by the relation

$$\text{NEA} = \left(\frac{1}{1.51 \times 10^7} \right) \times \frac{\sqrt{0.5 \times C + B}}{0.5 \times C \times \sqrt{t}} .$$

The NEA is used by the proposal processing tool (APT) to set the default FESTIME time. The parameter C is the total count rate expected from the target summed over all four PMTs, B is the background count rate, and t is the FESTIME. The NEA is plotted as a function of magnitude and FESTIME in [Figure 4.1](#). C as a function of filter and magnitude for FGS1r is given by:

$$C = 20776 \times f\text{-factor} \times 10^{-0.4(V-13)} .$$

The constant $f\text{-factor}$ is a function of the filter and the target's spectral color. [Table 4.3](#) provides the $f\text{-factor}$ for each combination of filter and color. The default FES times used by the proposal processing software for Position mode measurements are listed in [Table 4.1](#).

Table 4.2: Default FES Times

V Magnitude	FESTIME (seconds)
8-12	0.025
13	0.050
14	0.1
15	0.4
16	1.6
17	3.2

Figure 4.1: Default FESTIME as a Function of V Magnitude for F583W FGS1r: NEA as a Function of Magnitude and FESTIME

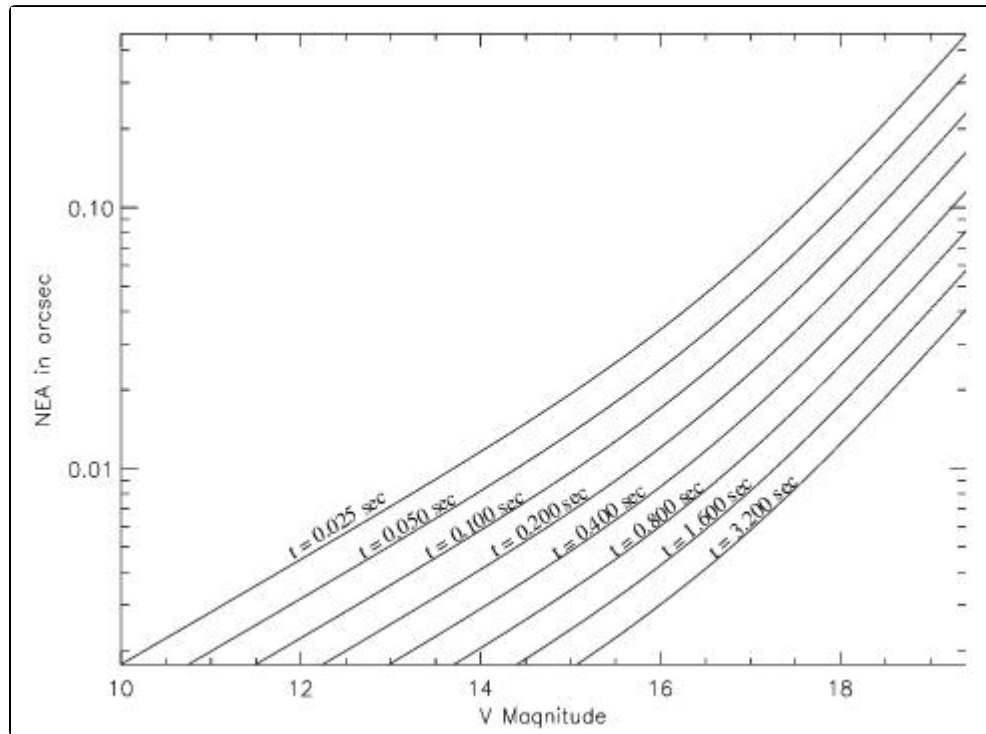


Table 4.3: F-factor Transmission Estimator for Combination of Filter and Color

Filter	B-V			
	+1.78	+0.60	+0.040	−0.24
	F583W	1.000	1.000	1.000
PUPIL	0.491	0.491	0.491	0.491
F5ND	0.010	0.010	0.010	0.010
F550W	0.356	0.354	0.331	0.331
F605W	0.860	0.700	0.624	0.575

4.2.3 Background

Background noise includes cosmic ray events, particle bombardment during passages through the South Atlantic Anomaly (SAA), and scattered light falling in the $5 \times 5''$ IFOV. Cosmic ray events are suppressed by special circuitry and the FGS is prohibited from operating while transiting regions of heaviest impact from the SAA. [Table 4.4](#) gives the typical dark + background counts for FGS1r in 0.025 seconds. Typically these values appear to be valid for all observations of isolated targets (suggesting that the dark counts dominate the background contribution). If the background counts for a specific observation are needed for the analysis of the observation, such as when the source is embedded in significant nebulosity or in a crowded star field, it can be obtained from the photometry gathered during the slew of the IFOV to (or away from) the target position. These data extracted by

the FGS pipeline package CALFGSA from the FITS files that input are cleaned of spikes from “interloping stars” and can be used to estimate the background levels during post-observation data reduction.

Table 4.4 lists the average dark+background counts/25 msec for each of the FGS1r PMTs. These data were serendipitously gathered over a 45 minute interval from a failed science observation (the target was not acquired due to a guide star problem). These data have proved invaluable for the analysis of Transfer mode observation of faint stars ($V>15$).

Table 4.4: FGS1r: Dark Counts

FGS1r PMT	Average Background + Dark Counts per 0.025 sec
Ax	3.623
Ay	1.566
Bx	3.658
By	5.893

4.2.4 Position Mode Exposure Time Calculations

The exposure time is the minimum time that an object will be tracked in FineLock. Based the rate at which the measured location (or centroid) of a star converges (from analysis of FGS1r data) Table 4.5 lists the recommended exposure times as a function of target magnitude. We note that:

- Exposures should be as short as possible to allow for more individual observations during the visit, but should be longer than *HST*’s mid-frequency oscillations (~10 seconds).
- Usually, Position mode observations yield an additional 10 to 20 seconds of FineLock data in excess of the exposure time specified in the phase II proposal (a result of unused overheads). Hence, specifying a 10 second exposure results in 20 to 30 seconds of FineLock data.

Table 4.5: Recommended FGS1r Exposure Times

Magnitude	phase2 exposure time (in sec)
8-14	10
15-17	25

4.2.5 Exposure Strategies for Special Cases

Observing Binaries and Extended Sources in Position Mode

Multiple or extended sources in the FGS’s IFOV will result in a reduction of the amplitude of the observed interferometric fringes (relative to that of a point source). This occurs because light from multiple sources in the IFOV do not interact coherently (the observed rays originate from different

angles on the sky). Therefore, multiple point source fringes will be superimposed upon one another, each scaled by the relative brightness of the source and shifted by its relative angular displacement on the sky. The result is a composite Transfer Function with reduced fringe visibility.

The fringe visibility reduction for the brighter component of a binary system with an angular separation along the X or Y axis greater than about 80 mas (i.e., when the individual S-Curves are fully separate) is given by:

$$F_r = \frac{f_a}{(f_a + f_b)},$$

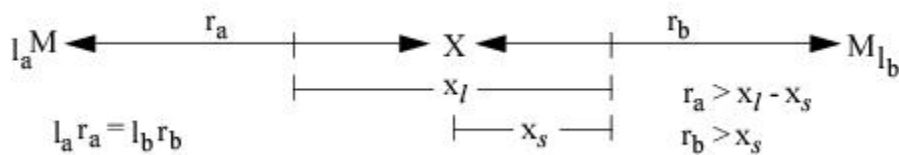
where f_a and f_b are the intensities of the brighter and fainter components, respectively. A similar expression, but with I_b in the numerator, is appropriate for the faint star S-curve (see [Figure 4.3](#) for examples).

For projected angular separations less than 80 mas, the Transfer Function will be a blend of the merged point source S-Curves. The resultant fringe visibility will depend on the relative brightness and the angular separation of the components (i.e., F_r is more difficult to predict).

Even significant loss of fringe visibility does not pre-dispose the object from being successfully observed in Position mode. To be acquired in FineLock, an object's *Fine Error Signal* (see [Appendix A](#)) must exceed a fringe detection threshold (see [Figure A.2](#)). The threshold is set on the basis of the target's V magnitude, as entered in the proposal, to accommodate the acquisition of faint targets. (The fainter the target the more effectively the background and dark counts reduce the fringe amplitude, hence lower detection thresholds must be applied.) If the GO were to state the V magnitude of a binary system or extended source to be sufficiently faint, (regardless of its true value), then the observed fringes will exceed the (lower) detection threshold, and the FGS will successfully acquire the object. However, if a false magnitude is specified, one should also manually set the FESTIME (an optional parameter) to the value appropriate to the object's true magnitude. Otherwise, the observation's overheads will be excessively long.

Some binary systems are not *reliably* observed in Position mode, even with the adjustment to the fringe detection threshold. Objects in this category include those with components exhibiting small magnitude differences ($\Delta m < 1$) and angular separations greater than 60 mas but less than 800 mas (as projected along an interferometric axis). In these cases, either star may be acquired. There have been cases where one component was acquired on the X-axis while the other was acquired on the Y-axis. Such data are still useful, but care must be applied in the post- observation data processing.

There is a class of binary stars which *cannot* be observed in Position mode. In a FineLock acquisition (see [Appendix A](#)), the WalkDown to FineLock is a finite length path (approximately 0.810") beginning at a point which is "backed off" a fixed distance from the object's photocenter. If the fringes of both stars lie outside this path, then neither will be encountered and the FineLock acquisition will fail. The condition for such a *failure* is the following,



where X is the location of the system’s photocenter, r_a and r_b are the distances from the photocenter to the fringes of the components “a” and “b” respectively, I_a and I_b are the flux from each component, x_s is the starting position of the WalkDown, and x_l is the length of the WalkDown. If the position of the binary along either the X or Y axis is known to meet this failure requirement, Position mode observations of this system should not be attempted.

It is recommended that a proposer contact the [STScI Help Desk](#) for assistance with Position mode observations of binary systems.

4.2.6 Sources Against a Bright Background


For sources against bright backgrounds, the fringe visibility function is reduced by $I / (I + B)$ where I is the point source flux and B is the background flux. The proposer should contact the [STScI Help Desk](#) for assistance with such observations.

4.2.7 Crowded Field Sources

Crowded fields create two problems for FGS observations:

- A nearby star (< 10 arcsec away) of similar magnitude could be acquired during the search phase.
- The background brightness in the 5 × 5 arcsec aperture may be increased by the presence of numerous faint stars or nebulosity.

The proposer should consult the [STScI Help Desk](#) for assistance with such observations.

**Proposers should document—in the proposal—the logic for selecting a -FESTIME or entering a false apparent magnitude of a target.**

4.3 Position Mode Observing Strategies

- [4.3.1 Summary of Position Mode Error Sources](#)
- [4.3.2 Drift and Exposure Sequencing](#)
- [4.3.3 Cross Filter Observations](#)
- [4.3.4 Moving Target Observation Strategy](#)

Measurement errors can be minimized by carefully structuring the order of exposures in a visit. This section describes strategies which maximize science return.

4.3.1 Summary of Position Mode Error Sources

The reduction of a Position mode data set requires several corrections and calibrations:

- ***Exposure Level:***
 - Background determination.
 - Star Selector encoder positions (7 LSB).
 - PMT response.
 - Optical Field Angle Distortion calibration.
 - Differential velocity aberration.
 - Lateral color aberration.
- ***Visit Level***
 - Vehicle jitter.
 - Drift of FGS's FOV.
 - Cross filter (F583W v. F5ND, if used).
- ***Program Level***
 - Plate solutions (4 or 6 parameter fits).
 - Plate scale.

Each of the corrections and calibrations are briefly discussed in [Chapter 5](#), and are thoroughly reviewed in the [FGS Data Handbook](#). Many of the corrections specified on the list are determined by analysis of individual observations and removed later in the data reduction processing, (e.g., jitter data is retrieved from the guide star telemetry and removed from the target data). Calibrations, such as the plate scale, the OFAD, lateral color, and cross filter effect are derived from STScI calibration programs. A potentially dominant source of error, the FOV drift (time scale of several minutes), must be measured during the visit, and to that end, the sequence of exposures must be carefully arranged.

4.3.2 Drift and Exposure Sequencing

Stars observed more than once per visit (“check stars”) are typically seen to drift across the FGS by ~ 2 to 6 mas when two FGSs guide the telescope (or ~ 5 to 20 mas with only one FGS guiding). Because astrometry observations execute sequentially, the errors in the measured angular separations between objects increase as the time between the measurements lengthens. If uncorrected, this drift will overwhelm the astrometry error budget.

Whatever causes the position of an object to “drift” in the astrometer’s FOV affects the guiding FGSs as well. The apparent motion of the guide stars are interpreted as “errors” by the pointing control system and are “corrected” by a small vehicle maneuver. The astrometry FGS witnesses the pointing change. Therefore, the check star motion will have a contribution from all three FGSs.

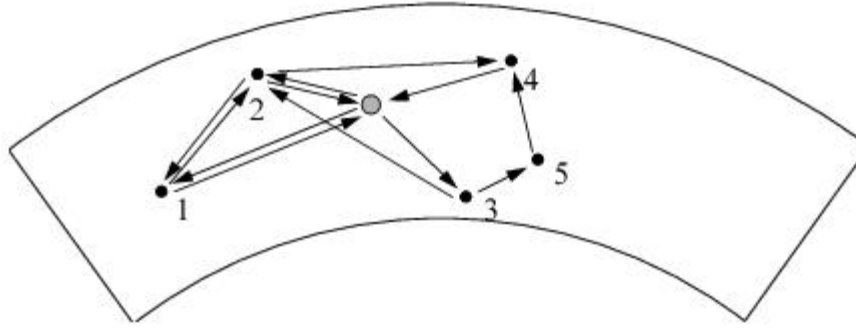
When only one FGS is used for guiding, the telescope is not roll-constrained, and large motions in the astrometric FGS - up to 10 mas - are not uncommon. Nevertheless, this drift can be successfully removed from the astrometry data, provided the proposal specifies an adequate check star sequence. The more check star observations, the more precise the drift correction. Check stars can be reference or science targets. Ideally, both rotation and translation corrections should be applied to the data, implying the use of at least two check stars with at least three measurements each.

The need to observe check stars can be in conflict with other aspects defining an optimal observing strategy, so compromises will be necessary. Overall an optimal Position mode visit is scripted to:

- Define a check star strategy which will be robust against FOV drift.
- Maximize the number of reference stars observed.
- Maximize the number of observations of each object.

For example, a visit could contain 10–35 exposures, provided the overheads are minimized and exposure times are less than 20 seconds. A sample geometry is given in [Figure 4.2](#), where the science target is represented by the central object.

Figure 4.2: A Sample Visit Geometry



For the geometry specified above, the exposures may be sequenced as follows:

1 - 2 - **target** - 3 - 2 - 4 - **target** - 3 - 5 - 4 - **target** -->
--> 2 - 1 - **target** - 3 - 5 - 4 - **target** - 2 - 1 - **target**.

Additional examples expressed in proposal logsheet syntax are given in [Section 6.5](#).

4.3.3 Cross Filter Observations

Targets brighter than $V = 8$ cannot be observed with the F583W. The F5ND attenuator must be used for such observations. If the visit includes observations of fainter objects with the F583W, a cross-filter correction will be needed for the data reduction. For FGS3, the F583W/F5ND cross-filter effect was found to be astrometrically large (~ 7 mas) and varied with location in the FOV. This effect has been calibrated at the center of FGS1r's FOV by STScI calibration programs. If needed at other locations in the FOV, special calibrations by the proposer might be required.

4.3.4 Moving Target Observation Strategy

In Position mode, the FGS can track a bright target ($V < 14.0$) whose motion is less than ~ 0.1 arcsec per second. However, planning the observation requires extreme precision: the moving target must be accurately located, to within 10 arcsec, in the IFOV at the start of the exposure, implying a very accurate ephemeris. Transfer mode observations of moving targets are discussed in the next section.

4.4 Transfer Mode Overview

4.4.1 The FGS Response to a Binary

4.4.2 The Transfer Mode Exposure

4.4.1 The FGS Response to a Binary

If the source is a double star, then its wavefront has two components, each incoherent with respect to the other. Two propagation vectors characterize this wavefront and the angle between them is directly related to the angular separation of the stars on the sky. As the FGS's IFOV scans across the object, each component of the wavefront can be thought of as generating its own interferogram (or "S-Curve"), whose modulation is diminished by the non-interfering "background" contributed by the other component. The resulting relationship between the position of the IFOV to the normalized difference of the PMTs depends on the separation of the stars and their relative brightnesses. *The composite interferogram of a multiple system is the linear superposition of the fringes from the individual components, scaled by their relative brightness and shifted with respect to one another by their separation on the sky.* Given this, the fringe pattern of a binary system, whose components have an angular separation α (as projected along the X-axis) and fluxes f_a and f_b is given by

$$S_{binary}(x)l_1 S_{single} S_{binary}(x)l_2 S_{single} = +(x + \alpha) ,$$

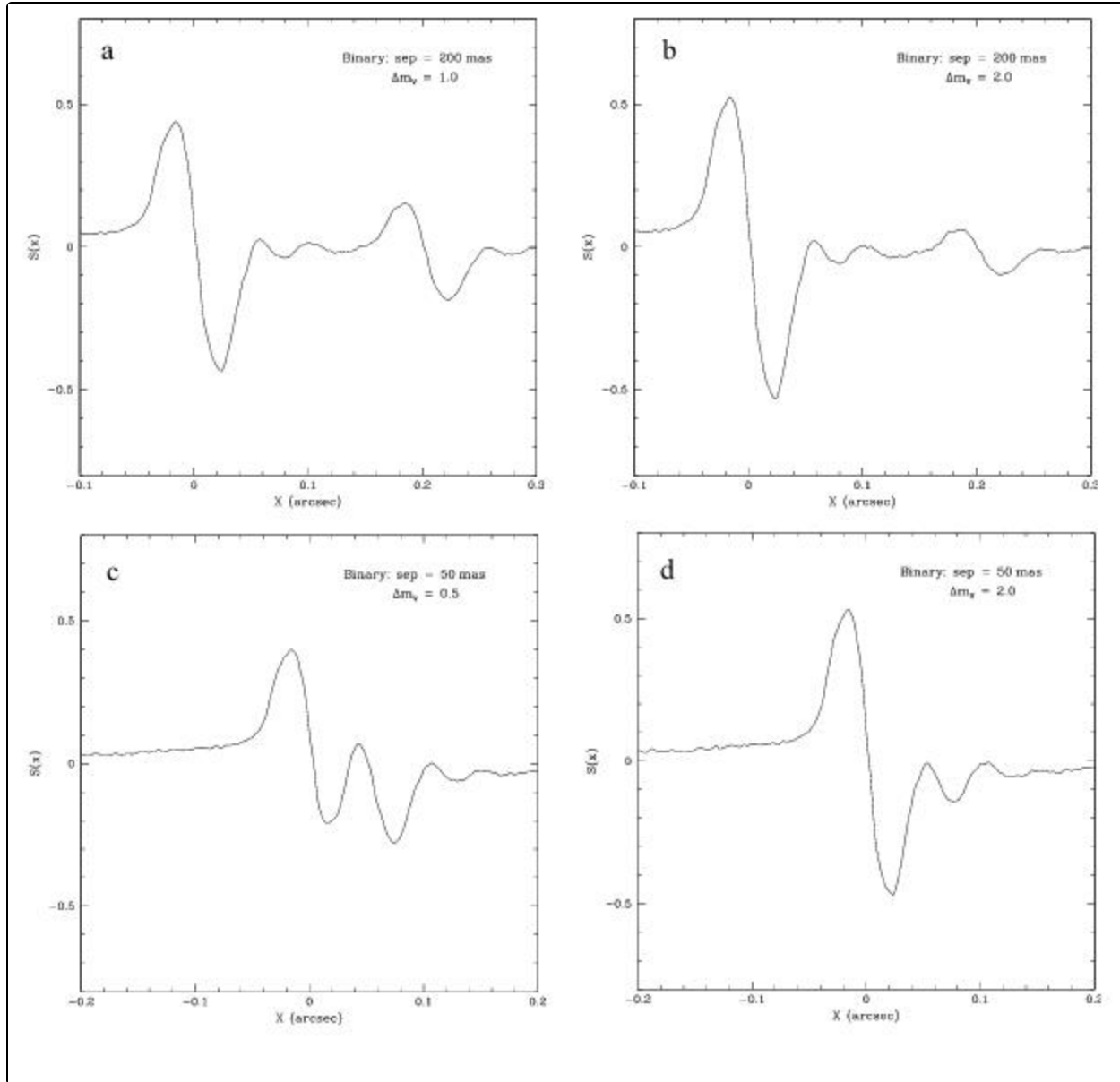
where:

$$l_1 = \frac{f_a}{f_a + f_b}$$

$$l_2 = \frac{f_b}{f_a + f_b} .$$

Figure 4.3 shows the changes in the observed FGS1r interferogram due to binary systems of varied separations and magnitude differences. In Figure 4.3a we display the interferogram of a wide binary pair with component separations and magnitude differences of (200 mas, 1.0) respectively. Figure 4.3b is an example of a system with the same separation, but with a magnitude difference of $\Delta m = 2.0$. The binary system in Figure 4.3c has a smaller separation and magnitude difference (50 mas and 0.5 respectively), while in Figure 4.3d increases the magnitude difference to $\Delta m = 2.0$ for a component separation of 50 mas.

Figure 4.3: Binary S-Curves Generated from FGS1r X-Axis Data



If the angular separation of the stars is greater than the width of the S-Curve, two distinct S-Curves are apparent, but the modulation of each will be diminished relative to that of a single star by an amount depending on the relative flux from each star (see [Figure 4.3a](#) and also [Figure 3.1](#)). On the other hand, if the angular separation is small, the S-Curves will be superimposed, and the morphology of the resulting blend complicated (as in [Figure 4.3d](#)). In either case, the composite S-Curve can be deconvolved using reference S-Curves from point sources, provided the angular separations are not too small and the magnitude difference is not too large. To be more precise, fitting the observed double star S-Curve with two appropriately weighted, linearly superimposed reference S-Curves from single stars leads to the determination of the angular separation, position angle, and magnitude difference of the binary's components. The modulation, morphology, and temporal stability of the point-source calibration S-Curves determine the resolving power of the FGS. For FGS1r, this is about 7 mas for $\Delta m < 1.0$.

4.4.2 The Transfer Mode Exposure

Rather than tracking the fringe as in Position mode observation, the IFOV is scanned across the object along a 45 degree path (with respect to the FGS detector axes) in a Transfer mode exposure. Every 25 milliseconds, star selector angles and data from the four PMTs are recorded. From these data, the fringes of the object can be reconstructed. The number of scans and the length of each scan are derived from the Phase II proposal.

For each target, the step size and scan length must be adjusted as necessary to accomplish the goals of the observation:

- **Step Size:** The step-size refers to the angular distance covered by the IFOV along an axis during a 25 millisecond interval. The default step-size is 1.0 mas. Higher resolution is achievable using step sizes as fine as 0.3 mas. However, such a small step size may prohibitively increase the total time to complete a scan, and as a result of least significant bit (LSB) constraints and vehicle jitter, the effective resolution may not be better than 1.0 mas. The goal is to execute as many scans as possible, with the smallest StepSize (0.6 or 1.0 mas), to achieve the highest S/N ratio.
- **Scan Length:** The required scan length is depends on the geometry of the target. A minimum of scan length of 0.3" is needed to fully sample the fringes of a point source along with a sufficient segment of the wings to either side. For binary systems, the scan length should be at least as wide as the component separation plus 0.3".



The point-source calibration S-Curves are obtained only at the center of the FGS1r FOV. Other locations in the FOV are not routinely calibrated.

4.5 Planning a Transfer Mode Observation

- 4.5.1 Target Selection Criteria
- 4.5.2 Transfer Mode Filter and Color Effects
- 4.5.3 Signal-to-Noise
- 4.5.4 Transfer Mode Exposure Time Calculations

4.5.1 Target Selection Criteria

Other than the brightness restrictions specified in [Table 4.6](#) there are several additional considerations when selecting targets for Transfer mode observations.

- **Position in the FOV:** The morphology of the fringe varies considerably with position in the FOV, as shown for FGS1r in [Figure 2.6](#). As explained in [Chapter 2](#), this field dependence is the manifestation of small misalignment between the star selector optics and the Koesters prism which is greatly magnified by *HST*'s spherical aberration. To obtain the highest quality data with the best resolution, all Transfer mode observations should be obtained at the AMA optimized position at the center of the FOV. *Under normal circumstances, STScI will provide reference S-Curve calibrations only at the center of the Field of View.*
- **Color:** The FGS's interferometric response is moderately sensitive to the spectral color of the target. The FGS calibration library contains interferograms from point-source objects with a variety of (B-V) colors. The GO is encouraged to inspect this library to ascertain whether a suitable reference ($\delta(B-V) < 0.3$) is available for data analysis. If not, the FGS group should be alerted, and efforts will be made to enhance the library. The color calibrations available in the FGS library are listed in [Chapter 5](#). Up-to-date additions can be found on the FGS Web site: <http://www.stsci.edu/hst/instrumentation/fgs>
- **Minimum Scan Length:** In order for Transfer mode observations to achieve the highest possible signal-to-noise, the length of the scan should be as short as possible (to allow for more scans in the allotted time). The minimum scan length is determined by the expected angular separation of the components of the binary being observed plus the recommended minimum size (for a point source) of 0.3", or,

$$\text{Min Scan Length (arcsec)} = 0.7 + 2x$$

where the value x is the largest anticipated angular separation of the binary along either axis.

- **Minimum Scan Length:** In order for Transfer mode observations to achieve the highest possible signal-to-noise, the length of the scan should be as short as possible (to allow for more scans in the allotted time). The minimum scan length is determined by the expected angular separation of the components of the binary being observed plus the recommended minimum size (for a point source) of 0.3", or,
- **Maximum Scan Length:** When considering the maximum scan length, three concerns should be addressed:
 - Masking by the field stops becomes relevant when the FOV is moved beyond 2 arcsec from the photocenter. False interferometric features become prevalent.
 - Beyond 2.5 arcsec from the photocenter, the intensity of the target's light drops off considerably, resulting in poor signal-to-noise photometry.
 - Maximum commandable scan length is 6.7".

- **Target Orientation:** If the approximate position angle of the non-point source is known, then specifying an orientation for the observation may be advantageous. If possible, (for wide binaries) avoid the situation where the projected angular separation along one of the axes is less than 20 mas. Specific orientations are achieved by rolling the *HST* to an off-nominal roll attitude or by scheduling an observation at a time when the nominal roll is suitable. It should be noted however that special orientations are considered as special scheduling requirements which affect schedulability.
- **Target Field:** The Search and CoarseTrack acquisition are vulnerable to acquiring the wrong object if the field is too crowded (with neighbors of comparable brightness within 8 arcseconds of the target). Hence, the problem addressed in [Section 4.2.7](#) for Position mode observations applies equally to Transfer mode observations.

4.5.2 Transfer Mode Filter and Color Effects

[Table 4.6](#) is a summary of the available filters and associated restrictions governing their use.

Table 4.6: FGS1r Transfer Mode Filters to be Calibrated During Cycle 8

Filter	Calibration Status at FOV Center	Comments	Target Brightness Restrictions
F583W	Full	Monitoring of Reference Standard star Upgren69 and single epoch color calibrations as required by the GO proposal pool.	Recommended for $V > 8.0$; Not permitted for $V < 8.0$
F5ND	Single-epoch color calibrations as needed	Supported by the STScI Observatory Calibration program.	Required for $V < 8.0$; Not recommended for $V > 8.0$
PUPIL	Single-epoch color calibrations as needed	Not part of the STScI Observatory calibration program. GO must request time from TAC for any calibrations.	Not permitted for $V < 7.5$
F605W	Single-epoch color calibrations as needed	Not part of the STScI Observatory calibration program. GO must request time from TAC for any calibrations.	Not permitted for $V < 8.0$
F550W	Single-epoch color calibrations as needed	Not part of the STScI Observatory calibration program. GO must request time from TAC for any calibrations.	Not permitted for $V < 7.5$

The S-Curve morphology and modulation have a wavelength dependence. Experience with FGS3 has shown that the color of the reference star should be within $\delta(B-V) = 0.1-0.2$ of the science target. We endeavor to maintain a library of single reference stars which accommodate the color requirements of the GO proposals in the Cycle. These color standards are usually observed once during the Cycle, while Upgren69 is observed every 6 months to monitor S-curve stability.

4.5.3 Signal-to-Noise

In essence, the “true” signal in a Transfer mode observation of a binary system is the degree to which the observed Transfer Function differs from the S-curve of a point source. The signal-to-noise (S/N) required of an observation will depend upon the object being observed; a wide binary whose stars have a small magnitude difference and separation of 200 mas will be much easier to resolve than a pair with a larger magnitude difference and a separation of only 15 mas.

The “noise” in an observation has contributions from both statistical and systematic sources. Photon noise, uncertainty of the background levels, and spacecraft jitter comprise the statistical component. The temporal variability and spectral response of the S-curves dominate the systematic component (these are monitored and/or calibrated by STScI). Provided that at least 15 scans with a 1 mas step size are available, observations of bright stars ($V < 13.0$) suffer little from photon noise and uncertain background levels, and show only slight degradations from spacecraft jitter (with high S/N photometry, the segments of the data which are degraded by jitter are easily identified and removed from further consideration).

Maximizing the S/N for observations of fainter objects requires a measurement of the background level (see [Chapter 6](#)) and a larger number of scans to suppress the Poissonian noise in the photometry of the co-added product. But with lower S/N photometry in a given scan, corruption from spacecraft jitter becomes more difficult to identify and eliminate. Therefore, the quality of Transfer mode observations of targets fainter than $V = 14.5$ will become increasingly vulnerable to spacecraft jitter, no matter how many scans are executed.

Systematic “noise” cannot be mitigated by adjusting the observation’s parameters (i.e., increasing the number of scans). To help evaluate the reliability of a measurement made in Transfer mode, STScI monitors the temporal stability and spectral response (in $B-V$) of FGS1r’s interferograms. As discussed elsewhere, the FGS1r S-curves appear to be temporally stable to better than 1%, and the Cycle 10 calibration plan calls for observations of single stars of appropriate $B-V$ to support the data reduction needs of the GOs (this calibration will be maintained in Cycle 29). This should minimize the loss of sensitivity due to systematic effects.

4.5.4 Transfer Mode Exposure Time Calculations

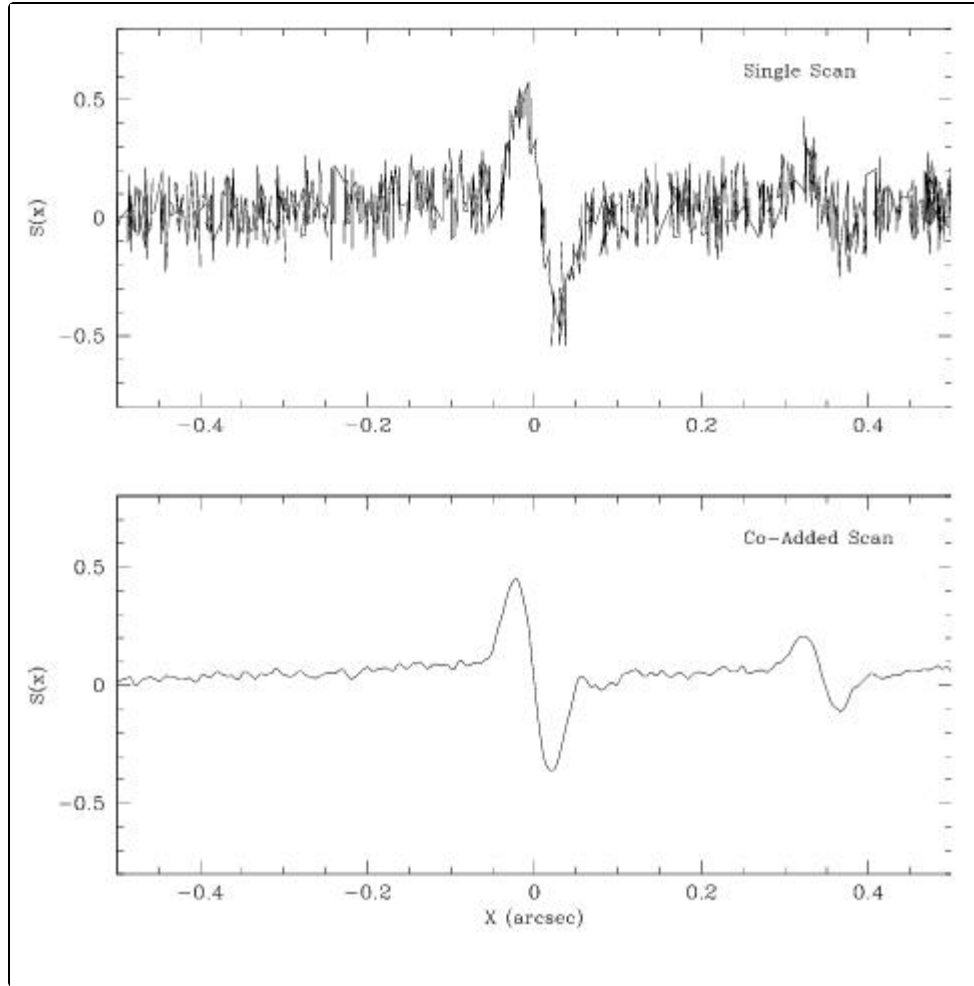
The step_size and number of scans determine the number of photometric measurements available for co-addition at any given location along the scan path. Typically, up to 50 scans with 1mas step_size are possible within a 53 minute observing window, (after accounting for overheads and assuming a scan length ~ 1.2 arcsec per axis). The step size and number of scans that should be specified are in part determined by the target’s magnitude and angular extent and also by the need to allocate time within the visit to any other objectives, such as Position mode observations of reference stars (to derive a parallax for the binary). The total exposure time for a Transfer mode observation (excluding overheads) is:

$$T_{\text{exp}} = \frac{\text{ScanLength}}{\text{StepSize}} \times (0.025 \text{ sec} \times N_{\text{scans}}) ,$$

where T_{exp} is the total exposure time in seconds, N_{scans} is the total number of scans, 0.025 is the seconds per step, ScanLength is the length of the scan *per axis* in arcsec, and StepSize is given in arcsec.

Photon noise is reduced by increasing the number of scans, N_{scans} , as displayed in [Figure 4.4](#), which demonstrates the benefits of binning and co-adding individual scans. Trade-offs between step size, length, and total duration of an exposure are unavoidable especially when considering visit-level effects such as *HST* jitter.

Figure 4.4: FGS1r (F583W) S-Curves: Single and Co-Added



Simulations using actual data scaled by target magnitude are needed to relate the Transfer Function signal-to-noise (described in the previous section) to the resolving performance of the instrument. A robust exposure time algorithm is in development. In [Table 4.7](#), we offer some guidelines on the minimum number of scans to use in a visit for various binary parameters. These are derived for a step size = 1.0 mas, so that in a 1 mas bin there would be NSCANS samples per bin. Smaller step sizes facilitate the use of less scans to achieve the same signal-to-noise ratio. (Specificity fewer scans with smaller step sizes can reduce the observational overhead, which can increase the time on target and hence the overall signal-to-noise ratio. However, intermittent vehicle jitter may corrupt the data from some scans to the degree that such data is useless for scientific purposes. These trade off need to be considered when planning the observations).

Table 4.7: Suggested Minimum Number of Scans for Separations < 15 mas

V Mag	$\Delta\text{mag} = 0.0$	$\Delta\text{mag} = 1.5$	$\Delta\text{mag} = 3.0$
5	18	20	40
9	10	15	40
12	15	20	40

14	30	40	40
15	35	50	50
16	50	60 ¹	60 ¹

¹Note that 60 scans is about the maximum that can be performed in a single *HST* orbit (assuming a scan length of $\sim 1''$). Multi-orbit visits do not necessarily increase the achievable S/N for targets of $V > 15$ since photometric noise makes cross correlation of scans across orbital boundaries questionable. In other words, the data gathered during one orbit is not reliably combined with data from another orbit for faint, close binary systems.

4.6 Transfer Mode Observing Strategies

- 4.6.1 Summary of Transfer Mode Error Sources
- 4.6.2 Drift Correction
- 4.6.3 Temporal Variability of the S-Curve
- 4.6.4 Background and Dark Counts Subtraction
- 4.6.5 Empirical Roll Angle Determination
- 4.6.6 Exposure Strategies for Special Cases: Moving Targets

4.6.1 Summary of Transfer Mode Error Sources

The Transfer mode corrections and calibrations are:

- *Exposure Level:*
 - Background subtraction.
 - Star Selector Encoder correction (7 LSB).
 - Cross-correlating and co-adding individual scans.
 - Availability of a suitable point-source reference S-Curve (color response).
- *Program Level:*
 - Roll dependence of the FGS plate scale.

Each of the corrections and calibrations are discussed briefly in [Chapter 5](#) and more thoroughly in the [FGS Data Handbook](#). Those corrections that could result in an enhanced observation strategy are discussed here.

4.6.2 Drift Correction

As discussed in the Position mode section, targets observed multiple times per Position mode visit typically drift across the FGS by about 6 to 12 mas when two FGSs guide the telescope. This drift is also apparent in Transfer mode observations, but the cross-correlation of S-Curves prior to binning and co-adding automatically removes the drift. Each single-scan S-Curve is shifted so that the particular features of the S-Curve used for the cross correlation coincides with that of the fiducial S-Curve. The reliability of implicitly removing the drift is only as good as the accuracy of the cross correlation procedure, which, for bright objects ($V < 14.5$) is accurate to < 1 mas. Analysis is underway to determine the procedure's accuracy for fainter objects.

4.6.3 Temporal Variability of the S-Curve

Measurements of the standard star Uggren69 over the lifetime of FGS3 indicated a 10 – 18% variability of the S-Curve morphology on orbital timescales. The amplitude of these changes have important consequences on the analysis of binary star observations when the separation of the components is less than 30 mas and the magnitude difference exceeds 1.6. These temporal changes also affect analyses of extended source observations. The cause of this relatively high frequency variability in FGS3 has not been determined.

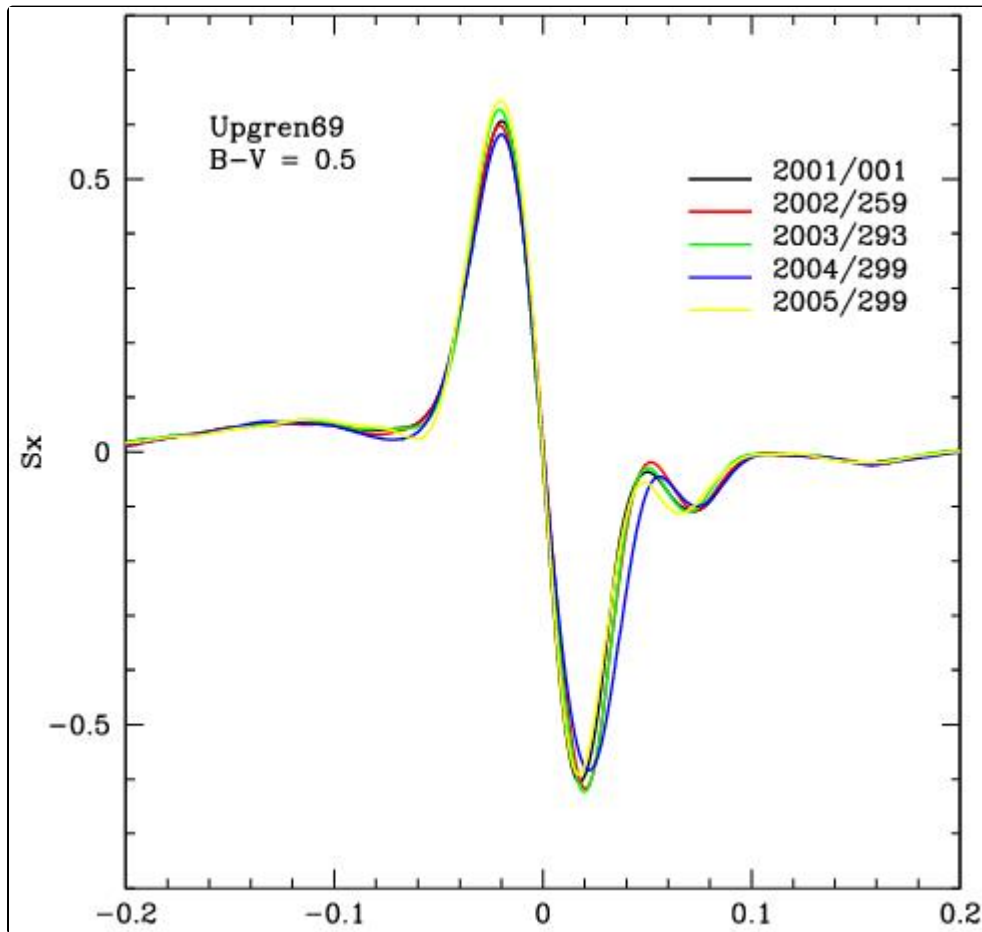
FGS1r appears to be stable at the 1% level over periods of many months to perhaps years (as of July 2002). There appears to have been a slow evolution of the y-axis S-curve however, as shown in [Figure 4.5](#). The changes along the X-axis have been much less. On the assumption that this evolution is due to changes in the alignment of the interferometer with respect to HST' OTA as water vapor outgasses from the instrument's graphite epoxy composites, it is expected that FGS1r will become more stable as time goes on (the rate of outgassing slows with time in orbit). STScI will continue to monitor FGS1r's S-Curves so that this evolution can be calibrated and its effect on science data minimized.

4.6.4 Background and Dark Counts Subtraction

For programs with isolated targets, background is not an issue. For programs with targets embedded in nebulosity, knowledge of the background is required. In order to obtain a background measurement, it is necessary that there be at least two targets in the observing sequence, separated by at least 60". The background will be measured during the slew of the IFOV from one target to the next. If necessary, the proposer should specify a false target at some location in the FOV at least 60" from the science object, and observe it in Position mode for approximately 30 seconds with the same filter as the science target. Care must be taken to avoid observing "background: objects brighter than $V = 8.0$ with F583W.

Dark counts become important for stars fainter than $V=14.5$. STScI has calibrated the FGS1r dark counts. Therefore there is no need to acquire such data as part of a science observing program. Likewise, the dead time correction is needed for stars brighter than about $V=9$, but STScI has already acquired the data needed to support this correction.

Figure 4.5: Evolution of S-curve morphology along the FGS1r Y-axis



4.6.5 Empirical Roll Angle Determination

The science data headers contain the commanded HST roll angle, not a measured angle. The errors that contribute to a difference between the commanded and actual roll include: the relative guide star positional error, the FGS-FGS alignment error, and errors in the predicted ephemeris. The actual roll angle is calculated from the guide star telemetry by the observatory monitoring system, and is reported in the STScI Observation Logs that accompany the science data. More information is available on the following Web page:

<http://www.stsci.edu/hst/observing/program-information>

The error in the calculated roll angle is estimated to be about 0.04 degrees. If a more accurate determination is needed, the position angle of the observed binary with respect to the local reference frame can be measured via Position mode observations of the target and a reference star (or two reference stars if the target cannot be acquired in Position mode—see [Section 4.2.5](#)) should be included in the visit along with the Transfer mode exposures. Please confer with STScI for help designing the visit and calculating the roll from Position mode measurements.

4.6.6 Exposure Strategies for Special Cases: Moving Targets

For Transfer mode observing, a moving target represents a special case. The flight software which enables HST to track a moving target has not been implemented for FGS observations. Nonetheless, the FGS is quite capable of acquiring a moving target provided that the object's angular speed is less than 80 mas/sec. However, during the observation, the scan path is not adjusted to accommodate for the object's motion. The target's fringe will be displaced in each subsequent scan until it moves completely out of the scan path. A method to work around this problem is to specify several observations of the object during the visit. For example:

1. The target should be observed in several short exposures rather than in one or two long exposures. The FGS would re-acquire the target with each new Search, CoarseTrack acquisition regardless of the target's motion. The target list should contain enough entries to cover the swath of sky traversed by the moving target, e.g., if the motion takes the object 10 arcsec across the FOV, then at least two sets of target coordinates should be specified.
2. The number of individual observations (entries in the exposure logsheet) and number of scans in an observation will be dictated by the object's angular speed.
3. Plan the observation when the target is moving its slowest, e.g., at opposition (if possible).
4. Take advantage of rolling the telescope to adjust the angle between the target motion vector and relevant FGS reference directions (-please contact STScI for assistance).
5. Choose the exposure times to be as short as possible.

Chapter 5: FGS Calibration Program

Chapter Contents

- [5.1 Position Mode Calibrations and Error Sources](#)
- [5.2 Transfer Mode Calibrations and Error Sources](#)
- [5.3 Linking Transfer and Position Mode Observations](#)
- [5.4 Cycle 21 Calibration and Monitoring Program](#)
- [5.5 Special Calibrations](#)

5.1 Position Mode Calibrations and Error Sources

[5.1.1 Position Mode Exposure Level Calibrations](#)

[5.1.2 Position Mode Visit Level Calibrations](#)

[5.1.3 Position Mode Epoch-Level Calibrations](#)

FGS science data is processed at three distinct levels: the exposure, the visit, and the epoch. Each of these levels is subject to different sources of error. [Table 5.1](#) summarizes the accuracies of Position mode calibrations. Most of the errors listed are statistical. Multi-epoch observations reduces the impact of these errors in the science data.

Table 5.1: FGS1r Position Mode Calibration and Error Source Summary

Type of Calibration Correction	Pre-Calibration Error Extent	Calibration Error (mas)	Comments
<i>Exposure Level (per observation) Calibration Corrections:</i>			
background and detector dark counts	-	-	Addressed by increasing the integration time for each centroid determination when observing faint stars. (to preserve the NEA).
Star Selector Encoder fine bit errors	~1 mas	0.1	Correction applied in the SSA,B->X,Y conversion.
Centroid errors	Magnitude Dependent	~ 1, V < 15 ~ 2, V > 15	Apply median filter.
Relative PMT sensitivity	~4 mas (V>15)	0.1 mas	Analysis removes PMT mismatch effect; used to adjust for position centroid errors.
Differential velocity aberration	± 30 mas (function of geometry)	0.1	Depends on HST velocity vector and target geometry, ephemeris errors
Relative distortion across FOV (OFAD)	~ 500 mas	~0.3 mas	STScI calibration in filter F583W.
Lateral color correction	~1 mas relative shift for $\delta(B-V) = 1$	0.1 mas	STScI standard yearly calibration at center of FOV.
Cross filter calibration	~7 mas	< 0.2 center	Relative positional shifts are calibrated for filters F583W and F5ND at FOV center.
<i>Visit Level Calibration Corrections:</i>			

HST jitter	2–4 mas: quiet; 10–150 mas: extreme incidents	< 0.1 during quiescence.	Correction derived from guide star motion. Large jitter excursions could cause loss of lock or corrupt a data set; disqualify outliers.
Drift	5–20 mas: two GS FineLock. 12–60 mas: one GS + gyro roll control	< 0.2	Special observing strategy for check stars; Drift models derived from check star motion and applied to target data.
<i>Epoch-Level Calibration Corrections:</i>			
Temporal evolution of OFAD and plate scale.	<100> mas /year	0.2 mas	Long-term stability monitor program: update OFAD coefficients and FGS star selector calibration.

Exposure level calibrations address the per observation errors. The visit level corrections address the errors after an entire orbit of astrometry data are combined. The epoch-level corrections include the long term changes in scale and distortion of the instrument. The residuals after combining data from multiple visits include the plate overlays and, for example, the determination of an object's parallax and proper motion.

5.1.1 Position Mode Exposure Level Calibrations

The corrections and calibrations described below are applied by the FGS Calibration Pipeline.

Star Selector Encoder Fine Bit Errors

The star selector rotation angles are read as 21 bit integers. The 7 least significant bits (LSBs) are read by an optical resolving device that was calibrated during the manufacturing process. The size of the calibrated correction is about 1 mas with a residual of about 0.1 mas. Errors in the 14 most significant bits (MSBs) are absorbed by the OFAD calibration.

Position Centroiding

The location of a star in the FOV during a Position mode observation is determined by identifying the median of the 40 Hz SSA or SSB samples (while the target is being tracked in FineLock). The median measurement is robust against most spacecraft jitter, short-interval transients and telemetry dropouts. If *faint* targets ($V > 16.0$) are observed, the photometric noise results in a large noise equivalent angle. Spacecraft jitter and photometric noise contribute to the standard deviations about the median of up to 2 mas per axis for $V < 14.5$ and up to 3 mas per axis for $V > 15.0$. However, the repeatability of the centroid measurement (over smaller intervals of the exposure) is the true assessment of the precision of the measurement, typically 0.7 mas and 1.5 mas for targets where $V < 14.5$ and $V > 15.0$ respectively.

PMT Sensitivities and Position Centroid Adjustment

The effect of PMT sensitivity on FGS observations is discussed in [Appendix A](#). In order to accommodate the differences between the two PMTs along each axis, the FGE computes an average difference (DIFF) and average sum (SUM) of their photometric response to the star over the first few FESTIMES in the WalkDown. These values are used in the calculation of the Fine Error Signal. The results are accurate for bright ($V < 14.0$) objects but become unreliable for fainter targets, a result of the short integration period and increasingly noisy photon statistics. The pipeline gathers photometric data over the entire WalkDown (typically 80 times as many samples) to achieve a better signal-to-noise and more reliable values of DIFF and SUM. These are used to recompute the Fine Error Signal and adjust the (x,y) centroids in post-observation data reduction.

Differential Velocity Aberration

Differential velocity aberration arises as a result of small differences in the angle defined by the HST velocity vector and the line of sight to targets in the FGS FOV. The HST PCS guides for zero differential velocity aberration (DVA) at one position in the FOV. The positions of targets elsewhere in the FOV must be corrected for DVA. Calibration errors in the relative alignment of the FGSs, catalog position errors of the guide stars, and ephemeris errors all contribute—though negligibly—to the errors in the differential velocity aberration correction. The actual adjustment to the target's positions can be as large as ± 30 mas (depending on the target and velocity vector geometry) but are corrected by post-observation data processing to an accuracy of ± 0.1 mas.

Optical Field Angle Distortion (OFAD) Calibration

Field angle distortion introduces errors in the measurement of the relative angular separation of stars at varied positions across the FGS FOV. The distortion errors originate from:

- Radial distortions induced by the Ritchey-Chretien design of the OTA.
- Manufacturing irregularities in the FGS/OTA optical train.
- The optical reader produces errors in the 14 most significant bits of the 21-bit Star Selector A and B encoder values.

The distortion is independent of target magnitude, color, or exposure time, and depends only on the location of the object in the FGS FOV. The Space Telescope Astrometry Science Team (STAT) has calibrated the optical field angle distortion (OFAD) in FGS3 and maintained this calibration (the OFAD has a slow time dependence).

The data for calibrating FGS1r became available in December 2000. The analysis (by the STAT) was completed in June 2001. The distortion, on average about 500 mas across the FOV, is represented by two fifth-degree two-dimensional polynomials. Post-calibration residual errors are typically ~ 0.3 mas throughout most of the FOV. The OFAD calibration of FGS1r was part of the FGS1r commissioning calibration plan.

The OFAD residuals for FGS1r are smaller than those of FGS3 due to the design of the calibration test. The FGS3 data were acquired at a time when the roll of HST was restricted to be within 30 degrees of nominal for the date of the observations. The FGS1r test executed when the target field (M35) was close to the “anti-sun” position, i.e., when HST could be rolled over a full 360 degrees. [Figure 5.1](#) shows an overlay of the pointings used for the FGS3 calibration, while [Figure 5.2](#) shows the same for the FGS1r calibration. The freedom to rotate the field of view maximized the apparent effect of the distortions, making them more easily measured compared to the FGS3 test.

The accuracy of the astrometric catalog generated from ground based observations is insufficient for calibrating an FGS as a science instrument. As part of the OFAD calibration, it was necessary to derive an accurate star catalog. This requires that selected stars be observed at several HST pointings. In [Figure 5.1](#) and [Figure 5.2](#), the bold symbols denote stars that were observed as part of the calibration. For the FGS1r calibration, special care was taken to maximize the number of pointings which measured every star.

Figure 5.1: Overlay of the pointings used for the FGS3 OFAD calibration

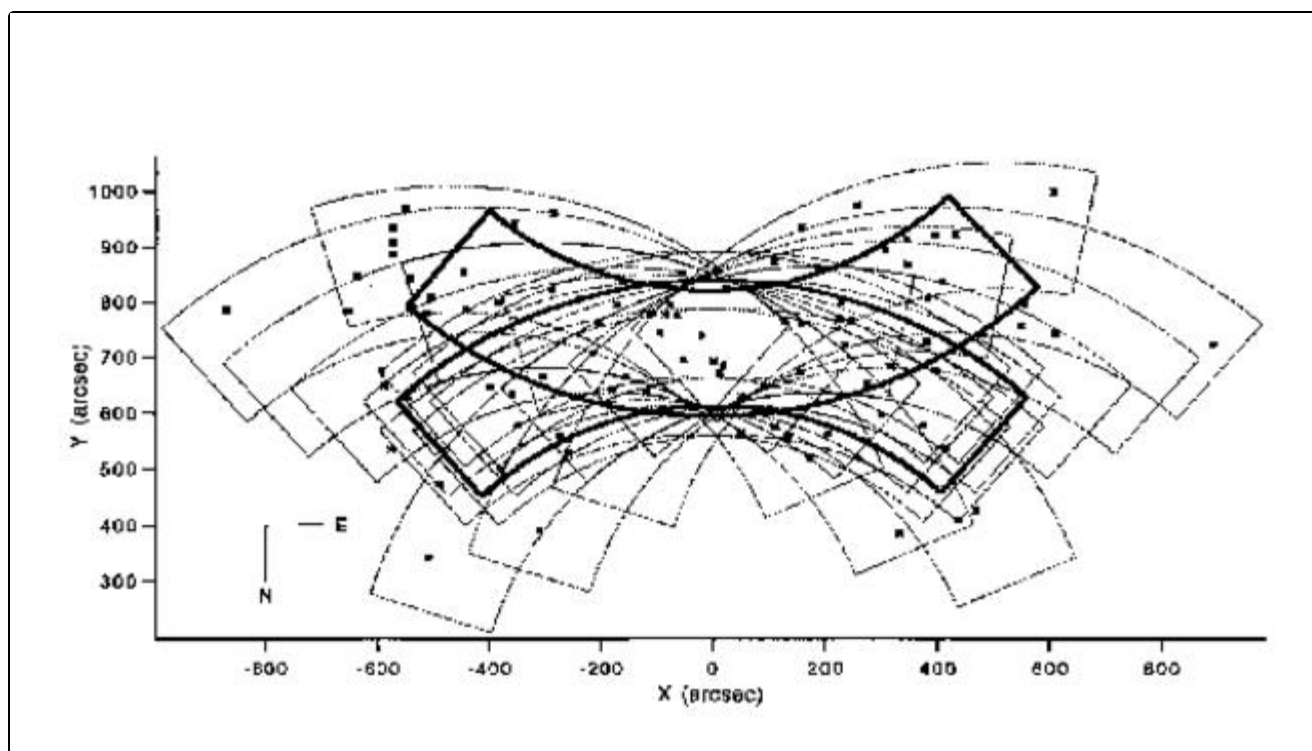
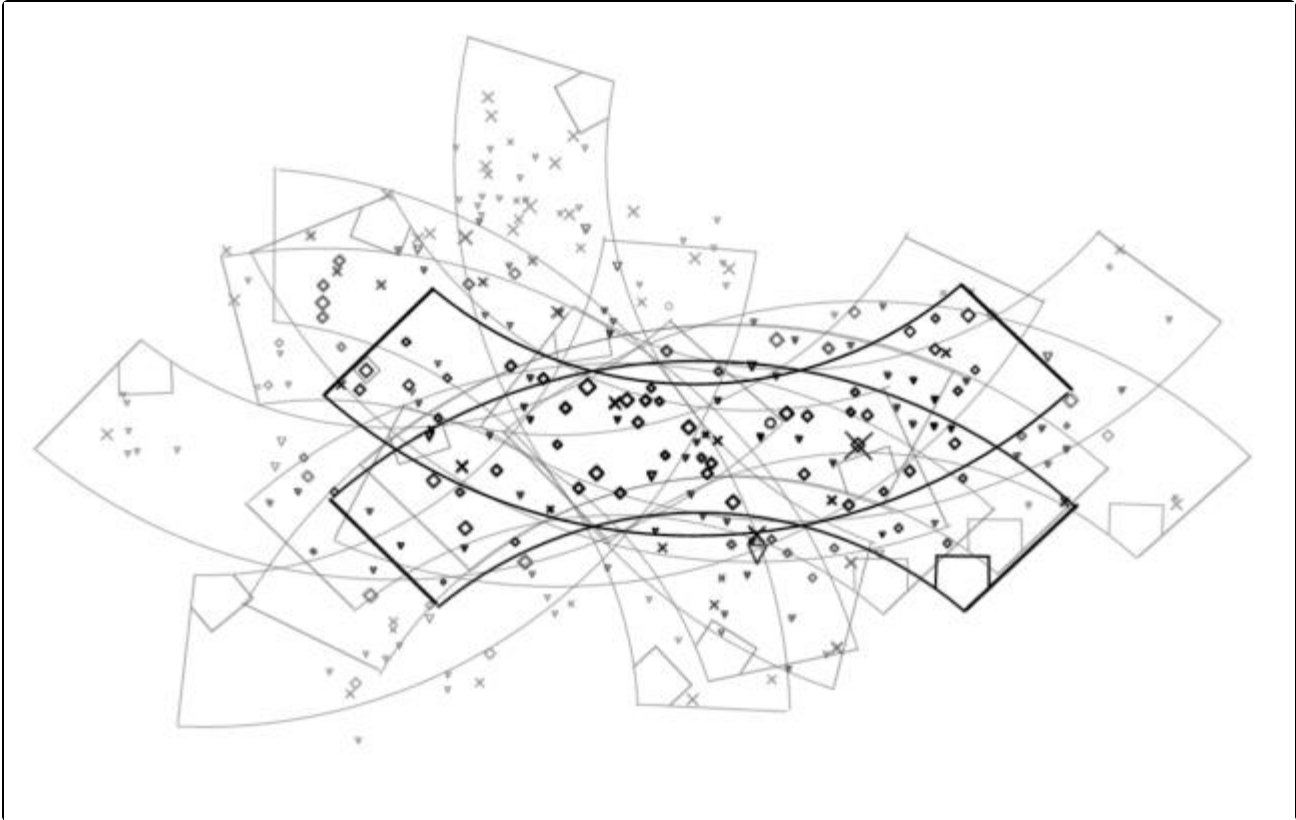


Figure 5.2: Overlay of pointings used for the FGS1r OFAD calibration



Lateral Color

The five-element corrector group (see box in [Figure 2.1](#)) is a collection of refractive elements tasked with the removal of astigmatism and the final collimation of the beam. It's refractive properties introduce subtle changes to angle of propagation of the beam as a function of the spectral color of the source. This change causes the apparent position of the star in the FOV to shift slightly, an effect referred to as *lateral color*. The positional error introduced by is relevant when comparing the relative positions of two targets of extreme colors: for example, a color difference of $\delta(B - V) = 1$ between two targets could introduce a ~ 1 mas positional shift. An in-orbit assessment of lateral color associated with FGS1r was performed in December 2000 and again in December 2001 (and will be repeated in December 2002). A dedicated on orbit calibration of the lateral color shift in FGS1r was first performed in December 2000. A field of stars containing a blue star (A0) and a red star (M3) was observed at three *HST* roll angles that differed by about 60 degrees (the field was near anti-sun, so *HST* roll angle was unconstrained). The three-orbit test was repeated in December 2001. Since then the lateral color calibration has been monitored every two years. The results of these tests are available from the FGS Web site at:

<http://www.stsci.edu/hst/instrumentation/fgs>

5.1.2 Position Mode Visit Level Calibrations

Jitter

Significant enhancements to the HST pointing control system and the replacement of the original solar arrays have reduced quiescent vehicular jitter to 2–4 mas. Although small for most HST science applications, the jitter must be removed from astrometry data.

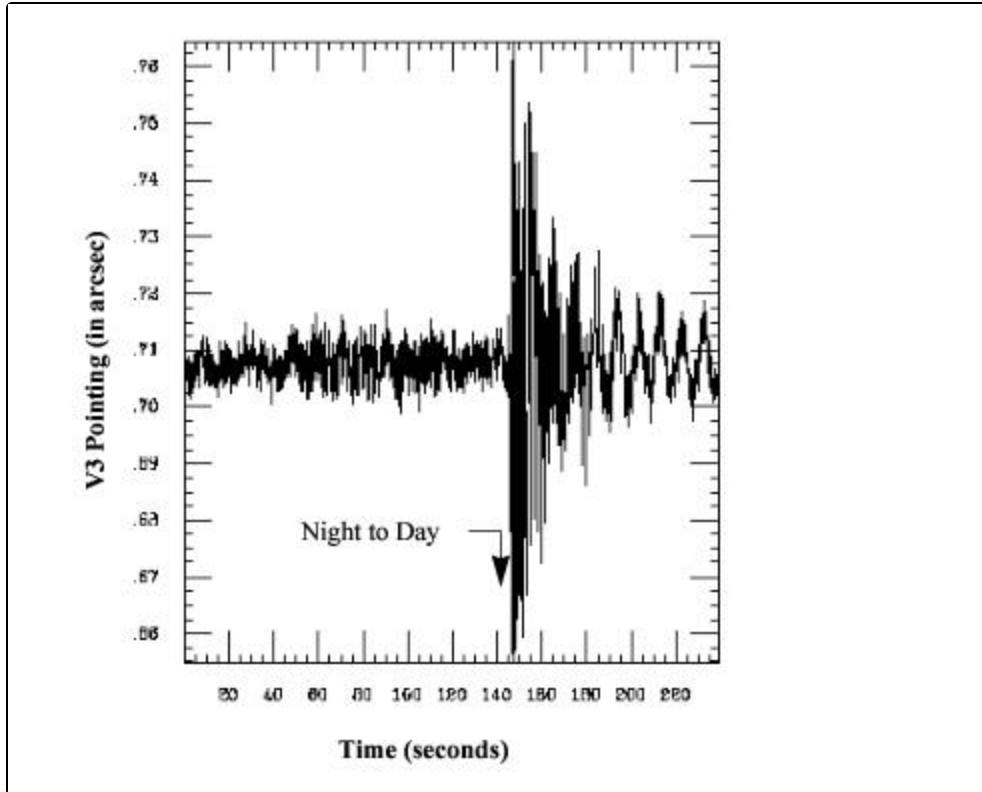
Since astrometric measurements are made sequentially, relating the measurements to one another requires a mapping of each measurement onto a fixed common reference that defines the visit. Guide star positional data, also telemetered at 40 Hz, are used to define jitter characteristics over the course of the visit. Using the time dependent guide star centroids, low frequency jitter (on time scales of minutes) can be removed from the target data.

The pre-SM3B solar panels caused high frequency, large-excursion jitter, as HST transitioned to and from orbital day and night. These disturbances ranged in amplitude from 50 to 150 mas and lasted up to several tens of seconds. If particularly frenzied, a temporary or total loss of lock of the guide stars would result. An example of the jitter during the onset of a day/night transition is shown in [Figure 5.3](#). The large vibrations increase the standard deviations of FineLock tracking in the three FGSs by up to a factor of eight over the pre-transition values. Fortunately, such instances were rare.

With the new solar arrays installed during SM3B, the day/night disturbances no longer cause significant vehicle jitter. With the new arrays, HST jitter is characterized by two low amplitude (~5 mas) vibrational modes at 0.5 and 1.2 Hz. A larger, intermittent (and infrequent) disturbance of up to 100 mas persists, however. Fortunately HST's pointing control law damps this jitter away in about 10 seconds or less.

The overall residual from the “de-jittering” process is only ~ 0.1 mas, the small value testifying to the advantages of using a median filter in the centroid computation and to the excellent tracking of guide stars by the guider FGSs.

Figure 5.3: FGS2 Guide Star Motion at the Onset of a Day/Night Transition



This plot shows the relative position of a guide star in FGS2 along the HST V3 axis as a function of time. The large disturbance at about 157 seconds occurred as HST transitioned from orbit night into daylight. This was typical until the new solar panels were installed in March 2002 (SM3B). Significant jitter is no longer present at day/night or night/day transitions.

Drift

FGS drift was discussed in [Chapter 7](#) with regards to observation strategy, i.e., the use of check stars to track apparent motion of the FOV during the visit so it can be removed during post-observation processing. There are two different classes of drift, depending on whether one or two FGSs guided the HST during the visit. With two FGSs guiding, drift is identified as a slow but correlated wander of the targets observed more than once during the visit. The amount of drift *appears* to be related to the intensity of the bright Earth entering the telescope during target occultations. Accordingly, the drift is highest for targets in HST's orbital plane (~ 10 mas) and lowest for those at high inclination (~ 2 mas).

When only one FGS is used to guide the telescope, the drift is typically 20 mas over the course of the visit. The single guide star controls the translational motion of the spacecraft while the HST roll axis is constrained by the gyros. Gyro-induced drift *around the dominant guide star* ranges from 0.5 to 5 mas/sec, and is typically of order 1 mas/sec. Note the gyro drift is a spacecraft roll, and does not represent the translational motion of a target at the FGS (which will typically be ~ 0.01 mas/sec). Over the course of a visit, the roll drift error measured by the astrometer can build up to 40 mas or more (but is typically less than 20 mas).

Regardless of the size of the drift, it can be characterized and removed by applying a model to the check star motions, provided the visit includes a robust check star strategy: a check star observation every 5–6 minutes (described in [Chapter 7](#)). At a minimum, two check stars measured three times each are needed to model translational and rotational drift.

Cross Filter Calibrations

For a target star (or any reference stars) brighter than $V = 8.0$ to be included as part of an FGS observation, it must be observed with the neutral density attenuator F5ND. As a result of the differing thicknesses of F583W and F5ND, and possibly a wedge effect between the two filters, the measured position of the bright target in the FOV will shift relative to the (fainter) reference stars. A cross-filter calibration is required to relate these observations, as relative positional shifts may be as high as 7 mas. Also, further evidence from FGS3 indicates these shifts are field dependent. If the effect is uncorrected, a false *parallax* will occur between the science and reference targets as the star field is observed at different orientations in the FOV. Since it would be prohibitive to calibrate the cross-filter effect as a function of field location, FGS1r cross-filter calibrations will be restricted to the center of the FOV. For reference, the uncertainty after the FGS3 cross-filter calibration is ~ 0.5 mas.

5.1.3 Position Mode Epoch-Level Calibrations

Plate Scale and Relative Distortion Stability

For FGS3, the plate scale and OFAD exhibits a temporal dependence on an average time scale of ~ 4 months and a size of several tens of milli arcseconds (predominately, a scale change). The evolution of the FGS3 OFAD revealed that the variability is probably due to the slow but continued outgassing (even after 10 years!) of the graphite epoxy structures in the FGS. A long-term stability monitoring test is executed bi-monthly to help measure and characterize the distortion and relative plate scale changes and thus update the OFAD. Post-calibration residuals are on average ± 1 mas along the X-axis and Y-axis. Better performance (of order ± 0.5 mas) is achieved in the central region of the FOV.

The FGS1r Position mode stability was coarsely monitored during Cycle 7. Large scale changes in its S-Curve, attributed to outgassing effects, show that the instrument was unstable (for high accuracy astrometry) during its first year in orbit, as expected. In early 1998 the evolution slowed, and by April 1998 FGS1r's S-curves fully stabilized; a major prerequisite for the OFAD calibration was met.

The OFAD and lateral color calibrations were to have been performed during cycle 8 when the target field was at anti-sun and HST would not be roll constrained. Unfortunately this coincided with and was preempted by the Servicing Mission 3a. Rather than perform the calibrations under less favorable, roll-constrained conditions, STScI decided to defer the observations until December 2000, when the target field again has an anti-sun alignment. The analysis of the OFAD data were carried out as a “calibration out sourced” proposal led by members of the STAT from the University of Texas at Austin. The results of this calibration have been made available to STScI and reside as reference files used by the FGS calibration pipeline.

The science data that has accumulated since the beginning of cycle 8 can be fully calibrated with the OFAD calibration. Any temporal evolution since the beginning of cycle 8 is back-calibrated away by use of the long term monitoring observations that have been executing all along. Check the [FGS Web pages](#) for updates with regard to the OFAD calibrations.

Errors Associated with Plate Overlays

The errors associated with several of the corrections described above will not manifest themselves until data from individual visits are compared. The most dominant source of Position mode error are the OFAD and changes in the plate-scale. The derivation of a plate scale solution is described in the [FGS Data Handbook](#). In general, for regions near the center of the pickle, residuals are smaller than 1 mas if the reference star field is adequately populated.

5.2 Transfer Mode Calibrations and Error Sources

[Table 5.2](#) summarizes Transfer mode sources of error and associated calibrations. Each entry is described in the subsections below.

A Transfer mode observation contains multiple scans of a target. To obtain optimal S/N values, the individual scans are cross-correlated, binned, and co-added. The reliability of this process is dominated by spacecraft jitter for targets with $V < 14.5$, and by photometric noise for fainter targets.

Background and Dark Subtraction

Targets fainter than $V \sim 14.5$ are increasingly affected by dark counts which reduces the amplitude of the S-Curve (since these contributions are not coherent with the light from the star. see [Chapter 7](#)). The instrumental dark counts have been measured as part of the STScI FGS calibration program (and are listed in [Table 2.1](#)). These values are needed for the analysis of data from Transfer mode observations of stars with $V > 14$.

Table 5.2: FGS1r Transfer Mode Calibrations and Error-Source Summary

Correction	Pre-Calibration Error Extent	Calibration Error (mas)	Comments
Background and detector noise	-	-	For bright backgrounds, use data serendipitously acquired during the FGS servo slew to the target. For dark measurements, use STScI calibration data.
HST jitter	2-4 mas: quiet; 50-150: extreme	< 0.1 during quiescence	Use guide star data to remove HST jitter. Highly corrupted scans are deleted.
Drift	5-20 mas: 2 guide star FineLock. 12-60: 1 guide star plus gyro roll control	< 0.5	Cross correlation of S-Curve scans during post observation data processing removes drift errors.
S-Curve temporal variability	~1% in FGS1r	limits resolution	Monitor standard star (Upgren69).
S-Curve color dependence	~2%	limits resolution	Use calibration point source (i.e., an unresolved star) of appropriate (B-V) color.

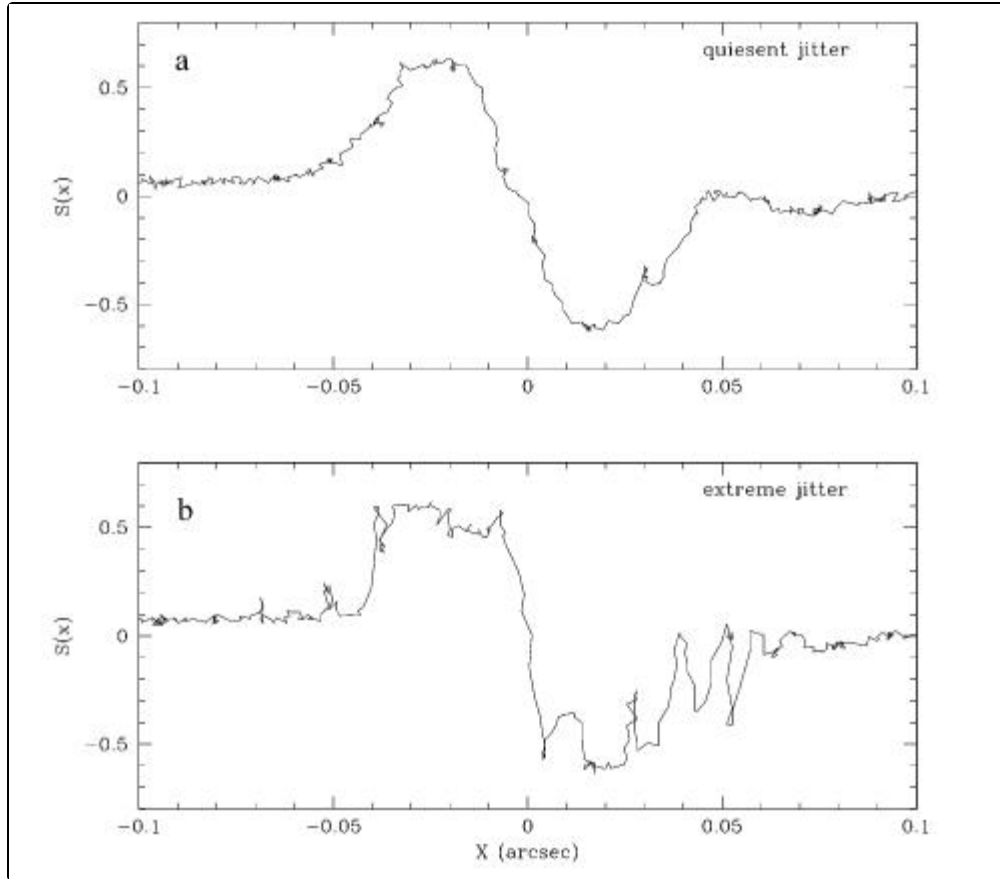
PMT Sensitivity Differences

Although individual PMT sensitivities in an FGS differ, these differences do not introduce a significant source of error in Transfer mode observations. Differences in the PMT response manifest themselves as a bias (offset) of the S-Curve. This bias is present in the calibration standard star S-Curves (the single stars) as well, and so the effect is neutralized when deconvolving the science target Transfer Function into its component single S-Curves (provided the spectral colors of the science and reference targets are well matched).

Jitter

Typically, quiescent vehicular jitter is about 2–4 mas in amplitude on timescales of minutes. With the solar panels installed in March 2002 during SM3B, the large 150 mas amplitude disturbances associated with the day/night orbital transitions of *HST* do not occur. Spacecraft jitter is removed by using the guide star centroids for quiescent times, or by eliminating intolerably corrupted scans or segments of scans from the co-addition process. For illustration, [Figure 5.4](#) shows the effects of jitter on the FGS1r interferogram (single scan).

Figure 5.4: Effects of Jitter on an FGS1r S-Curve (single scan)



The quiescent scan ([Figure 5.4a](#)) shows features due to jitter - like the jump in $S(y)$ around 0.03 arcsecond - which can be filtered out during post-observation processing. Unfortunately, the extreme effects of vehicle jitter on the S-Curve shown in [Figure 5.4b](#) cannot be corrected. Scans such as this are deleted from further consideration in the analysis. Note the small variations in the S-Curve's wings seen near the extreme edges of the plot (i.e., $\pm 0.08''$) are due to photometric noise (the data presented in this example are from an observation of a bright $V=9$ star).

Drift

Drift is defined in [Chapter 7](#), and its application to Position mode observations has been discussed earlier in this chapter. Drift is also apparent in Transfer mode observations but its removal from the raw data is straightforward; the cross-correlation of S-Curves, prior to binning and co-adding, automatically accounts for drift. Each individual S-Curve is shifted so that the particular feature of the S-Curve used for the cross correlation coincides with that of the fiducial S-Curve. However, the reliability of implicitly removing the drift is only as good as the accuracy of the cross correlation procedure, which becomes photon noise dominated for stars fainter than $V=15$ (i.e., cross correlation of scans is not reliable for $V>15$, hence drift can not be removed from such observations).

For bright stars with $V < 13$, FGS drift is estimated to degrade the resolution of Transfer mode observations by about 0.5 mas. For fainter stars, the degradation is worse. If an observation of a faint star ($V > 15$) was subject to typical drift (10 to 12 mas), then the estimated loss of angular resolution would be ~ 3 mas.

Instrumental Stability

Analysis of observations of resolved objects (i.e., binary systems or extended sources) involves the deconvolution of the observed transfer function using reference S-Curves of point sources. The repeatability, or temporal stability, of point-source S-Curves has a direct effect on the reliability (or accuracy) of the scientific result. FGS3 continued to demonstrate a variability of $\sim 15\%$ in its X-axis S-Curve (as determined from repeated observations of a standard star). This effectively rendered FGS3 unreliable for observing close (separations < 20 mas) binary systems. However, FGS1r has demonstrated repeatability at the 2% level, implying reliable measurements of binary systems down to 7 mas.

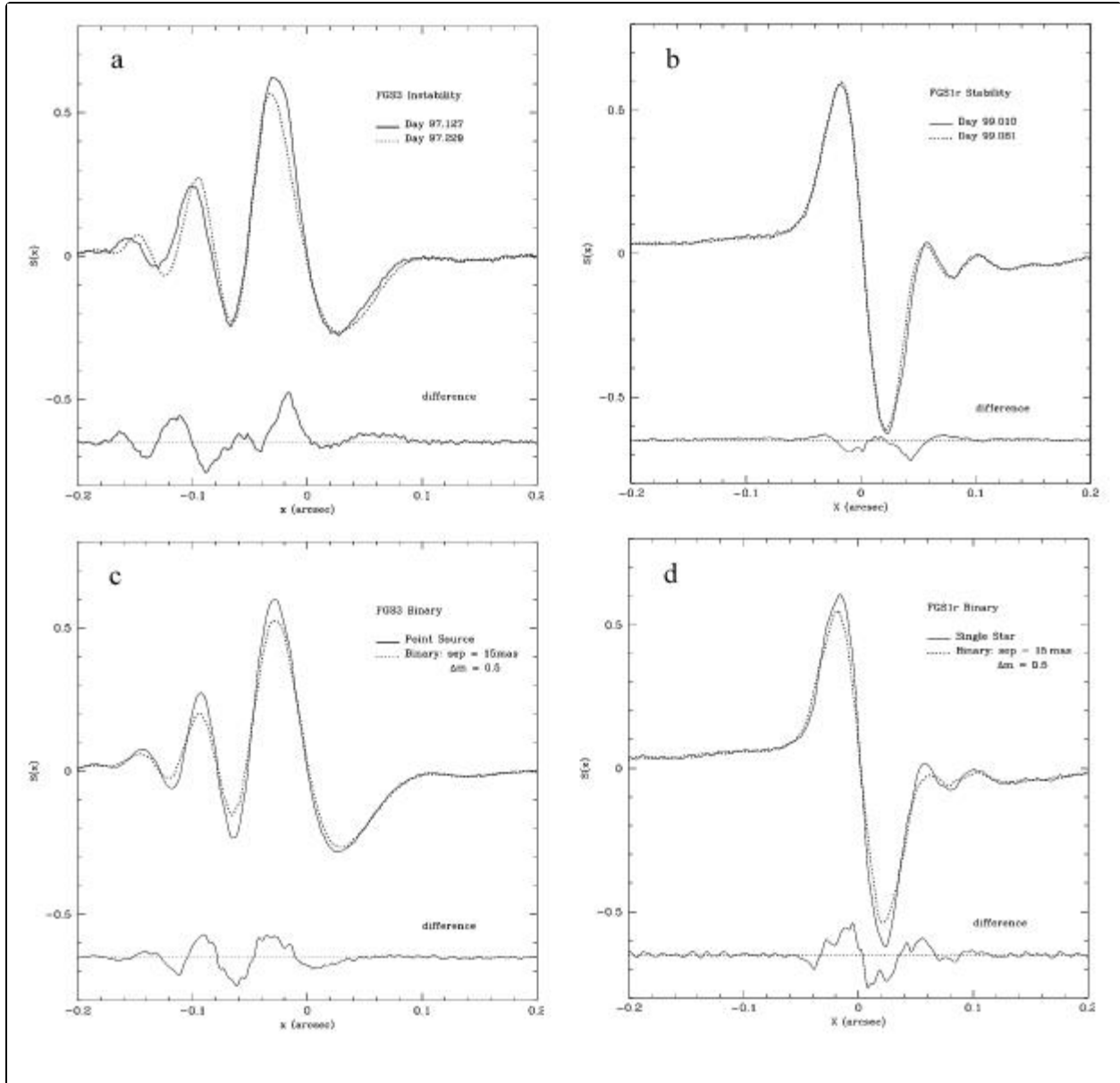
Figure 5.5 illustrates FGS3's persistent variability and FGS1r's stability over comparable timescales. Figure 5.5a shows FGS3's inherent variability in the S-Curves of the same point source over a 102-day span in 1997. Note this intrinsic variability in the instrument is indistinguishable from its interferometric response to a 15 mas binary with $\Delta m = 0.5$ mag (when compared with a point-source, as shown in Figure 5.5c). In contrast, the stability of FGS1r (Figure 5.5b) easily permits detection of the 15 mas binary system (Figure 5.5d) when compared to a point-source. We note the "difference" seen in Figure 5.5dd are due to systematic changes in the observed interferogram (i.e., the object is resolved), not random effects.

As was discussed in Chapter 4, FGS1r has shown a slow "evolution" of its y-axis S-curve. This should not compromise the reliability of this instrument for observing close binary systems; STScI will continue to observe calibration standards in each cycle as needed so that GOs have access to calibration data appropriate of a given epoch.

Interferometric Response and Source Color

The morphology and amplitude of the S-Curve is sensitive to the spectral color of the source. The point-source reference S-Curve used for comparison to the observed fringes of a science target should match the color of the target to within $\delta(B - V) = 0.3$, especially when analyzing observations of close binaries (separations $< \sim 40$ mas). The point source standards observed by FGS1r as part of the yearly observatory calibration plans are chosen to meet the needs of the cycle's GO science program. This includes consideration of both the science target colors as well as the filter (F583W or F5ND) to be used by the GOs. For example, the cycle 10 FGS1r reference star color library is given in the Table 5.3.

Figure 5.5: Temporal Stability: FGS3 v. FGS1r



The two plots at the top compare the fringes of FGS3 (left) and FGS1r (right) from observations of point sources taken at two different times. Clearly FGS3 shows significantly more variability than FGS1r. The plots in the bottom row compare the FGS3 and FGS1r fringes of a point source to that of a 15 mas binary. Given FGS3's temporal variability (top left plot), the detection of the binary (bottom left plot) is questionable, unlike the reliable detection by FGS1r.

⚠ The point-source calibration S-Curves are obtained only at the center of the FGS1r FOV. Other locations in the FOV are not routinely calibrated.

Table 5.3: Library of cycle 10 calibration point source S-curves

Star	R.A.	Declination	V mag	B-V	Filter
WD0148+476	01 52 02.9	+47 00 06	12.5	0.0	F583W
Latcol-B	05 59 27.3	+22 34 39	10.5	0.2	F583W
Upgren69	00 42 42.2	+85 14 14	9.6	0.5	F583W
HD 233877	11 52 54.1	+49 23 46	9.7	1.1	F583W
SAO185689	17 45 06.9	-29 08 37	9.3	1.5	F583W
Latcol-A	05 59 20.1	+22 34 50	9.7	1.9	F583W
μ Col	05 45 59.8	-32 18 23	5.2	-0.3	F5ND
HD 143101	16 01 06.5	-54 34 40	6.1	0.2	F5ND
HD 31975	04 53 05.6	-72 24 27	6.3	0.5	F5ND
HD 37501	05 34 57.4	-61 10 34	6.3	0.8	F5ND
HD 59149	07 29 30.7	+19 37 59	6.7	1.3	F5ND

Transfer Mode Scale as a Function of HST Roll Angle

Testing of FGS1r during its commissioning in Cycle 7 revealed that the measured separation and position angle of the stars in a binary system is sensitive to the system's orientation relative to the interferometer axis and hence the HST roll angle. Over time, as a system is observed at a variety of HST roll angles, this introduces systematic errors into the derivation of the binary's apparent orbit. The error in the measured separation of the stars can be as large as $\sim 1\%$ of the true projected separations, so measurements of wide binaries are affected more than those of close systems. The effect is believed to be due to a small rotation error of the Koesters prism(s) about the normal to its entrance face.

During Cycle 9 a wide binary (KUI 83, component separation $\sim 0.3''$) was observed with FGS1r in Transfer mode at three different *HST* roll angles ($V3_{\text{roll}} = 25, 43, 60$ degrees). The measured total separation of the components was constant to about 1 mas, indicating that the scale is not dependent upon vehicle roll, in contradiction to the Cycle 7 results. STScI will monitor this aspect of FGS1r's performance, but at a low frequency (approximately every 2 to 3 years).

5.3 Linking Transfer and Position Mode Observations

It is possible to use the FGS in both Transfer and Position mode during a given observing session (visit). As was mentioned in [Section 3.4](#), by using Transfer mode observations to determine a binary system's true relative orbit, and using Position mode observations of nearby reference stars (and perhaps the binary as well) to determine the binary's parallax, the system's total mass can be derived. Furthermore, if the data are of sufficient quality, i.e., if the uncertainty in the position of each component with respect to the reference stars is small compared to the semi-major axis of the binary's orbit, then the motion of each component about the system's barycenter can be determined. From this information, the mass ratio, and hence the mass to luminosity ratio of each of the two stars, can be calculated.

Investigations of an extended source, such as a giant star, can also benefit from a combination of Transfer and Position mode observations. If the FGS in Transfer mode can resolve the disk and measure its angular size, and nearby stars are measured in Position mode to derive the object's parallax, then the physical size of the disk can be determined.

In order to achieve these scientific objectives, the Transfer mode data must be related to the Position mode data. If the binary is observable in Position mode, then it is straightforward to determine the offsets between the Position mode reference frame and Transfer mode positions. If the binary cannot be observed in Position mode, then the task of relating the Transfer data to the Position data is more complex.

Linking a Transfer mode observation of a binary system to Position mode observations of reference stars in the same visit requires that the x,y coordinates of each of the binary's components, derived from analysis of the Transfer function, be mapped onto the same x,y coordinate system as the Position mode observations (the visit level "plate"). This implies that all pertinent corrections and calibrations applied to Position mode data must be applied to the Transfer mode centroids, i.e., visit-level corrections for low frequency oscillations of the spacecraft's pointing, FOV drift, the OFAD, and the differential velocity aberration. The level of difficulty in accomplishing this task depends on the structure of the binary (i.e., the separation of the components and their relative brightness).

More information on analysis techniques can be found in the [FGS Data Handbook](#).

5.4 Cycle 21 Calibration and Monitoring Program

5.4.1 Active FGS1r Calibration and Monitoring Programs

A short summary is given for each FGS1r calibration and monitoring observation included in the Cycle 21 calibration plan. For specific information, please refer to the STScI [FGS Web page](#) (under the topic FGS and Calibration Plans”) and to the *HST* Schedule and Program Information Web page: <http://www.stsci.edu/hst/observing/program-information>

5.4.1 Active FGS1r Calibration and Monitoring Programs

- 13607 Long Term Stability of FGS1r in Position Mode
 - This proposal uses FGS1r in POS mode to observe selected stars in M35 to obtain astrometric data used to update the values of the star selector servo parameters rhoA and kA, which are used to convert raw star selector encoder values to the local FGS (x,y) detector frame. Moreover, these data also allow both an on going monitoring of the OFAD calibration as well as updates to the M35 catalog accounting for proper motion of the observed stars. In this cycle, this program is one HST orbit that executes in August 2014, as that is the only time that FGS1r is used as a science instrument in POS mode (for the currently executing science programs).
- 13608 A Field Dependent Calibration of the F5ND-F583W Cross-Filter Effect
 - This is a two orbit *HST* proposal using FGS1r to observe two bright stars in the Hyades. These stars are approximately 90" apart. FGS1r is used to observe each star several time, alternating between F583W and F5ND, to measure the cross-filter shift (wedge effect) of the star's position. Orbit #1 places one of the stars at FGS1r center to update the Transfer mode S-curve library, as well as the F5ND-F583W wedge effect at pickle center. The *HST* orient is chosen such that second star is placed in the vicinity go the FGS FOV where science targets have been observed using the F5ND attenuator. The second *HST* orbit places the two stars in the vicinity of where other science programs observed science targets with the F5ND. The required *HST* orients cause these visits to schedule in late 2013.

5.5 Special Calibrations

It is expected that the same calibrations outlined here for recent cycles and the current Cycle 28 plan will be maintained for Cycle 29.

It is the intention of STScI to develop a calibration program that most effectively balances the needs of the community for obtaining excellent science results from the instrument with the limited resources available (e.g., a nominal limit of 10% time available for calibration). Common uses of the instrument will be fully calibrated.

In special circumstances proposers may wish to request additional orbits for the purpose of calibration. These can be proposed in two ways and should be for calibrations that are not likely to be in the core calibration programs. An example of a non-core calibration would be one that needs to reach precision levels well in excess of those outlined in [Tables 5.1](#) and [5.2](#).

The first type of special calibration would simply request additional orbits within a GO program for the purpose of calibrating the science data to be obtained (see the [Call for Proposals](#)). In this case the extra calibration would only need to be justified on the basis of the expected science return of the GO's program.

The second type of special calibration would be performed as a general service to the community via Calibration Proposals ([HST Proposal Categories](#)). In this case the calibration observations should again be outside the core responsibilities of the FGS group to perform, and furthermore should be directed at supporting general enhancement of FGS capabilities with the expectation of separately negotiated deliverables if time is granted.

Proposers interested in obtaining either type of special calibration should consult with Instrument Scientists from the FGS Group via questions to the [Help Desk](#) at least 14 days before the proposal deadline in order to ascertain if the proposed calibrations would be done at STScI in the default program.

Observations obtained for calibration programs will generally be flagged as non-proprietary.

Chapter 6: Writing a Phase II Proposal

Chapter Contents

- [6.1 Phase II Proposals: Introduction](#)
- [6.2 Instrument Configuration](#)
- [6.3 Special Requirements](#)
- [6.4 Overheads](#)
- [6.5 Proposal Logsheet Examples](#)

6.1 Phase II Proposals: Introduction

6.1.1 Required Information

6.1.2 STScI Resources for Phase II Proposal Preparation

6.1.1 Required Information

The information required for Phase II proposals are:

- Precise target information: positions accurate to $\pm 3''$, and V magnitude accurate to ± 0.5 magnitudes. If possible, the (B – V) color should be specified when known. The color is important for archival considerations as well to help the FGS Instrument Scientist determine if the standard calibrations support the needs of the proposal.
- Configuration and scheduling instructions for each exposure and visit, expressed in the specified proposal syntax.
- The relationship between the visits: scheduling, relative orientations, etc.
- Justification for special scheduling or configuration requirements.

 **Important:** A clear explanation for:

1) the use of special requirements;

2) the special design of a program; or

3) the calculation of an exposure time, orient angle, or target offset, etc., will help STScI during the review and verification process.

Text can be included in the “Additional Comments” section of the proposal or in the justification for real-time and special requirements. If an action is critical for the successful implementation of an exposure line, a short one-line comment (in the comments syntax) should be placed on individual exposure lines.

6.1.2 STScI Resources for Phase II Proposal Preparation

- **APT:** The Astronomer’s Proposal Tool is the STScI interactive graphical software interface for both Phase I and Phase II proposal preparation. It provides proposal preparation tools and several verification and error-checking phases: proposal syntax, operational feasibility, and schedulability. APT also will offer an option to prepare your Phase II program in a text format whose syntax is similar to the previous STScI proposal preparation system, RPS2. Examples of proposals in this syntax are provided in [Section 6.5](#). You are strongly encouraged to make full use of the APT software. It is available on the website at: apt.stsci.edu.
- **Program Status:** For proposal status, scheduling (visit level) information, weekly calendars, recent proposal listings, please consult the Hubble Space Telescope Web pages at: <http://www.stsci.edu/hst/observing/program-information>.
- **Contact Scientist:** After HST observing time has been allocated by the TAC, a Contact Scientist may be assigned to the proposal. The objective of the Contact Scientist is to ensure the scientific return of the observing program is maximized.

6.2 Instrument Configuration

6.2.1 Optional Parameters for FGS Exposures

This section is designed to complement the section on FGS instrument parameters contained in the Phase II Proposal Instructions. [Table 6.1](#) summarizes the FGS instrument parameters.

Table 6.1: FGS Instrument Parameters

Config	Aperture	Sp_Element	Opmode	Optional_Parameters
FGS	1, 2, 3 (FGS1=FGS1r)	F5ND F550W F583W F605W(FGS1r, FGS3) F650W (FGS 2) PUPIL	POS	ACQ-DIST, ACQ-MODE, COUNT, FESTIME, NULL, LOCK
			TRANS	ACQ-DIST, ACQ-MODE, SCANS, STEP-SIZE

Aperture

The aperture must be defined as either “1”, “2”, or “3”. Only FGS1r (aperture=1) is calibrated as a science instrument. FGS2 and FGS3 should not be used for science observing. For illustrations of the FGS1r field of view in the HST focal plane, refer to [Chapter 1](#).

Spectral Element

“Spectral Element” refers to filters, etc. chosen for the observation. For FGS1r, the available filters are: F583W, F5ND, PUPIL, F605W, and F550W. Only one filter can be in place for an exposure, though multiple filters can be used during a visit (check that calibrations are available for the configuration). Recommendations for specific mode and filter combinations are discussed in [Chapter 5](#) and [7](#). [Table 6.2](#) presents a summary of the calibrated modes and filter configurations.

Table 6.2: Summary of Calibrated Mode and Filter Combination

Mode	Filter	Status	Comments
Pos mode:	F583W	Calibrated across entire FOV	OFAD in F583W only
Pos mode	F5ND	Calibrated at the center and a small number of selected locations in the FOV	Cross-filter calibration with F583W

Trans mode:	F583W, F5ND; Others as needed	<ul style="list-style-type: none"> • All calibrations at FOV center • Select reference S-Curves from library of standard stars • If needed, propose for calibration time to observe a reference standard star at the same epoch as the science visit (see Chapter 7). 	Availability of standard stars with appropriate spectral energy distributions, i.e., colors of reference star and science target should differ by no more than $\delta(B-V) \sim 0.3$ for a given filter (F583W or F5ND).
-------------	-------------------------------	--	---

Mode

Two operation modes are available: Position mode (POS) for measuring relative astrometric positions of targets in the FGS FOV and Transfer mode (TRANS) for obtaining high angular resolution interferometry.

6.2.1 Optional Parameters for FGS Exposures

A program is customized by specifying optional parameters for each exposure. [Table 6.3](#) and [Table 6.4](#) list the optional parameters, default values, and recommended settings for Pos and Trans modes, respectively.

⚠ Many of the optional parameters have default values. In such cases, the entry for that optional parameters may be omitted. If an observer wishes to override the default value, the parameter and its value must be specified.

Table 6.3: Pos Mode Optional Parameters

Optional Parameter	Allowed Values	Comments and Recommendations
ACQ-DIST	DEF (default=10), 0.0 to 90.0 Units: arcsec	Determines the size (in arcseconds) of the search region. For ACQ-MODE=SEARCH, ACQ-DIST is the maximum radius of the search spiral. <i>Recommendation:</i> Although Search radii up to 90 arcsec are allowed, larger values <i>must be used with caution</i> , i.e., the larger the search radius, the more potential to acquire a spurious nearby star. If the target coordinates are expressed with respect to the Guide Star System, the default value of 10 arcsec (radius) should be sufficient to find the target. Typically the target is found with 0.3 to 1.0 arcsec. Note that large search radii incur a large overhead (time) cost. <i>Reference:</i> Appendix A: Target Acquisition

ACQ-MODE	SEARCH (default) Units: None	<p>Determines the strategy for locating the target. The Search Phase is the initial outward spiral to find and identify the target. The sequence of Search, CoarseTrack, WalkDown, and FineLock is the standard astrometry target acquisition scenario. No other options are available for GO programs.</p> <p><i>Requirement:</i> Default “SEARCH”</p> <p><i>Reference:</i> Appendix A: Target Acquisition</p>
COUNT	DEF (default), 1-2621400 Units: FGS PMT counts	<p>Expected count rate [target + background]. When the default is set, the count rate is calculated (by the proposal processing software) from the target V magnitude, filter, and aperture. The default background rate (from in-orbit measurements) is 712 counts/sec for all four PMTs.</p> <p><i>Recommendation:</i> Allow the system to select the default based upon the target’s specified visual magnitude. The default values are calculated using data from on-orbit photometric calibrations. The value of COUNTS is also used to determine the default FESTIME.</p> <p>A few special cases may require non-default values and are discussed in the text.</p> <p><i>Reference:</i> Chapter 7: See sections on Pos and Trans mode Signal to Noise and Exposure calculation sections.</p>
FESTIME	DEF (default), 0.025, 0.05, 0.1, 0.2, 0.4, 0.8, 1.6, 3.2 Units: seconds	<p>Sets the averaging time for the Fine Error Signal (in seconds). The FESTIME also determines the rate at which the star selectors are adjusted to null the fine error signal. <i>The default value for Pos mode is calculated from the COUNT parameter if explicitly entered, or if COUNT defaults to the V magnitude and the filter. All Trans mode observations use FESTIME = 0.025 seconds.</i></p> <p><i>Recommendation:</i> The algorithm that selects the default FESTIMEs from the specified brightness of the target is based on photon statistics and a conversion from photon noise to equivalent positional error. For fainter targets, longer integration times are supplied by the default algorithm to assure that the FGS can track the fringe and remain in FineLock.</p> <p>For non-point sources, the S-Curve amplitude is reduced because of the increased contribution of the background or companion. In these cases, it may be desirable to adjust the FESTIME. Please consult with STScI.</p> <p><i>Reference:</i> Chapter 7: See Sections on Pos and Trans mode Signal to Noise and Exposure calculation sections.</p>

LOCK	FINE (default), COARSE, 0.0–1.0 Units: None	<p>The method used by the astrometer to track the science or reference target. (Note, this parameter does not specify the HST guiding mode). Because of the excessive wear to bearings inside the instrument, CoarseLock, which is inferior to FineLock, is no longer allowed.</p> <p><i>Requirement:</i> Fine.</p> <p><i>Reference:</i> Chapters 5 and 7.</p>
NULL	YES, NO (default) Units: None	<p>Determines whether the next FESTIME begins immediately after the previous one or not until the star selectors have been repositioned. This parameter may be applicable for very fast moving target. Observers should consult with STScI before specifying non-default values.</p> <p><i>Recommendation:</i> This use of this parameter is limited to a few specific observation scenarios (tracking solar system objects). Most standard astrometry programs benefit from NULL=NO.</p> <p><i>Reference:</i> STScI will alert the proposer if a non-default value is required.</p>

Table 6.4: Trans Mode Optional Parameters

Optional Parameter	Allowed Values	Comments and Recommendations
ACQ-DIST	DEF (default = 10), 0.0 - 90.0 Units: arcsec	<p>Determines the size (in arcseconds) of the search region. For ACQ-MODE=SEARCH, ACQ-DIST is the maximum radius of the search spiral.</p> <p><i>Recommendation:</i> Although a search radius of up to 90 arcsec is allowed, larger values must be used with caution, i.e., the larger the search radius, the more potential to acquire a spurious nearby star (spoiler). If the target coordinates are expressed with respect to the Guide Star System, the default value of 10 arcsec (radius) should be sufficient to find the target. HST’s pointing accuracy usually places the target within 1 arcsec of the expected location in the FGS. Note that large search radii incur a large overhead (time) cost.</p> <p><i>Reference:</i> Appendix A: Target Acquisition</p>
ACQ-MODE	SEARCH (default) Units: arcsec	<p>Determines the strategy for locating the target. The search phase is the initial outward spiral to find and identify the target. The sequence of Search, CoarseTrack, WalkDown, and FineLock is the standard astrometry target acquisition scenario. No other options are available. (Trans mode fringe scanning commences after the FineLock acquisition.)</p> <p><i>Requirement:</i> Default “SEARCH”</p> <p><i>Reference:</i> Appendix A: Target Acquisition</p>

SCANS	1 (default) -200 Units: None	<p>Determines the number of separate scan lines. Successive scans are taken in opposite directions along a 45 degree diagonal path in the FGS detector space coordinates.</p> <p><i>Recommendation:</i> Determine the number of scans to achieve the required signal-to-noise.</p> <p><i>Reference:</i> Chapter 7</p>
STEP-SIZE	1.0 (default) 0.3-10.0 Units: mas	<p>The average angular distance (in mas) stepped by the IFOV along an interferometric axis in 0.025 seconds. To achieve the best results, step sizes of 0.3 or 1 mas should generally be selected.</p> <p><i>Recommendation:</i> Value depends on the science target and goals of the observation, required resolution and signal-to-noise.</p> <p><i>Reference:</i> Chapter 7</p>

6.3 Special Requirements

6.3.1 Visit-Level Special Requirements

6.3.2 Exposure-Level Special Requirements

In this section, we describe several special requirements which are often needed in an FGS Phase II observing proposal.

6.3.1 Visit-Level Special Requirements

Many visit-level special requirements are outlined in the Phase II Proposal Instructions. Those most applicable to FGS programs are:

Spacecraft Orientation ORIENT:

- **Definition:** The angle from North to the +U3 axis of the HST measured in the direction of +U2 (counter clockwise when North is up and East is to the left). The `ORIENT` special requirement is useful for orienting *HST* so that astrometric reference stars fall within the FGS FOV or for aligning a binary star's position angle relative to an FGS axis. Along with the `ORIENT` angle, a tolerance must be specified.
- **Calculation:** Two angles must be known in order to calculate a special `ORIENT` angle: the angle from North to the eigenaxis of the target or target field (measured in the direction of East), and the angle between the +U3 axis to the FGS $+Y_{\text{POSTARG}}$ axis measured in the direction of +U2. (Note that the values are different for FGS1r and FGS3.)
- **Accuracy:** The *HST* roll angle precision depends on the relative guide star position errors and the FGS alignment calibration errors (when two guide star FineLock is used). The pre-designated roll angle for a two-guide star FineLock tracking will be accurate to ≤ 0.04 degrees.
- **Recommendations when `ORIENT` is used in the proposal:**
 - Explain, in the "Additional_Comments" text section of the proposal, the method used to calculate `ORIENT` so that STScI schedulers and instrument scientists understand (and can defend the requirement).
 - `ORIENT` is considered a Special Scheduling Request and as such, must be justified in the proposal and will affect the schedulability of the visit. Setting the `ORIENT` tolerance to as large a range as possible (and still be within the bounds of the scientific requirements) will help to lessen the scheduling impact.

Timing Requirements:

- **Definition:** Timing links between visits are fairly common for FGS observations. For parallax programs, timing requirements are generally invoked so that a target field is observed at times of maximum parallax factor (every six months). Trans mode observations may also make use of timing requirements, such as observing a binary system at specific orbital phases. Timing links on the Visit level include: BEFORE, AFTER, BETWEEN [dates], GROUP [the following visits] WITHIN [xxx hours, or xxx orbits], etc. See the [Phase II Proposal Instructions](#) for the complete list.
- **Note:** Timing requirements place restraints on the schedulability of the visit. Specify the largest tolerance on the timing constraint that the science can accommodate.

6.3.2 Exposure-Level Special Requirements

All available exposure-level special requirements are described in detail in the Phase II Proposal Instructions. Of these, the following three types are most often used in connection with FGS observations.

POS TARG:


- *Definition:* The ΔX and ΔY offset of a target from the standard aperture reference position are the POS TARG coordinates. They are specified in arcseconds and with respect to special coordinate systems which are illustrated and described in Chapter 2 and in the [Phase II Proposal Instructions](#). (Note, the POS TAR reference frame is not in the same coordinate system as the FGS detect reference frame.) POS TARG is used to position a target at various points in the FGS FOV. For example, a common use in Pos mode observations is to place the science target at a position in the FOV such that reference stars will also be within the FOV. In Trans mode, since calibrations are only available at the center reference point, the non default (0,0) use of POS TARG is not recommended.

SAME POS AS:

- *Definition:* The position and orientation of the spacecraft will be held constant over the course of all exposures within a given visit when the special requirement SAME POS AS is invoked. This requirement is virtually always used for Pos mode visits.

SEQ NON-INT:

- *Definition:* To ensure that all exposures within a visit are scheduled in the same orbit, the SEQ NON-INT special requirement should be used, otherwise the system may divide the exposures over several orbits, requiring guide star re-acquisitions and incurring instrumental overheads taking up to 12 minutes, as well as exceeding the number of orbits awarded by the TAC to the proposal.

 ***Do not hesitate to explain the use of any special requirements in the proposal text. The more explanation, the easier for STScI to understand your requirements and schedule the proposal.***

6.4 Overheads

6.4.1 Pos Mode Overheads

6.4.2 Trans Mode Overhead

The assessment of the total spacecraft time needed by a program should take into account the overheads associated with various types of observations. Overheads are incorporated into the APT proposal processing algorithm. They are explicitly pointed out here for illustration.

6.4.1 Pos Mode Overheads

[Table 6.5](#) lists the estimated overheads associated with guide star acquisitions, the initial configuring (standby to operate) of the FGS for science observing, the time for slewing the IFOV from target to target in the observing plan, the acquisition of target stars, and finally configuring the FGS at the end of the observing sequence (operate to standby).

The acquisition time of an astrometric target depends upon the target's magnitude. Fainter stars require longer integration times (FESTIME) of the fine error signal during the walkdown to finelock. For example, the FESTIME used to acquire a $V=10$ star is 25 msec, while for a $V=16$ star $FESTIME=3.2$ seconds. Columns 2 and 3 in [Table 6.6](#) list an average overhead for each exposure and the recommended total exposure time to be entered on the phase2 proposal (see [Table 4.5](#)) as a function of target magnitude. Total time required for a given exposure is estimated by combining columns 2 and 3. The additional overheads indicated in [Table 6.5](#) must be included when determining the total time available for collecting science data. Fortunately, APT calculates and includes all of these overheads when processing a phase2 proposal.

Table 6.5: Pos Mode Overheads

Activity Description	Duration	Comments
Initial guide star acquisition	6 min	Two-guide star FineLock (5 min. for re-Acq)
Initial instrument configuration	4 min.	Incurred at the beginning of every orbit
IFOV slew to target	17 sec + 6 x dist (in arcmin)	for slews between targets in the FOV.
Astrometry target acquisition: <ul style="list-style-type: none"> • Search • CoarseTrack • FineLock 	<ul style="list-style-type: none"> • 5 sec • 13, 21 sec • varies as V 	(Each science target and reference star) <ul style="list-style-type: none"> • For a 10 arcsec search radius. • For $V < 14$ and $V > 14$ respectively • For $V < 12$: ~3 sec; For $V > 16$: ~400 sec
Instrument shut down	2 min.	Incurred at the end of every orbit

Table 6.6: Pos Mode Overheads and Exposure Time vs. -Magnitude

V Magnitude	Estimated Overhead per exposure (minutes)	Exposure Time ¹ in seconds
8–12	0.6	20
13	0.7	20
14	2	30
15	3	45
16	8	45
17	8	50

¹ For total spacecraft time, add columns 2 and 3.

6.4.2 Trans Mode Overhead

The overheads for the activities which occur during Trans mode exposures are listed in [Table 6.7](#). The guide star acquisitions, instrumental configurations at the beginning and end of the observing sequence, and astrometry target acquisition activities for Pos mode and Trans mode are identical through the CoarseTrack phase. The FineLock phase in Transfer mode does not depend upon the star's magnitude. (The star is not really acquired in FineLock. Setting the FineLock flag allows for the transition to fringe scanning under the control of the 486 SSM computer.)

Table 6.7: Trans Mode Observing Overheads

Activity Description	Duration	Comments
Initial guide star acquisition	6 min	Two-guide star FineLock (5 min. for re-Acq)
Initial instrument configuration	4 min.	Incurred at the beginning of every orbit
Astrometry target acquisition: <ul style="list-style-type: none"> • Search • CoarseTrack • FineLock 	<ul style="list-style-type: none"> • 5 sec • 13, 2 1 sec • 1 sec 	(Each science target and reference star) <ul style="list-style-type: none"> • For a 10 arcsec search radius. • For V < 14 and V > 14 respectively • For V < 14 and V > 14 respectively
Time for IFOV to slow and reverse scan direction	12 sec /scan	This overhead is incurred for each scan, regardless of the scan length or step_size.
Instrument shut down	2 min.	Incurred at the end orbit

6.5 Proposal Logsheet Examples

- [6.5.1 Parallax program using FGS1r in Pos mode](#)
- [6.5.2 Determining a binary's orbital elements using FGS1r in Trans mode](#)
- [6.5.3 Mass determination: Trans and Pos mode](#)
- [6.5.4 Faint binary with Trans mode: special background measurements](#)

This section provides several examples of RPS2 formatted proposal logsheets for the following types of investigations:

- Parallax program using FGS1r in Pos mode
- Determining a binary's orbital elements using FGS1r in Trans mode.
- Mass Determination: Trans and Pos mode
- Faint binary with Trans mode: special background measurements.

While formatted exposure logsheets became obsolete when APT replaced RPS2, the logsheets provided here are intended to assist proposers in to obtain a high level understanding of an FGS observing program within a single HST orbit.

6.5.1 Parallax program using FGS1r in Pos mode

- **Goal:** Determine the parallax and proper motion of star, "OGF_1".
- **Scenario:**
 - The program requires three visits, at 0, 6, 12 months intervals, each of which is timed to occur at epochs of maximum parallax factors. During each visit the science target and reference stars will be observed multiple times in Pos mode.
 - A special orientation is needed to align the FGS FOV so that the target and selected reference stars fall within the FOV (and hence are observable!). The appropriate Orient range can be determined by using special tools (e.g., PICKLES or VTT)
 - Filter for all targets with $V > 8$: F583W.
 - Reference Star Geometry: Six reference stars near science target; POS TARG required to fit all reference stars in the pickle. See [Figure 6.1](#).
- **Special Considerations:**
 - The need for special orientation must be explained in the text justification section.
 - The science target must be shifted from FGS1r aperture reference point (center of FOV) in order to fit all (i.e., OGF-21-REF) stars in the FOV. Appropriate POS TARG can be determined from PICKLES or VTT. Contact STScI Help desk for assistance if necessary.
- **Target Logsheet:**
 - See the [HST Phase II Proposal Instructions](#) for assistance.
 - Please include color information on all targets if available so the need for color-related calibrations can be assessed by STScI.

Figure 6.1 illustrates the field geometry and the orient angles of a typical FGS observation, while Table 6.8 summarizes the details of the exposures in the visit.

Figure 6.1: Example 1: Field of View at Special Orientation

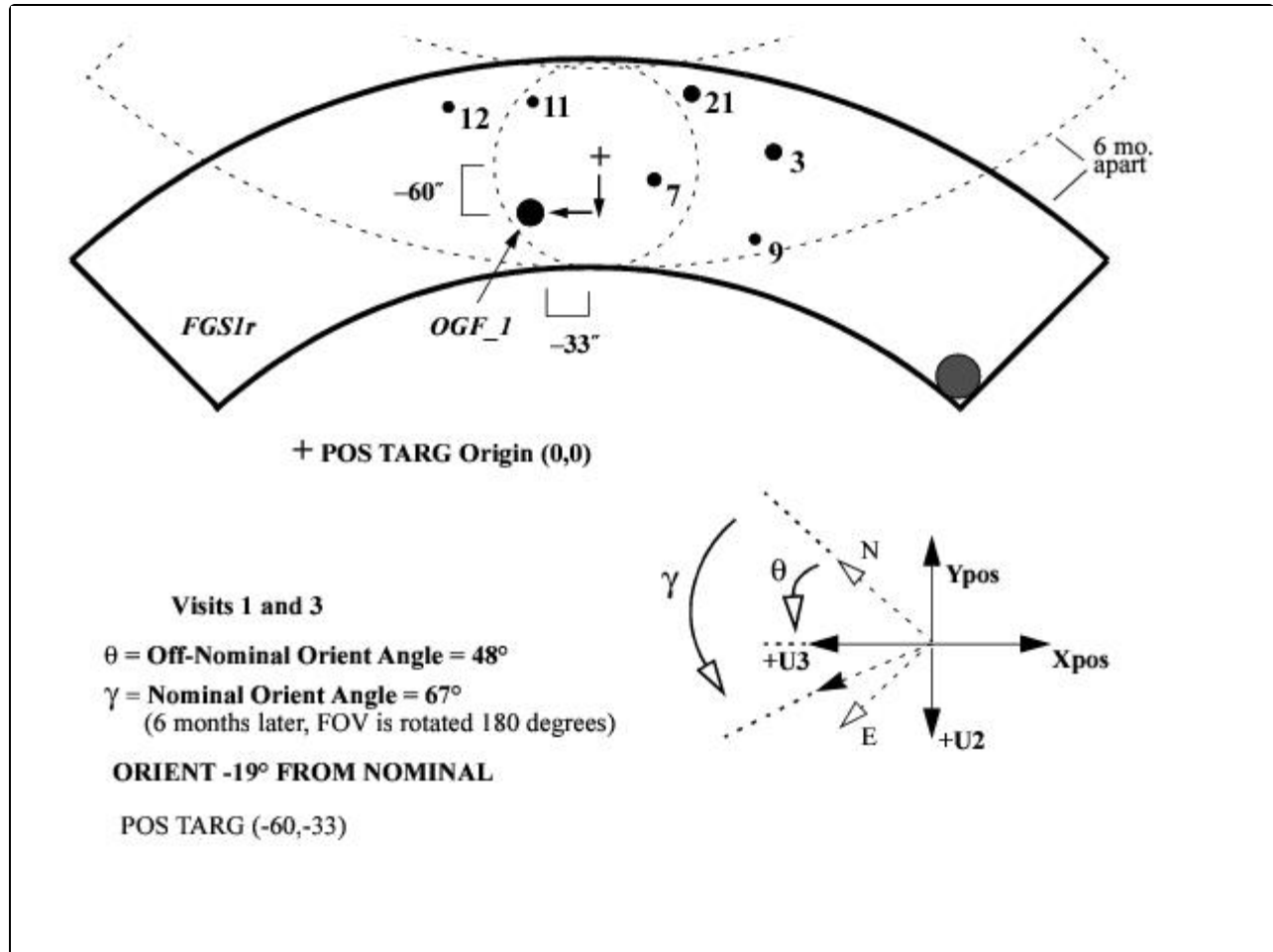


Table 6.8: Target and Exposure Input for Example 1

Target	V	FILTER	FESTIME (default)	Exposure Time (seconds)	~NEA for Single Exposure (mas)
"OGF_1"a	9	F583W	0.025	20	< 1.0
OGF-3-REFa	11.1	F583W	0.025	20	< 1.0
OGF-7-REF ¹	10.3	F583W	0.025	20	< 1.0
OGF-9-REF	10.2	F583W	0.025	20	< 1.0
OGF-11-REFa	13.3	F583W	0.050	30	3.1
OGF-12-REF	13.6	F583W	0.050	30	3.5
OGF-21-REF	11.5	F583W	0.025	20	1.0

¹ The “REF” appendix is not required. Rather its use is suggested simply for book keeping purposes.

- **Reference/Check Star Pattern:** Check Stars in this observation are REF-7, REF-11, and OGF_1. Observing sequence:

```
OGF_1--> 12 -- 11 -- 7 -- OGF_1 -- 11 -- 21 -- 3 -- 7 -- OGF_1
-----> 9 -- 7 -- 11 -- OGF_1 -- 21 -- 12 -- 11 -- 9 -- OGF_1
```

- **The Exposure Logsheet Template:** The Optional_Parameters entry is missing since, for this example, all Pos mode optional parameters are DEFAULT values

```
Visit_Number: 1
Visit_Requirements: BETWEEN 14-MAR-1998 AND 15-MAR-1998
ORIENT -18.5D TO -19.5D FROM NOMINAL
Visit_Comments: Two Guide Star FineLock Required.Exposure_Number: 01
    Target_Name: OGF_1
    Config: FGS
    Opmode: POS
    Aperture: 1
    Sp_Element: F583W
    Time_Per_Exposure: 20S
    Special_Requirements: SEQ 1-4 NON-INT;POS TARG -33,-60.

    Exposure_Number: 02
    Target_Name: OGF-12-REF
    Config: FGS
    Opmode: POS
    Aperture: 1
    Sp_Element: F583W
    Time_Per_Exposure: 30S
    Special_Requirements: SAME POS AS 1;

    Exposure_Number: 03
    Target_Name: OGF-11-REF
    Config: FGS
    Opmode: POS
    Aperture: 1
    Sp_Element: F583W
    Time_Per_Exposure: 30S
    Special_Requirements: SAME POS AS 1;
    Comments:

    Exposure_Number: 04
    Target_Name: OGF-7-REF
    Config: FGS
    Opmode: POS
    Aperture: 1
    Sp_Element: F583W
    Time_Per_Exposure: 20S
    Special_Requirements: SAME POS AS 1;
    Comments:
```

...and continues until the orbit is filled.

6-months after Visit 1, the HST Nominal Orient Angle is 180° from the Nominal HST Orientation in Visit 1. Nominal orient angle = 247°, off-nominal orient angle = 228°, pos targ = (+60,+33).

```

Visit_Number: 2
Visit_Requirements: BETWEEN 14-SEP-1998 AND 15-SEP-1998;
                    ORIENT -18.5D TO -19.5D FROM NOMINAL
Visit_Comments: Two Guide Star FineLock Required.
Exposure_Number: 01
    Target_Name: OGF_1
    Config: FGS
    Opmode: POS
    Aperture: PRIME
    Sp_Element: F583W
    Time_Per_Exposure: 20S
Special_Requirements: SEQ 1-4 NON-INT;POS TARG +33,+60
Comments:
    Exposure_Number: 02
    Target_Name: OGF-12-REF
    Config: FGS

```

...Continues until the orbit is filled. Visit 3 is identical to Visit 1 except that it executes 1 year later.

Running the proposal template file through APT will inform the observer whether the syntax is correct, whether the exposures fit in an orbit and how much time is left, and finally whether the observing dates are viable for the requested ORIENT angle.

6.5.2 Determining a binary's orbital elements using FGS1r in Trans mode

- **Goal:** Observe a known faint ($V=16$) close (separation ~ 40 mas) binary in Trans mode in order to determine the system's relative orbit from which the orbital element, and hence, the system's mass can be derived.
- **Scenario:**
 - Program requires 4 single orbit visits to observe the binary at different orbital phases. These shall be timed accordingly.
 - Target is faint enough ($V>8$) for filter F583W.
 - The expected separation of binary is ~ 40 mas. Its position angle is expected to be approximately 180 deg at the time of the first planned observation. This will have implications for the ORIENT of HST for the visit (see below. Note that special orients also imply scheduling constraints. Use of APT will facilitate resolving these constraints.)
 - Reference Star Geometry: Six reference stars near science target; POS TARG required to fit all reference stars in the pickle. See [Table 6.1, Example 1: Field of View at Special Orientation](#).
- **Special Considerations:**
 - Include B-V color information. STScI will use such information to plan the calibration observations of the color reference standard stars.
 - ScanLength: 0.5 arcsec.
 - The expected separation of binary is ~ 40 mas. Its position angle is expected to be approximately 180 deg at the time of the first planned observation. This will have implications for the ORIENT of HST for the visit (see below. Note that special orients also imply scheduling constraints. Use of APT will facilitate resolving these constraints.)

-Reference Star Geometry: Six reference stars near science target; POS TARG required to fit all reference stars in the pickle. See [Table 6.1, Example 1: Field of View at Special Orientation](#).

- **Exposure Time Calculation**

-target magnitude = 16.0, use F583W

-An ORIENT range is used to avoid the binary's projected separation along either of the FGS axis to be less than 20 mas (to assure an accurate determination of the system's total projected separation and position angle.).

-StepSize: 0.6 mas.

-target visibility period: 58 Minutes.

-guide star acq and instrument overheads: ~12 min.

-available observing time: ~ 46 min.

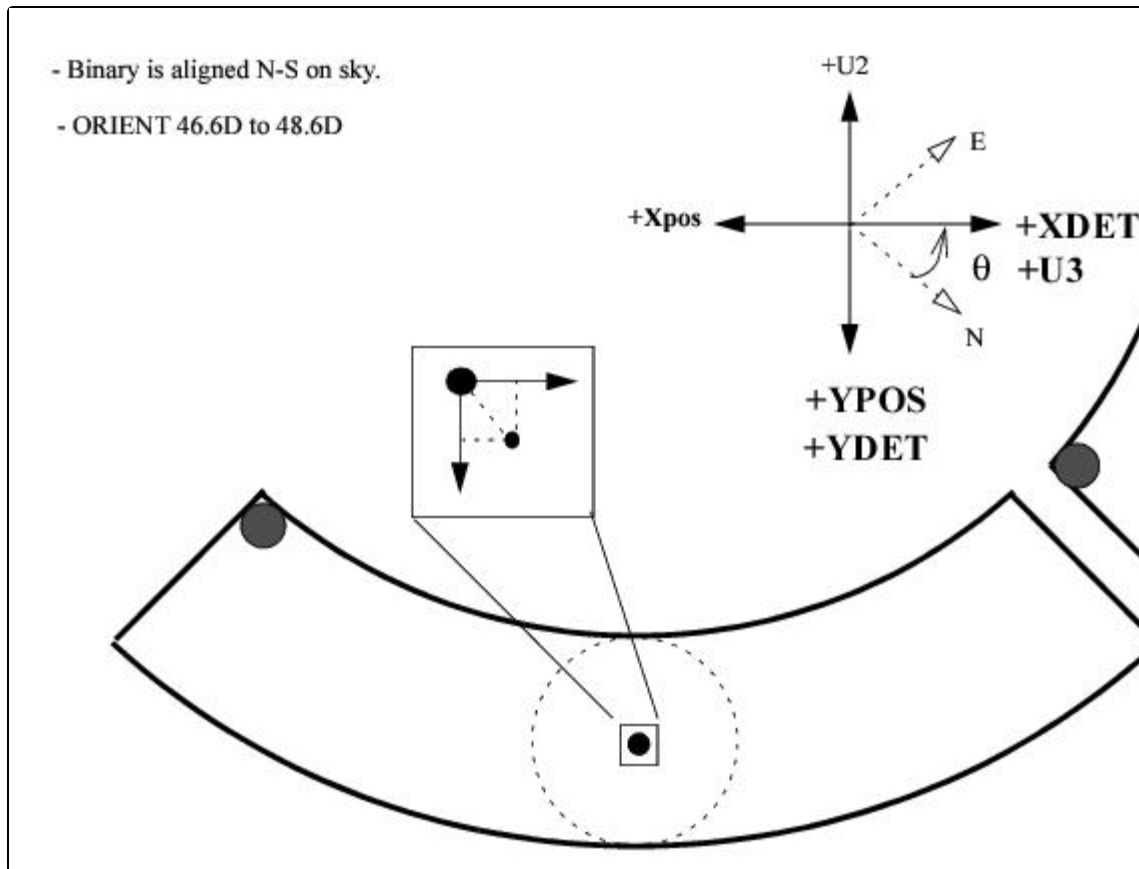
-time (sec) per scan = $0.025 * [\text{ScanLength}/\text{StepSize}] + 12 = 33$. (note, the 12 sec is the per scan overhead.)

-the number of scans that can fit in within this observing window is $N_{\text{scans}} = 46*60/33 = 83$

-exposure time = $N_{\text{scans}} * 0.025 * [\text{ScanLength}/\text{StepSize}] = 1730$ sec. (note the scan's overheads are not included in the user specified exposure time)

[Figure 6.2](#) illustrates the geometry of the binary with respect to the POS TARG and detector reference frames.

Figure 6.2: Example 2: Field of View at Special Orientation



- The Exposure Logsheet Template:

```

Visit_Number: 1
Visit_Requirements: ORIENT 46.6D TO 48.6D
Visit_Comments: Two Guide Star FineLock Required. Please notify Contact Scientist if two guide stars cannot be found.
Exposure_Number: 01
    Target_Name: Close_Binary
    Config: FGS
    Opmode: TRANS
    Aperture: 1
    Sp_Element: F583W
Optional_Parameters: SCANS=83, STEP-SIZE=0.6
    Time_Per_Exposure: 1729S
Special_Requirements:
Comment:
Visit_Number: 2
Visit_Requirements: AFTER 1 BY 30D TO 32D
    ORIENT -24D TO -25D FROM NOMINAL
Visit_Comments: Two Guide Star FineLock Required.
Exposure_Number: 01
    Target_Name: Close_Binary
    Config: FGS
    Opmode: TRANS
    Aperture: 1
    Sp_Element: F583W
Optional_Parameters: SCANS=83, STEP-SIZE=0.6
Number_of_Iterations: 1
    Time_Per_Exposure: 1729S
Special_Requirements:

```

And similar Visits for 3 and 4.

Running the proposal template file through APT will inform the observer whether the syntax is correct, whether the exposures fit in an orbit and how much time is left if they do not; and finally, whether the observing dates are viable for the requested ORIENT angle.

6.5.3 Mass determination: Trans and Pos mode

- **Goal:** A bright ($V=13$), wide binary system (separation = 0.4") is to be observed with FGS1r. Pos mode observations of the binary and neighboring reference stars will be used to determine the binary's parallax, proper motion, and barycenter. Trans mode observations will be used to establish the system's relative orbit so that its orbital elements can be derived. Combining these data from several epochs will allow for a dynamical mass determination of the system's components.
- **Scenario:**
 - program requires two visits every six months for three years.
 - reference star distribution: six reference stars near science target; science target must be placed at aperture reference position for Trans mode observations.
- **Special Considerations:**
 - include B-V color information on all targets, if available, so STScI can determine the need for specific calibrations.
 - target magnitude = 13.0, use F583W

- ScanLength: 1.6 arcsec.
- StepSize: 0.6mas.
- target visibility: 63 minutes.
- total Trans mode exposure time: 28 minutes.
- exposure time calculation:

$$T_{\text{exposure}} = 0.025 * [\text{ScanLength}/\text{StepSize}] * N_{\text{scans}}$$

where in this example ScanLength = 1.6 arcsec, StepSize = 0.0006 arcsec, and the number of scans $N_{\text{scans}} = 25$

[Figure 6.3](#) illustrates the geometry of the target and reference stars, while [Table 6.9](#) and [Table 6.10](#) summarize the details of the exposures in the visit.

Figure 6.3: Example 3: Trans + Pos Mode Visits

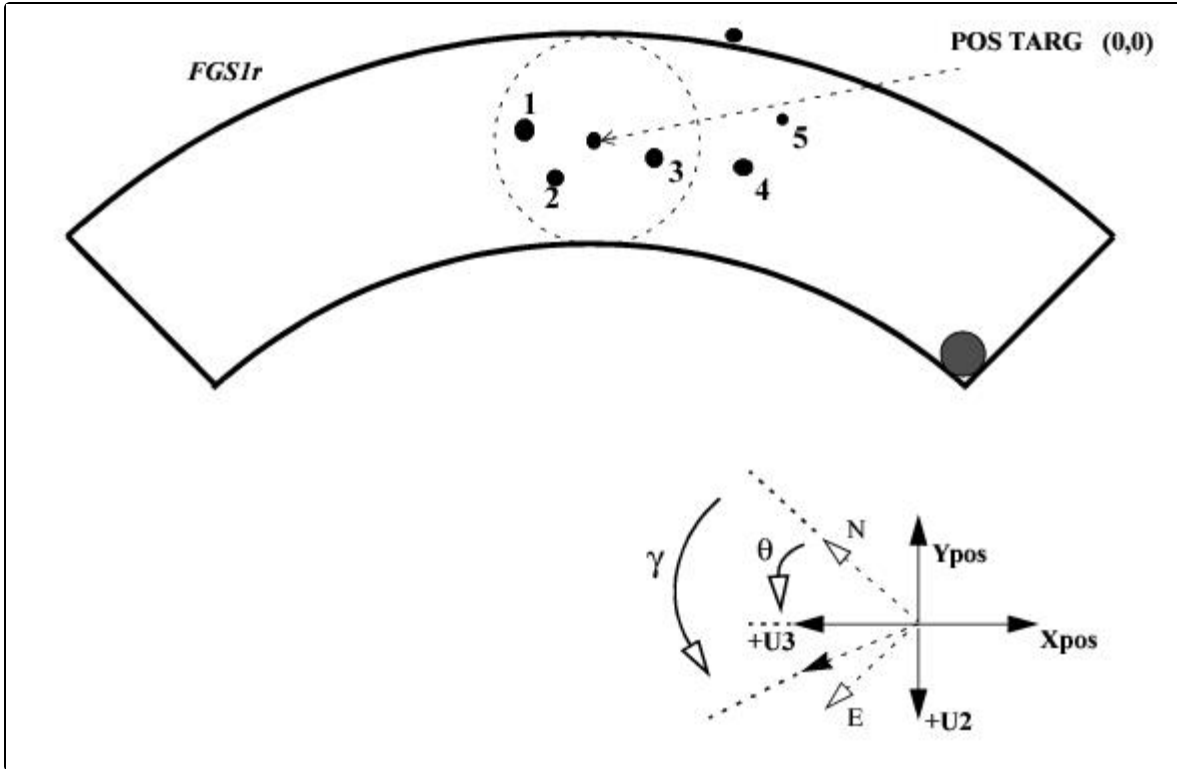


Table 6.9: Target and Exposure Input for Example 3

Target	V	FESTIME (use defaults)	FILTER	Total Exposure	~NEA for one exposure (mas)
Wide_Binary ¹ Pos mode	13.0	0.050	F583W	20 sec	2.0
Wide_binary Trans mode	13.0	0.025	F583W	28 min	$\sigma_{Sx} = 0.008$
BL-1-REF ²	10.8	0.025	F583W	20 sec	<1.0
BL-2-REF	14.1	0.100	F583W	35 sec	5.0
BL-3-REF	11.5	0.025	F583W	20 sec	1.0
BL-4-REF	12.5	0.025	F583W	20 sec	1.7
BL-5-REF	13.0	0.050	F583W	20 sec	2.5

¹ The primary target needs only be listed once in the fixed target list.

² The "REF" appendix is not required. Rather its use is suggest simply for book keeping purposes.

Table 6.10: Reference/Check Star Pattern

Mode	Overhead + Exposure Time (Minutes)
GS ACQ + Instrumental Overheads.	12
Trans mode	
• Wide_Binary	28
Pos mode:	
• Wide_Binary	2
• BL-3-REF	1
• BL-2-REF	2.5
• BL-1-REF	1
• Wide_Binary	2
• BL-3-REF	1
• BL-4-REF	1
• Wide_Binary	2

6.5.4 Faint binary with Trans mode: special background measurements

- **Goal:** A faint ($V=15$) object suspected to be a close ($\text{sep} < 30 \text{ mas}$) binary is embedded in nebosity which contributes about 20% of the light in the vicinity of the target. The putative binary is to be observed in Trans mode. Special additional observations are needed accurately measure the background. To do so, the RA,Dec of two points on the sky about 1 arcmin from the target and to either side of it are specified as “targets” in the proposal. These “targets” are to be observed in Pos mode after the Trans mode observation of the faint science target (the FGS high voltage, which enable the PMTs to count photons, does not get turned on until after the IFOV is placed at the expected location of the first target to be observed in the visit. The background data is to be acquired as the IFOV slews away from the science object to the reference “targets”. During this time the PMTs record the background counts.)
- **Scenario:**
 - Program requires a single one orbit visit.
 - Target Filter: F583W.
 - Reference Star Filter: F583W.
 - Geometry: Science target is placed at center of the FGS1r FOV; the background data are obtained en route to and while observing the reference points (specified in the proposal as a pointed targets) in Pos mode for 1 minute.
- **Exposure Time Calculation**
 - target magnitude = 15.0, use F583W
 - target visibility period: 54 minutes..
 - GS acq and instrumental setup time: 12 min.

- available observing time: 42 min.
- ScanLength: 0.5 arcsec.
- StepSize: 0.6 mas.
- time per scan = $0.025 * (0.5/0.0006) + 12 = 33$ sec
- time for two Pos mode observations (include overheads): 3 min.
- approximate number of scans that can fit within orbit: 69

Figure 6.4 illustrates a possible geometry of the field, while Table 6.11 summarizes the total exposure times for the target and reference star, and dark sky observations.

Figure 6.4: Example 4: Trans + Pos Mode Exposures

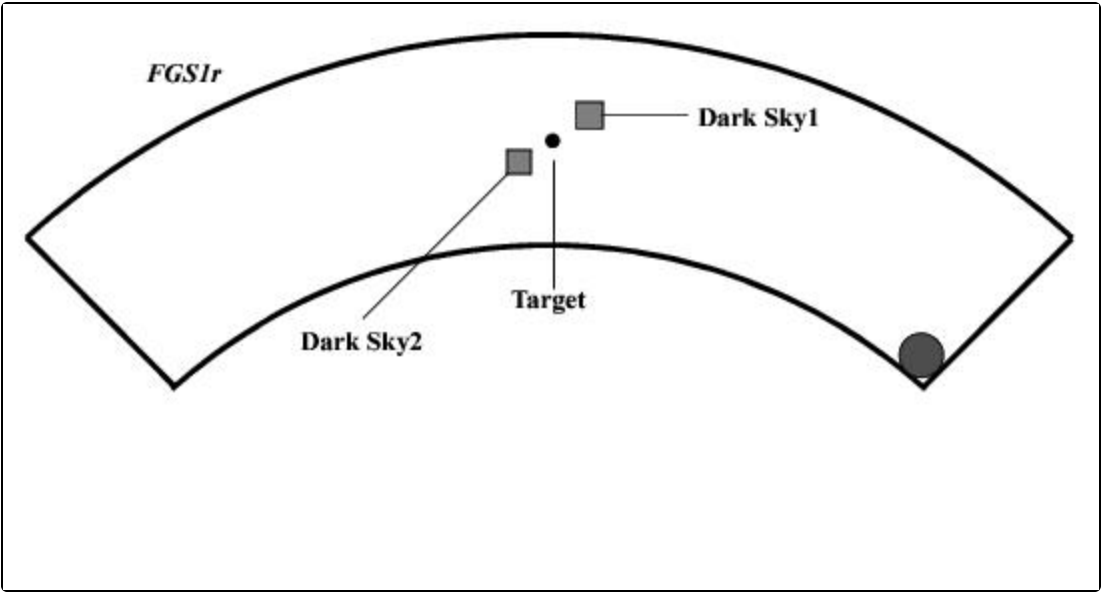


Table 6.11: Target and Exposure Input for Example 4

Target	V	FILTER	Total Exposure
HDFAINTE Trans mode	15	F583W	39 min.
Dark_Sky1 Pos mode	10	F583W	1 min.
Dark_Sky2 Pos mode	12	F583W	30 S

Specify the background targets to be bright (V=8) to minimize target acquisition overheads. Note: these targets will fail to be acquired in FineLock since no coherent source is present. However, the desired photometry will be recorded.

- Exposure Logsheet Template:

Visit_Number: 1
 Visit_Requirements:
 Visit_Comments:

Exposure_Number: 01
 Target_Name: HDFAINT
 Config: FGS
 Opmode: TRANS
 Aperture: 1
 Sp_Element: F583W
 Optional_Parameters: SCANS=69, STEP-SIZE=0.6
 Time_Per_Exposure: 1380S
 Special_Requirements: POS TARG = 0,0 SEQ 1-3 NON-INT

Exposure_Number: 02
 Target_Name: DARK_SKY1
 Config: FGS
 Opmode: POS
 Aperture: 1
 Sp_Element: F583W
 Optional_Parameters:
 Time_Per_Exposure: 60 S
 Special_Requirements: SAME POS AS 1

Exposure_Number: 03
 Target_Name: DARK_SKY2
 Config: FGS
 Opmode: POS
 Aperture: 1
 Sp_Element: F583W
 Optional_Parameters:
 Time_Per_Exposure: 60 S
 Special_Requirements: SAME POS AS 01

Chapter 7: FGS Astrometry Data Processing

Chapter Contents

- [7.1 Data Processing Overview](#)
- [7.2 Exposure-Level Processing](#)
- [7.3 Visit-Level Processing](#)
- [7.4 Epoch-Level Processing](#)

7.1 Data Processing Overview

FGS Astrometry observations are analyzed at three distinct levels, the exposure-level (individual observations), the visit-level (all observations within the HST orbit), and the *epoch-level* (relating data from one visit to others). The astrometry data pipeline processes the observations up to and including the visit level. Epoch-level analysis requires tools beyond the scope of the FGS data pipeline.

The exposure- and visit-level corrections and calibrations are performed by the observer using *calfgsa* and *calfgsb*. *calfgsa is a standalone executable (currently supported on Unix operating systems, including MAC OSX), while calfgsb* is implemented as tasks in STScI's STSDAS system. These tasks are semi-automated and require little user input to process the individual exposures that comprise the typical astrometry visit. Reference files used by these tasks are maintained by STScI and can be found by following the links to the calibration sections of the FGS website at:

<http://www.stsci.edu/hst/instrumentation/fgs>.

Epoch-level analysis of FGS data is not, by its nature, a procedure which lends itself to generic pipeline processing. However, tools to provide the observer with some of the more common manipulations encountered in data analysis of FGS astrometry observations are being made available to the general FGS user. Currently, these tools are not STSDAS tasks, but a collection of stand-alone scripts and executable files to achieve plate solutions for Position mode observations and the deconvolution of binary star transfer functions from Transfer mode observations.

The processing and analysis applied at each level is discussed below. Interested readers are encouraged to monitor the STScI newsletter or visit the [FGS web page](#) for updates to the status of these tools. More detailed discussions can be found in the [FGS Data Handbook](#) version 4.0 or later.

7.2 Exposure-Level Processing

7.2.1 Initial Pipeline Processing

7.2.2 Observing Mode Dependent Processing

The term “exposure-level processing” refers to pipeline corrections that are applied to the individual FGS observations. These are discussed in this section.

7.2.1 Initial Pipeline Processing

Regardless of the observing mode, several activities are carried out during the initialization of the astrometry pipeline. This begins with the usual file management, data quality assessments, and the determination of the required reference files and their availability status. At this early stage, the data are inspected to determine the identification of the astrometer FGS, its mode of operation, and the availability of guide star data from the guiding FGSs. The astrometer’s data are inspected to evaluate the outcome of the Search, CoarseTrack, and FineLock target acquisitions, while the guide star data are inspected to identify the guiding mode (i.e., was the spacecraft guided by one or two guide stars, and were the guide stars tracked in FineLock?).

If the astrometry target acquisition failed, the FGS flags and status bits are inspected to determine the cause. In this case, data processing proceeds as far as possible (in the event that the observation was a partial success), output files are generated and populated appropriately, and pipeline processing of the observation terminates.

7.2.2 Observing Mode Dependent Processing

After pipeline initialization and data quality assessments, successful observations (i.e., those that acquired the target), are processed according to the FGS observation mode: Position or Transfer.

Position mode

The goal of exposure-level Transfer mode pipeline processing is to determine the centroid of the IFOV while the FGS tracked the object in FineLock. A collateral objective is to analyze the individual PMT data, both to determine the small angle corrections that need to be applied to the centroids as well as to provide photometric information about the target and the sky background.

The guide star data are analyzed in the same way as the astrometer data, over the identical intervals of time. For example, the guide star centroids and average photometry are computed over the time the astrometer was in FineLock.

The corrections applied to the FGS data are as follows:

1. The FineLock centroids are computed by finding the median, from the 40 Hz data - of the X,Y location of the IFOV (computed from the Star Selector A,B encoder angles). PMT data are averaged for astrometer and guiding FGSs.
2. For the astrometer only, the PMT data are evaluated to determine the fine angle adjustments to the centroids.
3. The Optical Field Angle Distortion (OFAD) calibration is applied to remove distortions of the sky in the FOV.

4. Differential velocity aberration correction is applied to the adjusted FineLock centroids of the astrometer and guiding FGSs.

Steps 1 and 2 are carried out in *calfgsa*, while steps 3 and 4 are performed in *calfgsb*. Please see [Figure 7.1](#) and [Figure 7.3](#), the flow chart descriptions of *calfgsa* and *calfgsb* respectively.

Transfer mode

During a Transfer mode observation, the data retrieved from the astrometric FGS will include PMT counts and star selector positions from the slew of the IFOV to the target object, the Search and CoarseTrack target acquisition, and the individual Transfer scans. Corresponding data acquired from the guiding FGSs will include FineLock tracking of the guide stars.

The astrometer's data are analyzed to evaluate the background counts, if available (see [Chapter 7](#)), and to locate and extract the individual scans. For each scan, the guide star centroids are computed and corrected for differential velocity aberration. Output files are generated with the appropriate information.

The data from the individual scans are used to compute the Transfer Function over the scan path. The quality of each scan is evaluated for corruption from high amplitude, high frequency spacecraft jitter, and, if unacceptably large, the scan is disqualified from further analysis.

The remaining scans are cross correlated, shifted as needed, binned as desired, and co-added to enhance the signal to noise ratio. The co-added Transfer Function can be smoothed if need be. The analysis tool which performs these functions is available from STScI. It is currently implemented as a standalone executable (FORTRAN + C) in the UNIX environment.

Although not part of pipeline processing, the analysis of observations of binary stars and extended objects will be briefly described here for completeness.

Binary Star Analysis

The Transfer Function of a binary system will be deconvolved, by use of the standard reference S-Curves of single stars from the calibration database, into two linearly superimposed point source S-Curves, each scaled by the relative brightness and shifted by the projected angular separation of the binary's components. This provides the observer with the angular separation and position angle of the components as well as their magnitude difference. These results will be combined with those obtained from observations at different epochs to compute the system's relative orbit.

Extended Source Analysis

For observations of an extended source, such as the resolved disk of a giant star or solar system object, the co-added Transfer Function will be analyzed to determine the angular size of the object. This involves application of a model which generates the Transfer Function of synthetic disks from point source S-Curves from the calibration database.

Transfer mode observations are processed by *calfgsa* to the point of locating and extracting the individual scans and computing the guide star centroids. Support for additional processing - including the automation of the data quality assessment (identifying those scans which have been unacceptably corrupted by space craft jitter, for example) and the cross correlation and co-adding of the individual scans - are available as data analysis tools. Upgrades to *calfgsa* will be noted on the [FGS web page](#). [Figure 7.2](#) displays the processing steps performed by the current version of *calfgsa* for Transfer mode observations..

7.3 Visit-Level Processing

7.3.1 Position Mode

7.3.2 Transfer Mode

Visit-level processing refers to those corrections that are applied to the individual exposures in order to map each onto a common reference frame. Since the FGS observes the targets sequentially, not simultaneously, any motion of the spacecraft or the FGS's FOV during the course of the visit will introduce uncertainties in the measured positions of the objects. The corrections discussed here restore the cohesiveness of the reference frame.

7.3.1 Position Mode

Position mode observations during the course of a visit must be corrected for two sources of error which render the FOV somewhat unstable: low frequency HST oscillations and residual drift of the FOV across the sky.

HST Oscillations: Using the Guide Star Data

The mapping of the individual astrometry observations onto a common reference frame begins with the analysis of the guide star data. As part of the exposure-level processing, guide star centroids are computed over the same time interval as for the astrometry targets. Generally *HST* is guided by two guide stars. The so-called “dominant” guide star is used by the pointing control system (PCS) to control the translational pitch and yaw of the telescope. The “sub-dominant” guide star, also referred to as the roll star, is used to maintain the spacecraft's roll or orientation on the sky. Any change in the guide star centroids over the course of the visit (after corrections for differential velocity aberration) is interpreted by the FGS Astrometry Pipeline as an uncorrected change in the spacecraft's pointing.

The pipeline defines an arbitrary fiducial reference frame based upon the location of the guide stars in the first exposure of the visit. Relative changes in the position of the dominant guide star for subsequent observations are assumed to be a translational motion of the HST focal plane. The pipeline “corrects” the position of the sub-dominant guide star and the astrometric target star. Any change in the angle defined by the line connecting the two guide stars and the spacecraft's V2 axis is interpreted as a rotation of the focal plane, and is removed from the astrometry data.

The correction of the astrometry centroids for vehicle motion (as determined by changes in guide star positions) is referred to as *pos-mode dejittering*. Transient corrections can be as large as 3 to 5 mas, such as when HST enters orbital day, but the adjustments are typically small—less than 1 mas. This underscores the excellent performance of HST's pointing control system under the guidance of the FGSs.

Drift Correction

“Drift”, as discussed in [Chapter 5](#), is defined as the apparent motion of the astrometer’s FOV on the sky during the course of the visit as detected by the astrometry targets that are observed more than once during the visit (the *check stars*). Drift must be removed from the measured position of all astrometry targets. This is accomplished by using check star data to construct a model to determine the corrections to be applied. If at least two check stars are available and were observed with sufficient frequency (i.e., at least every seven minutes), a quadratic drift model (in time) can be used to correct for both translation and rotation of the FOV. The availability of only one check star will limit the model to translation corrections only. If the check stars were observed too infrequently, then a linear model will be applied.

If no check stars were observed, the drift cannot be removed and the astrometry will be contaminated with positional errors as large as 15 mas.

It is important to note that the drift is motion in the astrometer which remains after the guide star corrections have been applied. Its cause is not well understood, but with proper check star observing, the residuals of the drift correction are tolerably small (i.e., sub-mas).

With the application of the guide star data for pos-mode dejittering and the check stars to eliminate drift, the astrometry measurements from the individual exposures can be reliably assembled onto a common reference frame to define the *visit’s plate*.

The visit level corrections to Position mode observations, i.e., pos-mode de-jittering and the drift correction are performed by *calfgsb* ([Figure 7.3](#)).

7.3.2 Transfer Mode

Transfer mode observations typically last about 20 minutes (or more), much longer than Position mode exposures (1 to 3 minutes). Therefore, it is far more likely that low frequency spacecraft jitter and FOV drift will have occurred during the Transfer mode exposure. These do not introduce uncorrectable errors since low frequency FOV motion is implicitly removed from the data by cross correlating the Transfer Function from each individual scan. However, relating the arbitrary coordinate system upon which the Transfer Function is mapped to the system common to the reference stars is an important and necessary prerequisite in linking the Transfer mode observation to the Position mode data.

Guide Star Data

Transfer mode data analysis, as discussed in the exposure level section, involves the cross correlation of the Transfer Functions from each of the individual scans. The first scan is arbitrarily designated as the fiducial; all other scans in the Transfer Function are shifted to align with that of the first (this automatically eliminates jitter and drift local to the observation). Therefore, in order to restore some level of correlation with the other observations in the visit, the guide star centroids are evaluated over each scan, and, along with the shifts, are recorded.

Drift Correction

The cross correlation of the individual scans removes the drift of the FOV from the Transfer mode data. However, this is a relative correction, local to only the Transfer mode observation. By recording the shift corrections applied to the individual scans, the visit level pipeline has visibility to the drift that occurred during the Transfer mode observation.

Transfer/Position Mode Bias

The presence of a small roll error of the Koesters prism about the normal to its entrance face (see [“Section 5.2 Transfer Mode Scale as a Function of HST Roll Angle”](#)) introduces a bias in the location of interferometric null as measured by Position mode when compared to the same location in Transfer mode. This bias must be accounted for when mapping of the results of the Transfer mode analysis onto the visit level plate defined by the Position mode measurements of the reference stars. This bias is removed by applying parameters from the calibration database.

7.4 Epoch-Level Processing

7.4.1 Parallax, Proper Motion, and Reflex Motion

7.4.2 Binary Stars and Orbital Elements

Astrometry takes time. This is true whether the goal is to determine the parallax, proper motion, or reflex motion of an object measured in Position mode, or the orbital elements of a binary system observed in Transfer mode. By its very nature, astrometry looks for changes to the arrangement of objects on the sky, and as a result, observations taken over several different visits must be compared to one another. Relating the observations from different epochs is discussed. A more detailed discussion is provided in then [FGS Data Handbook](#).

7.4.1 Parallax, Proper Motion, and Reflex Motion

In order to measure the proper motion and parallax of an object observed in Position mode with the FGS, the data from the individual visits must be combined to form a virtual plate. This virtual plate is derived from an optimal mapping of all of the visit level plates onto a common plate using the method of least-squares to minimize the residuals of all reference stars (the plate solution). This mapping function is used to map the science target at each visit onto the virtual plate. In this way, the parallax, proper motion, and perhaps reflex motion (perturbations caused by a gravitationally bound companion) can be determined.

If enough reference stars are available (> 5), six parameter plate solutions - allowing for independent scale adjustments along each of the astrometer's X and Y axes - can be applied. Otherwise the four parameter model must be applied.

The residuals of the reference stars in the plate solution determine the overall astrometric performance of the telescope as a function of the number of visits expended. FGS3 achieved ~ 1.2 mas (rms) precision per *HST* orbit, while FGS1r has demonstrated ~ 0.8 mas rms precision per *HST* orbit. Given that the overall astrometric accuracy scales as $\sqrt{1/n}$ while random (Poisson) errors dominate, it can be anticipated that, for example, FGS1r will yield parallax measurements accurate to 0.3 mas in as little as 12 *HST* orbits if an optimal observing strategy is employed. (Below ~ 0.2 mas irreducible systematic errors dominate, such as the conversion of relative to absolute parallax.)

STScI can provide the analysis tools (developed by the STAT at the University of Texas) needed to perform a plate solution from multiple Position mode visits. These tools are available as stand-alone software packages and scripts that can be delivered via ftp from STScI. Supporting documentation is being developed. Please see the [FGS web page](#) for further updates.

7.4.2 Binary Stars and Orbital Elements

Transfer mode observations of binary stars provide the angular separation and position angle of the components at each epoch (as well as their difference in brightness). Once the binary has been observed at a sufficient number of phases in its orbit, the system's orbital parameters can be solved. The result will be knowledge of the orbit's inclination, eccentricity, period, and angular extent of its semi-major axis. If the parallax of the object is known, then the physical size of the orbit can be computed to yield the total mass of the system.

For a binary that was observed along with Position mode observations of reference stars, it is possible to determine the binary's parallax and proper motion, and the motion of the components about the system's barycenter, which then yields the component masses. This, along with the differential and system photometry (also measured by the FGS), provides the mass-luminosity relation.

STScI can provide observers, via ftp, with the appropriate analysis tools needed to analyze Transfer mode observations of binary star systems. These tools are standalone software packages written by STScI based upon algorithms developed by the STAT at the Lowell Observatory. These packages allow one to *deconvolve* the binary star Transfer mode data in order to determine the angular separation and relative brightness of the components at each epoch of observation. Documentation of these packages will be made available during Cycle 278 Check the [FGS web page](#) for updates.

Figure 7.1: CALFGSA Common Processing Tasks

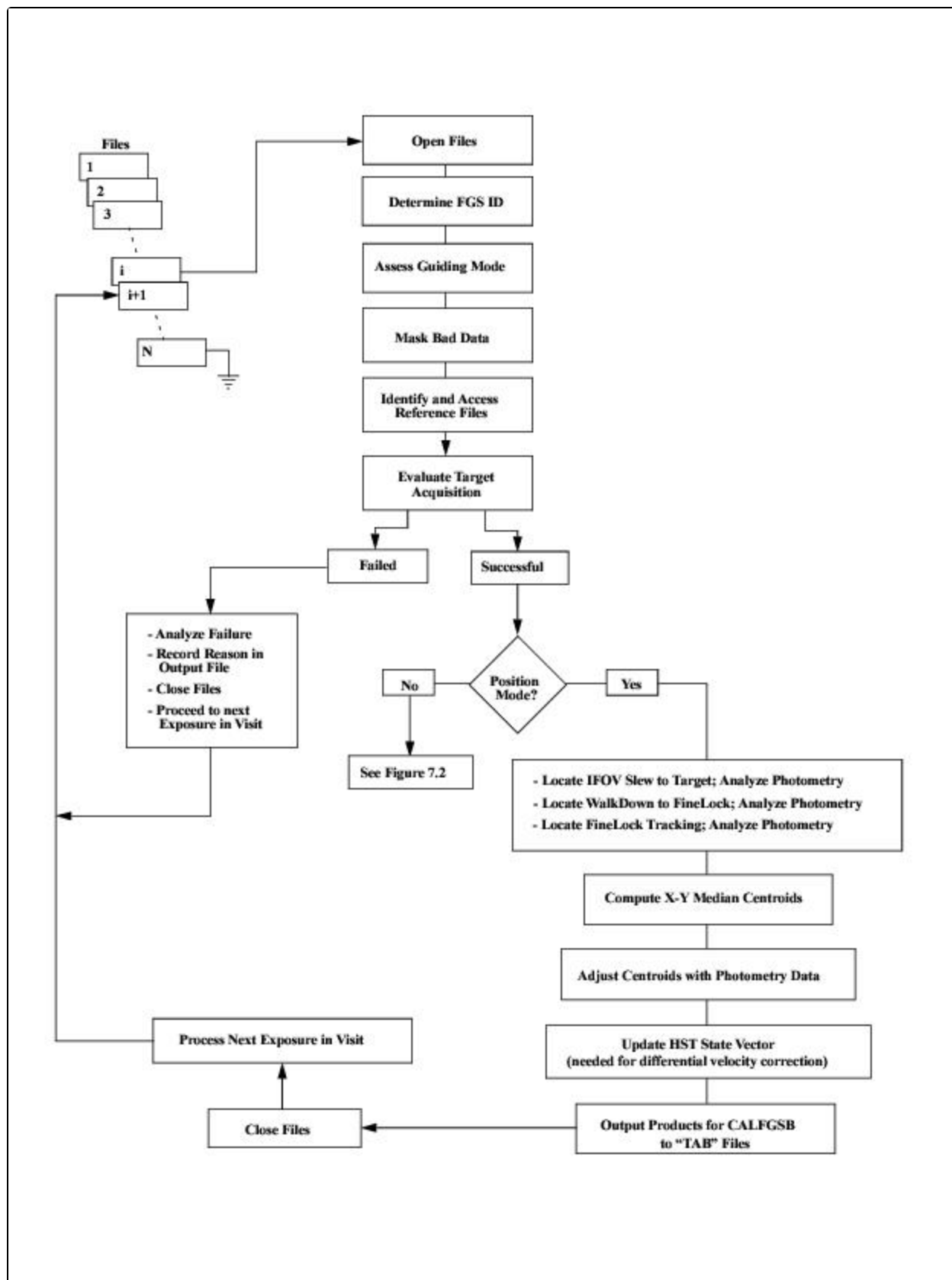


Figure 7.2: CALFGSA Transfer Mode Processing Tasks

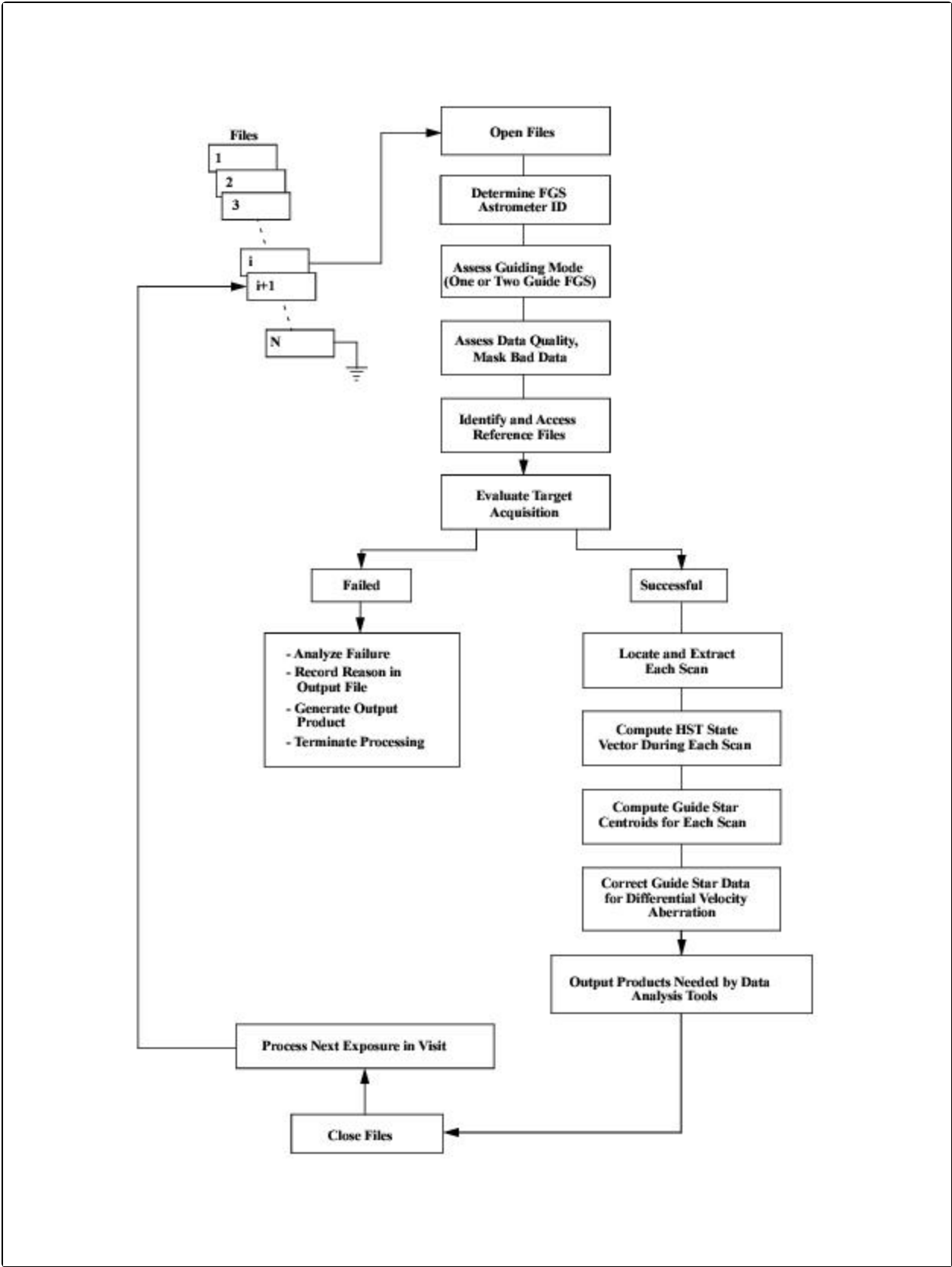
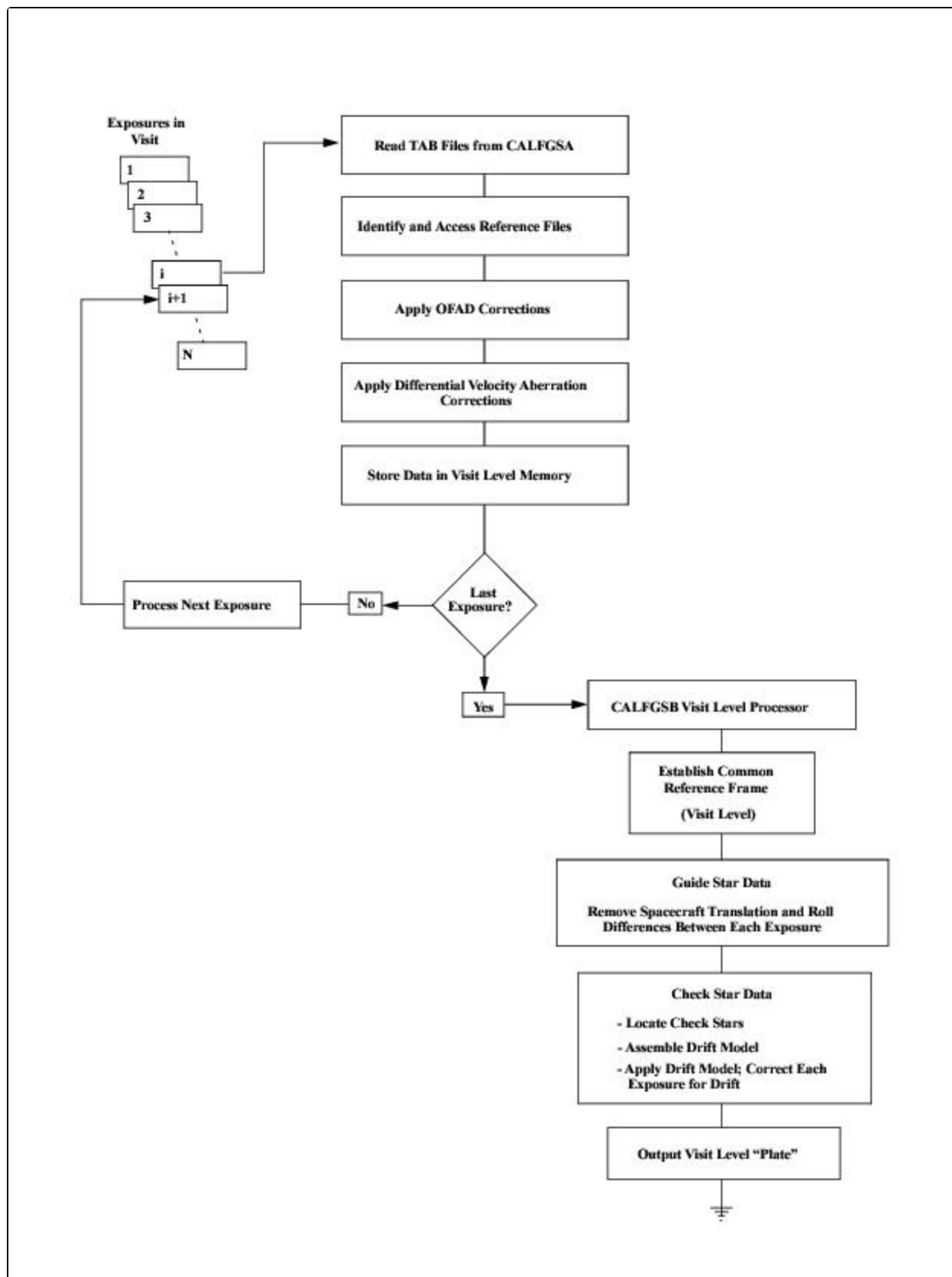


Figure 7.3: CALFGSB Position Mode Processing



Appendix A: Target Acquisition and Tracking

Appendix Contents

- [A.1 FGS Control](#)
- [A.2 Target Acquisition and Position Mode Tracking](#)
- [A.3 Transfer Mode Acquisition and Scanning](#)
- [A.4 Visit Level Control](#)

A.1 FGS Control

Two different computers interface with and control an FGS at various times. The first is the 486, which controls the *HST* spacecraft and its pointing control system. The second is the Fine Guidance Electronics (FGE) microprocessor associated with each FGS. Both the 486 and the FGEs control the FGSs while they are guiding *HST*. During astrometric science observations, control is shared by the two computers: the FGE operates the FGS during Position mode, while the 486 operates the FGS during Transfer mode scans.

A.2 Target Acquisition and Position Mode Tracking

[A.2.1 Slew to the Target](#)
[A.2.2 Search](#)
[A.2.3 CoarseTrack](#)
[A.2.4 FineLock](#)

In this section we review the acquisition and tracking sequence. The flags and status bits are defined in detail in the [FGS Data Handbook](#).

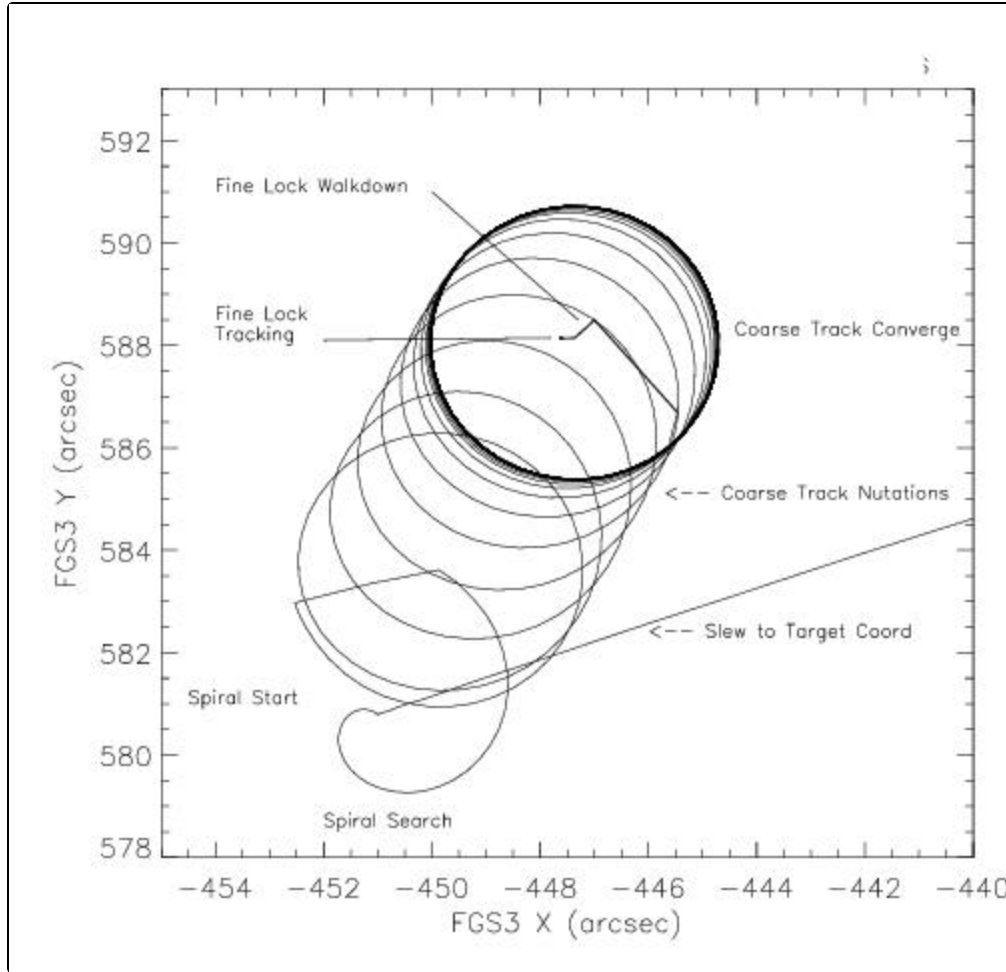
A.2.1 Slew to the Target

To initiate the acquisition of a target, the 486 slews the FGS Instantaneous Field of View (IFOV) to the expected location of the target. Upon arrival, the FGE initiates the search and track sequence: Search, CoarseTrack, and FineLock. [Figure A.1](#) demonstrates the actual movement of the IFOV during a target acquisition.

1. The end of the slew to the target's expected location.
2. A short spiral search.
3. CoarseTrack nutations to locate the photocenter.
4. WalkDown to locate interferometric null.
5. Tracking in FineLock.

Note: The example depicted in [Figure A.1](#) was chosen for its clear demonstration of the phases of the acquisition. *This example is atypical, as the 7" difference between the expected location and the true location of the target is unusually large. More typical miss-distances are 0.3" to 1.00".*

Figure A.1: Location of IFOV as FGS Acquires a Target



A.2.2 Search

In the search phase, the IFOV, under FGE control, steps every 25 msec along an outward spiral while the PMTs count the photons received from the $5'' \times 5''$ patch of sky observed in the IFOV. When the counts fall within a specified tolerance, the FGE declares the spiral search a success, and the instrument transitions to CoarseTrack. By default, the radius of the spiral search is 15 arcsec, but can be as large as 90 arcsec.

⚠ Unless the target's position is highly uncertain, there is no benefit in specifying a search larger than the default, since the HST Pointing Control System points the telescope with an accuracy of about $0.3''$. Large search spirals consume time better spent on science measurements.

A.2.3 CoarseTrack

After a successful search, the FGE attempts to acquire and track the star in CoarseTrack. The FGS locates the photocenter by comparing the photon counts from the four PMTs as the IFOV nutates in a $5''$ diameter circular path around the target.

If the PMT data ever indicate the star is no longer present, the FGS reverts back to Search mode, beginning where it left off on the search spiral to resume its outward search for the star.

A.2.4 FineLock

Upon completion of the CoarseTrack, the FGS attempts to acquire the target in FineLock. This activity involves the acquisition and tracking of an object's interferogram. The fundamental interval of time during FineLock is the Fine Error averaging time (denoted as FESTIME—see [Chapter 7](#)). During an FESTIME the FGS integrates the PMT counts while holding the IFOV fixed.

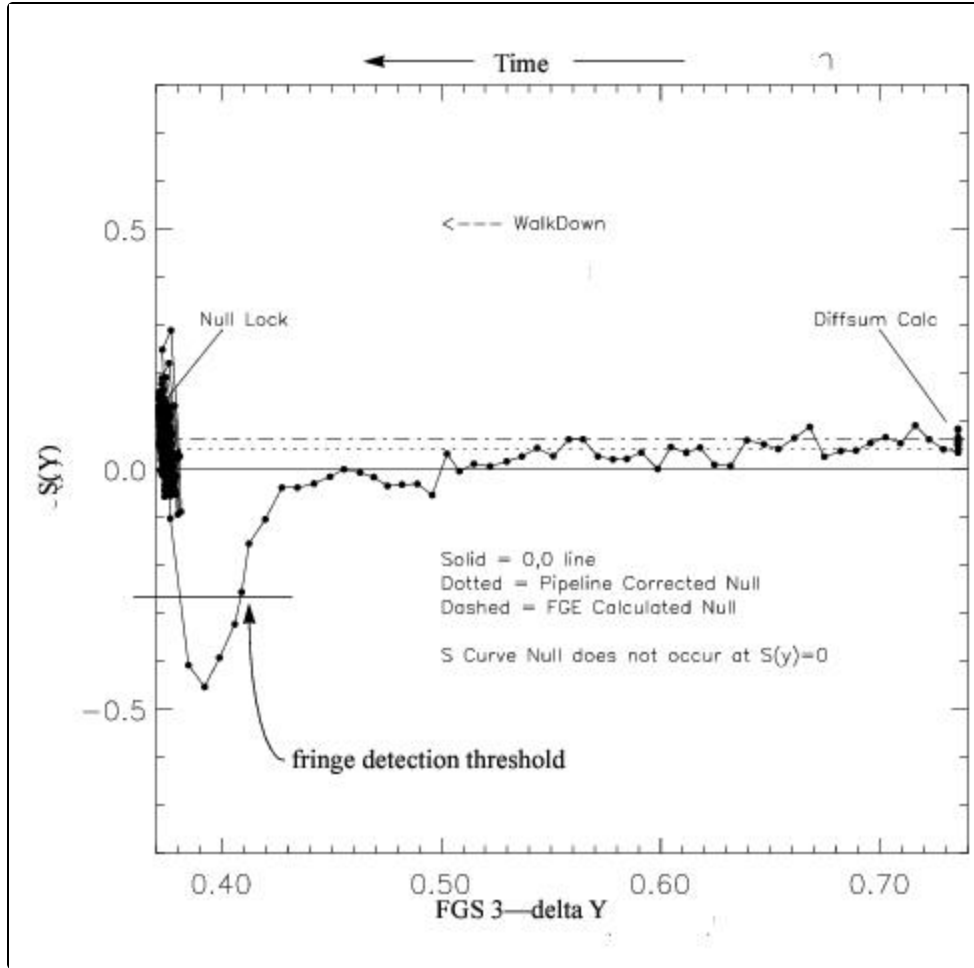
The acquisition begins with the “WalkDown to FineLock,” or simply the WalkDown. The FGE commands the FGS's IFOV to a position offset or “backed-off” from the photocenter (determined by CoarseTrack). Here at the very beginning of the WalkDown, while the IFOV is far from the fringe, the FGE collects data from the two PMTs on each of the X and Y channels to compute an average sum (SUM) and difference (DIFF) of the PMT counts on each channel. The integration time is 0.4 sec or one FESTIME, whichever is larger. The FGE then uses these values to compensate for any difference in the response of the two PMTs on a given axis. Thus, the X-axis Fine Error Signal (FES) for the remainder of the Position Mode observation will be:

$$Q_X = \frac{(A_X - B_X - \text{DIFF}_X)}{(\text{SUM}_X)}$$

where A_X and B_X are the average photon counts/25 msec (from PMTXA and PMTXB) integrated over the FESTIME, and DIFF_X and SUM_X are the average difference and sum of the PMTXA, PMTXB counts per 25 milliseconds (as computed at the start of the walkdown). The Y-axis FES is computed in a similar fashion.

[Figure A.2](#) shows the instantaneous value of the normalized difference of the PMT counts along the Y-axis during a WalkDown to FineLock. The fact that the null lies to the positive side of the Y-axis S-Curve ($S(y) > 0.0$) clearly demonstrates the need for the DIFF-SUM adjustment to locate the true interferometric null. The reference to “pipeline corrected null” in [Figure A.2](#) refers to the true values of DIFF and SUM as computed by the astrometry pipeline, which uses the photometry during the entire WalkDown to achieve a better signal-to-noise for these values. (See [Chapter 7](#) for additional details on the FGS pipeline.)

Figure A.2: Offset of True Null from $S_y = 0$

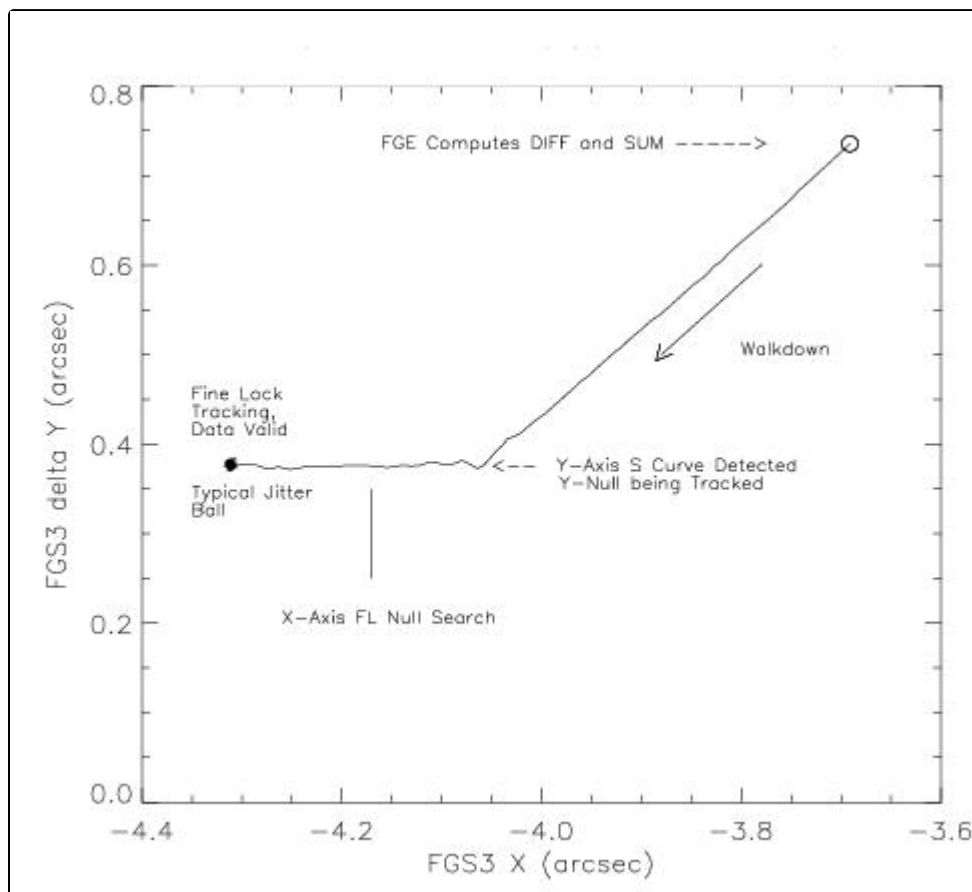


During the WalkDown, the IFOV creeps towards the photocenter in a series of equal steps of approximately 0.006" in X and Y. The IFOV is held fixed for an FESTIME after each step while the PMT data are integrated to compute the fine error signal on each axis. If the absolute value of the fine error signal for a given axis exceeds a specified threshold for three consecutive steps (satisfying the *3-hit algorithm*), the FGE concludes it has encountered the S-Curve on that axis. From this point, a continuous feedback loop between the star selector servos and the FES value governs the repositioning of the IFOV along that axis. For the remainder of the observation, the FGS continuously adjusts the star selector positions by small rotations every FESTIME to set the FES to zero. This repositioning of the IFOV ensures the wavefront at the face of the Koesters prism has zero tilt.

If the FGS does not detect the S-Curve after 130 steps (i.e., after having "walked" 810 mas), the FineLock acquisition fails and the "scan step limit exceeded" flag is set. The IFOV will then remain positioned at the end of the WalkDown path until the 486 slews it to the expected location of the next target in the observing sequence. The observer will be provided with the 40 Hz photometry and star selector angles from which the Fine Error Signal can be reconstructed and analyzed to determine the cause of the failure. *The star must be acquired on both axes for the observation to succeed.*

When the S-Curves on both axes have been encountered and the 3-hit algorithm satisfied, the FGS is said to be tracking the object in FineLock. [Figure A.3](#) shows the IFOV's position for both the WalkDown and FineLock tracking in local detector space. Notice the interferometric null is first encountered along the Y-axis. The IFOV must walk an additional 0.2" along the X-axis to find its interferometric null. This is typical FGS3, and is due to a bias in the CoarseTrack photocenter and the FineLock (interferometric) null. FGS1r has a different bias, with the X-axis null encountered some 0.440" before the Y-axis null. These biases do not degrade the instruments scientific performance.

Figure A.3: X,Y Position in Detector Space of FGS 3's IFOV During WalkDown to FineLock and Subsequent Tracking of a Star in FineLock



A.3 Transfer Mode Acquisition and Scanning

When the FGS is operated in Transfer mode, the acquisition is implemented in the same sequence as described in the previous section, with the exception that the FGS *remains in CoarseTrack until a specified spacecraft time*. Thereafter, the 486 slews the IFOV to the starting point of the first scan and steps it across the object along a diagonal path in detector space for a distance specified in the Phase II proposal. Each sweep across the target is referred to as a scan. After completing a scan, the 486 reverses the IFOV's direction and scans the object again until the total number of scans (as specified in the Phase II proposal) has been completed. Every 25 milliseconds, the PMT data and star selector rotation angles are reported in the telemetry. The FGS samples the entire S-Curve and its wings with sub-milliarcsecond resolution. The interferogram can be reconstructed by post-observation data processing.

A.4 Visit Level Control

After an observation is completed, the FGS's IFOV - under control of the 486 - is slewed to the expected location of the next target in the observing sequence. The search/track acquisition is initiated and the object, if acquired, is observed in either Position or Transfer mode. This process is repeated until all the exposures in the visit have been executed.

Appendix B: FGS1r Performance Summary

Appendix Contents

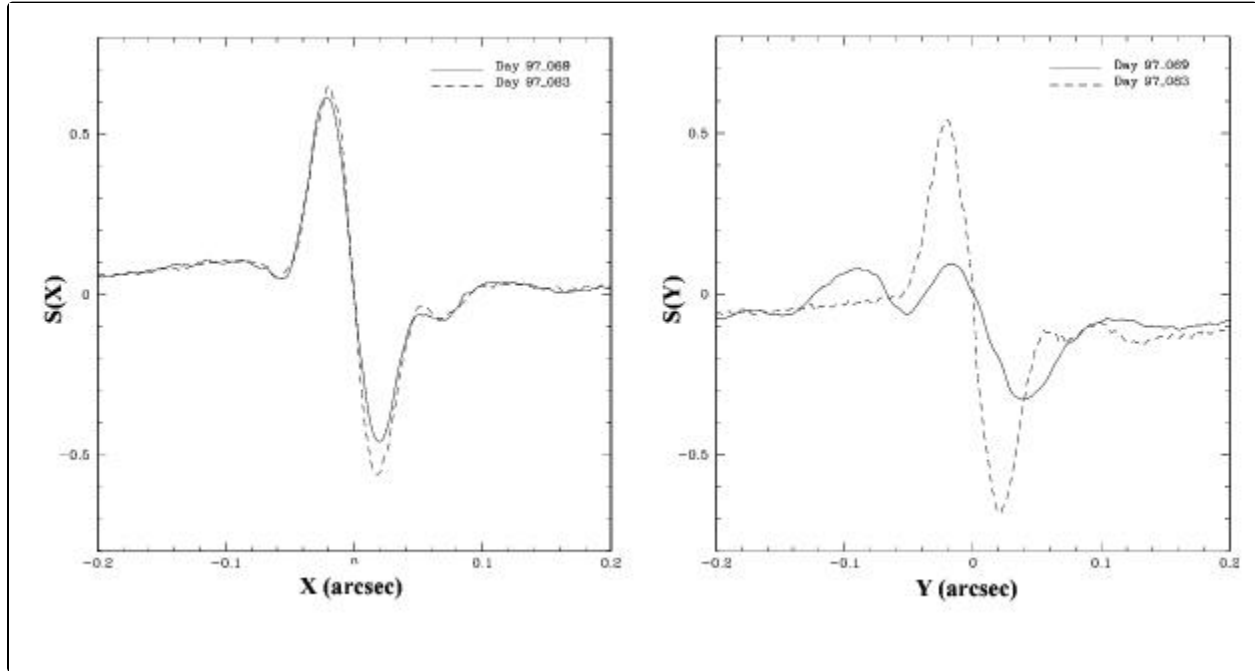
- [B.1 FGS1r's First Three Years in Orbit](#)
- [B.2 Angular Resolution Test](#)
- [B.3 FGS1r's Angular Resolution: Conclusions](#)
- [B.4 FGS1r: Second AMA Adjustment](#)
- [B.5 FGS1r: Third AMA Adjustment](#)

B.1 FGS1r's First Three Years in Orbit

As a result of the misfigured HST primary mirror, the FGSs must contend with a spherically aberrated wavefront. As discussed in [Chapter 2](#), this aberration amplifies the degrading effect of any misalignment of FGS optical elements that produces a shift of the beam at the Koesters prism. The result is a deformed S-Curve with reduced modulation. In order to provide an in-flight means to align FGS1r and thereby guarantee its interferometric performance, a stationary mirror was remounted on a commandable mechanism capable of tip/tilt articulation. This Articulating Mirror Assembly (AMA) is currently available in FGS1r and FGS2r.2 Without the AMA, FGS1r would most likely not have been suitable as a science instrument.

The first year of FGS1r's tenure in orbit is best described as an adjustment process. Upon reaching orbit, the instrument's interferometric response had already degraded, presumably due to a shift of the pupil at the Koesters prism induced by the launch stresses and gravity release. Early in the commissioning process, the AMA was adjusted to correct the instrument's alignment and restore its S-Curves to near ideal. [Figure B.1](#) compares the full aperture (F583W) S-Curves before and after the initial AMA adjustment.

Figure B.1: FGS1r S-Curves: Before and After AMA Adjustment



It was anticipated that FGS1r's performance would evolve during its first year in orbit due to the outgassing of the graphite epoxy composites upon which the instrument's optical bench is mounted. To monitor the changes, a standard star was observed in Transfer mode, once per month for the first 120 days, and then approximately every 3 months afterward. Consistent with the outgassing hypothesis, the S-Curves on both the X and Y axis were seen to change (degrade) quickly at first but eventually reached an approximate steady state by the first quarter of 1998. [Figure B.2](#) shows the early evolution of the full aperture (F583W) S-Curves, from initial optimization on March 24, to August 10, 1997, and [Figure B.3](#) shows the evolution from September 19, 1997 through February 23, 1998.

Figure B.2: FGS1r S-Curves: First Six Months After AMA Adjustment

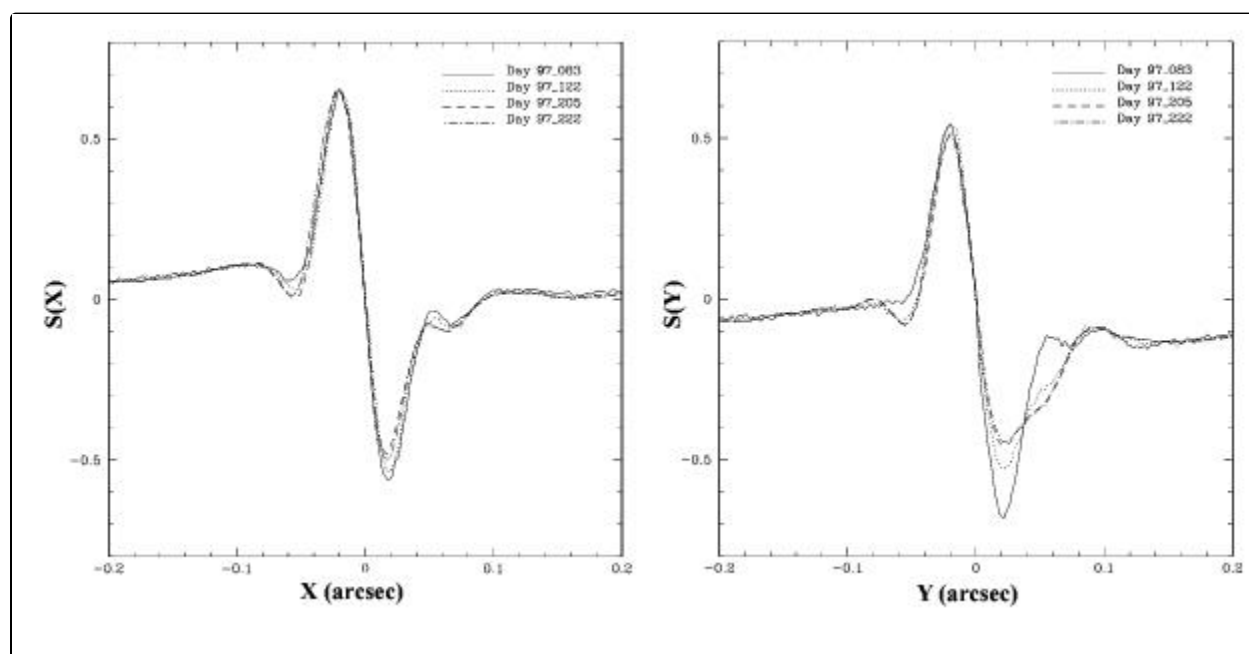
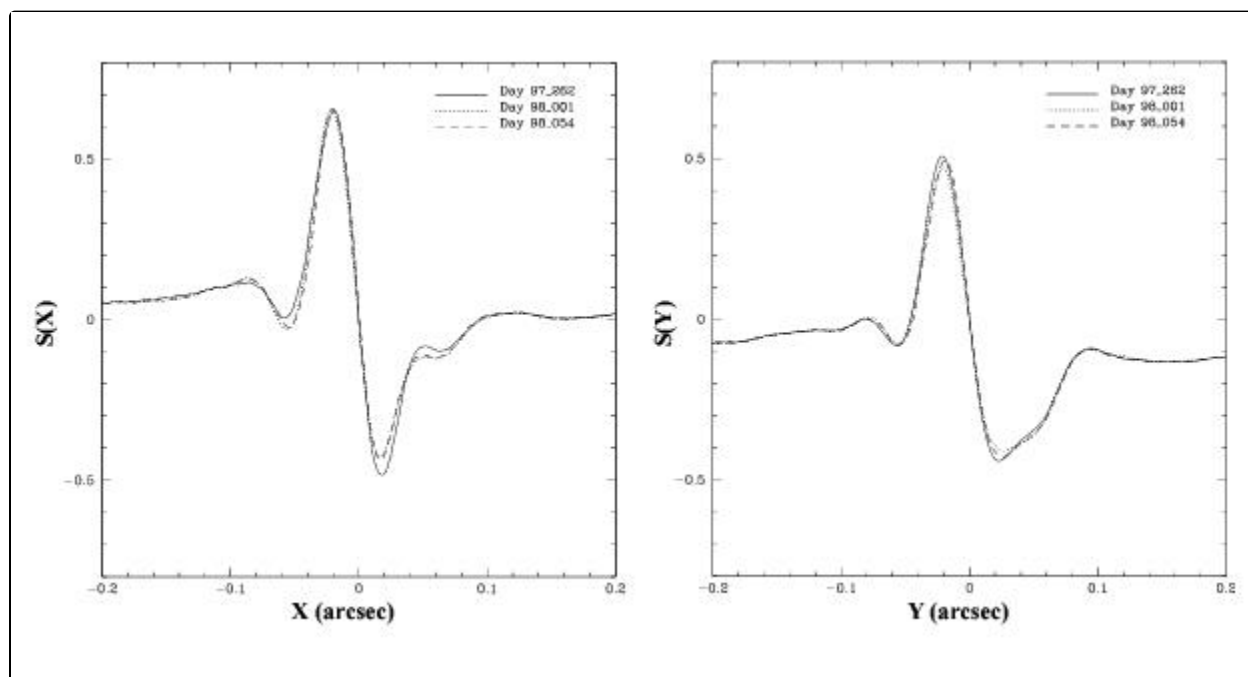
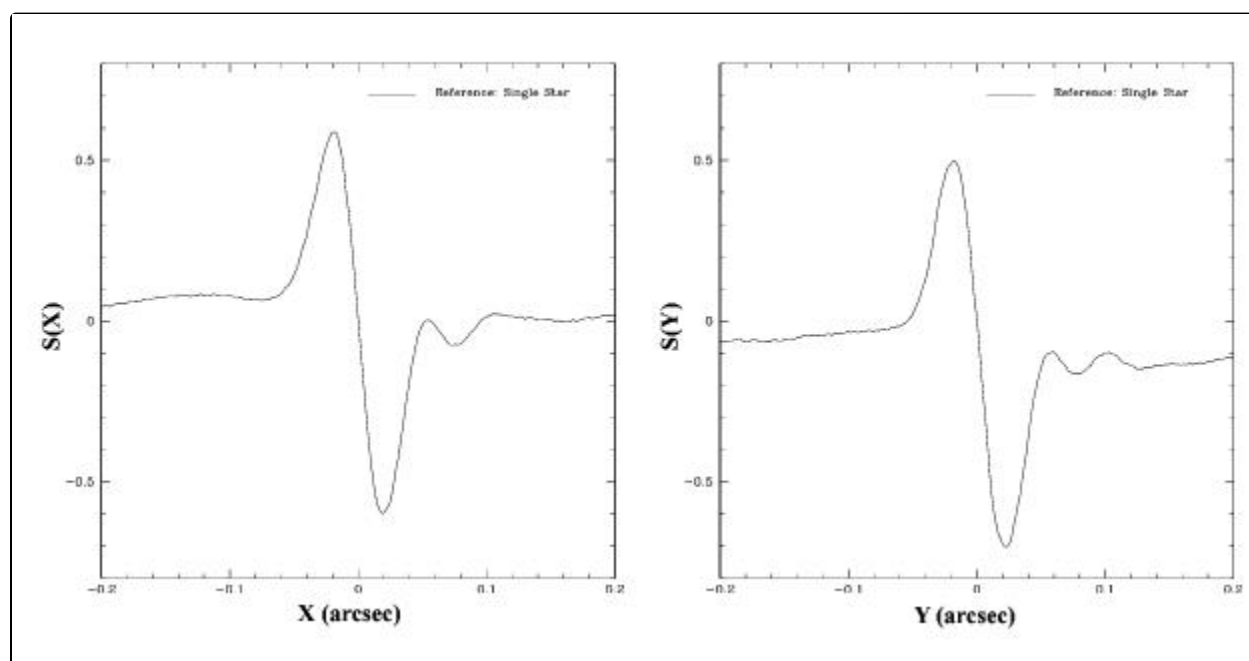


Figure B.3: FGS1r S-Curves: Second Six Months After AMA Adjustment



On May 8, 1998, the AMA was once again adjusted to restore the interferometer's performance to yield the S-Curves displayed in [Figure B.4](#). With near ideal S-Curves on both the X and Y axis, STScI executed an angular resolution test to assess FGS1r's potential as an astrometric instrument.

Figure B.4: Optimized FGS1r S-Curves Used in Angular Resolution Test



B.2 Angular Resolution Test

[B.2.1 Test Results: The Data](#)

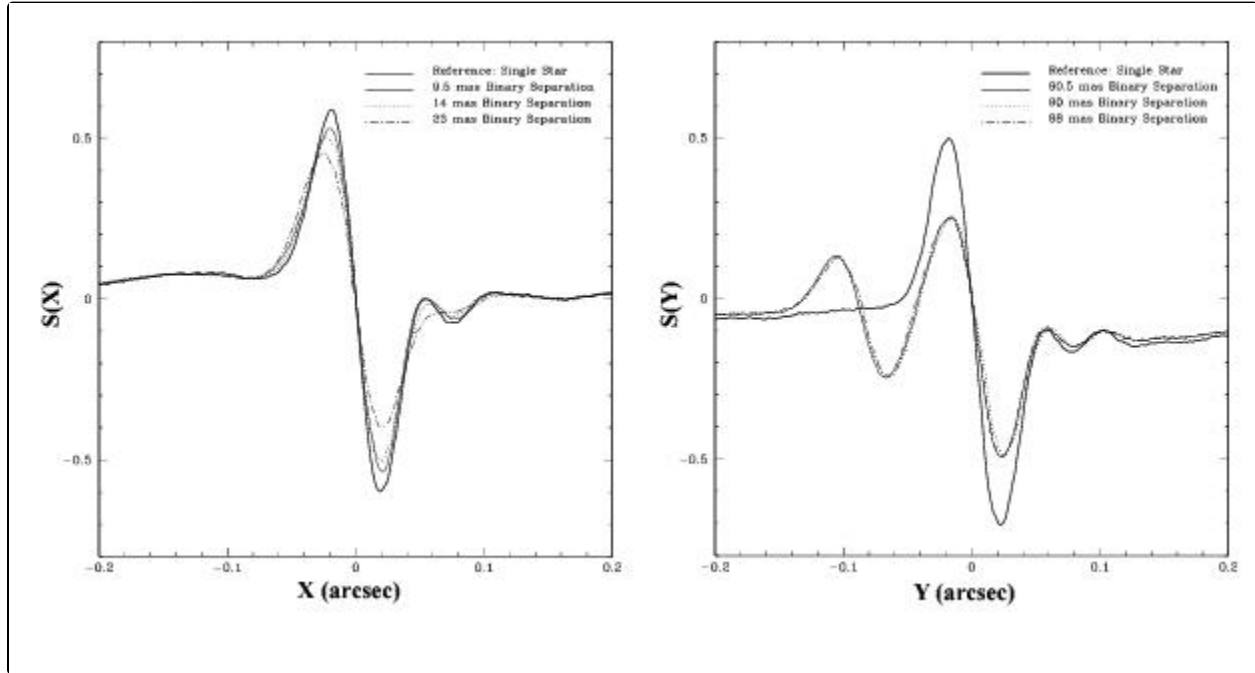
[B.2.2 Test Results: Binary Star Analysis](#)

Following the FGS1r re-optimization in early May 1998, STScI executed a test to determine the angular resolution limits of FGS1r and FGS3 by observing a known binary system at several small increments of telescope roll angle. The binary ADS11300 is an 9th magnitude system with components having a magnitude difference $\Delta m = 0.6$. At the time of the test, the predicted angular separation of the components was 0.085" (Franz and Wasserman, private communication). The test was designed such that the predicted position angle of the binary was (almost) aligned with the Y axis of the FGS, i.e., the projected angular separation of the two stars was large along the Y axis but small along the X axis. By rolling the HST in 6 increments, the projected separation along the X axis varied from the predicted angular resolution limit of FGS1r (~ 6 mas) to the resolution limit of FGS3 (~ 20 mas).

The true position angle and separation of the components were determined from both the FGS1r and FGS3 observations with the stars separated by 23 mas along the X axis. These values were used to determine the actual angular separation of the stars along FGS1r's X axis as a function of spacecraft roll, and the Transfer mode observations were analyzed to assess the instrument's ability to measure these separations. The test included actual separations of 7, 9, 12, 14, 17, and 23 mas (as compared with the intended separations of 6, 8, 10, 12, 15, and 20 mas).

FGS3 was tested only at the component separations of 14 and 23 mas since simulations of its X axis performance indicated that this instrument would not "resolve" the binary for separations less than 20 mas.¹

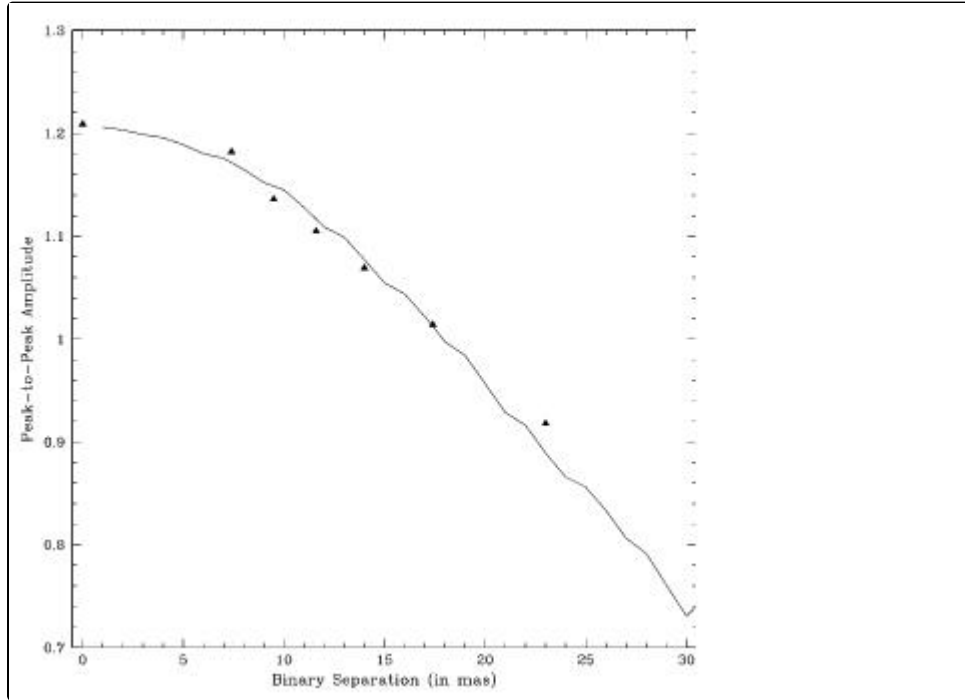
Figure B.5: FGS1r Transfer Function: Change in Angular Separation of a Binary



B.2.1 Test Results: The Data

For the six observations with FGS1r, [Figure B.5](#) compares the observed Transfer functions, and hence the response of the instrument to the angular separation of the stars as projected along the interferometer's X- and Y-axis. It is evident from these data that FGS1r easily detected the non-singularity of the source, and is sensitive to the change in separation of the two stars. [Figure B.6](#) plots the predicted vs. observed amplitude of the Transfer Function as a function of the binary's projected separation.

Figure B.6: FGS1r Transfer Function Amplitude w/ Binary Separation



The true “signal” in these observations can be thought of as the difference between the peak-to-peak amplitude of the binary star’s Transfer Function and that of the standard single star S-Curve. The statistical contribution to the noise can be calculated from the standard deviation of the normalized difference of the PMT counts in the wings of the fringe. With signal and noise defined in this way, [Table B.1](#) displays the signal-to-noise ratio for these six observations. These values underscore the validity of the instrument’s response displayed in [Figure B.5](#) and [Figure B.6](#).

Table B.1: FGS1r Angular Resolution Test: Effective Signal-to-Noise Ratios

Angular Separation (in mas)	Peak-to-Peak Amplitude	S/N
Single star	1.209	-
+7.4	1.182	48.9
+9.5	1.136	63.2
+11.7	1.105	105.7
+14.0	1.069	128.6
+17.4	1.014	156.7
+23.0	0.918	194.7

B.2.2 Test Results: Binary Star Analysis

The observations were analyzed, as described in [Appendix B: FGS1r Performance Summary](#), by finding a linear superposition of point source S-Curves that have been scaled and shifted to reproduce the observed Transfer function. Two separate techniques were employed. The most general model solves for the magnitude difference, angular separation, and parity of the binary's components. The second technique constrains the magnitude difference and solves for both the separation and parity.

[Table B.1](#) reports the results of these fits along the X axis for the FGS1r observations. In this table, a negative separation corresponds to a parity such that the faint star is to the “left” of the bright star, i. e., it is displaced in the $-X$ direction of the scan. Likewise, a positive separation places the faint star to the right of the bright star. For these observations, the parity was positive so a negative parity is incorrect. The formal error of each of these fits is about 0.5 mas.

Along the Y axis, where the components are widely separated by about 90 mas, the fits to the Transfer functions yielded accurate results for both the FGS1r and FGS3 observations.

The FGS3 observations succeeded in detecting the non-singularity of the source when the stars were separated by 14 mas along its X axis, but could not yield an accurate measurement of the separation. The observation with the 23 mas separation succeeded (as expected).

Table B.2: FGS1r Angular Resolution Test: Binary Star Analysis

Predicted Angular Separations (in mas)	Computed Separations (in mas)	
	No Constraints	Δmag Constrained
+7.4	+6.9	+7.5
+9.5	-11.1	+11.5
+11.7	-12.2	+12.5
+14.0	+13.6	+14.1
+17.4	+16.9	+18.0
+23.0	+23.0	+23.0

For FGS1r, as can be seen in [Table B.2](#), the unconstrained solution yields an incorrect parity for angular separations less than 14 mas. The models that constraining the magnitude difference reproduced the correct angular separations to within $\sim 5\%$, even at the smallest separation of 7.3 mas (though, not for the test at 9.5 mas separation).

¹ We express our greatest appreciation to O. Franz and L. Wasserman for researching the binary.

B.3 FGS1r's Angular Resolution: Conclusions

[Figure B.5](#) shows that FGS1r detects duplicity at component separations as small as 7 mas, and [Table B.1](#) shows that this instrument can accurately measure these separations if the magnitude difference is constrained (for projected separations $< \sim 15$ mas, no constraints are necessary for larger separations).

Details of the angular resolution test design and results are currently available on the [FGS web page](#).

B.4 FGS1r: Second AMA Adjustment

The second adjustment to FGS1r's AMA was performed on October 12, 1998. The results included near-ideal S-curves, essentially similar to those displayed in [Figure B.4](#). Since then, STScI has continued to monitor the temporal stability of these interferograms. Significant but tolerable changes in the amplitude and morphology of the y-axis S-curve have been seen. These appear to be due to a continuing, but very slow, shift of the y-axis Koester prism w.r.t. HST's OTA. To assure the reliability of measurements made by FGS1r on close ($< 25\text{mas}$) binary systems, standard calibration reference stars have been observed once per cycle (if that spectral type is needed by GO programs during the cycle).

B.5 FGS1r: Third AMA Adjustment

Long term monitoring of the FGS1r S-curves revealed a slow but continuous degradation of the Y-axis S-curve until about 2005. However, changes after 2005 were insignificant, indicating that FGS1r had finally reach long term stability. In late 2008, when *HST*'s science instrument compliment was reduced to ACS/SBC, WFPC2, and FGS, the reduced science pressure on access to *HST* assets motivated the decision to allocate the resources needed to re-optimize the FGS1r S-curves via an AMA adjustment. BF Goodrich optical engineers successfully executed the AMA adjustment (see Figures [2.7](#) through [2.9](#) for reference). It is expected that the current FGS1r interferometric performance, with its restored ability to detect and resolve close binary star systems, will be in place for the remainder of the *HST* mission.

Glossary of Terms

The following terms and acronyms are used in this Handbook.

Astronomer's Proposal Tool (APT)	Analog to Digital
articulating mirror assembly (AMA)	Commandable adjustable mirror assembly (replaces FF3 in FGS1r) capable of tip /tilt motion; allows for in-flight re-alignment of the beam at the Koesters prism to mitigate deleterious effects of HST's spherical aberration.
back-off distance	Distance ($+dx, +dy$) from target photocenter to which the FGS IFOV is moved before starting the Walkdown to FineLock phase of target acquisition.
beam walk	Movement of the axis of tilt of the collimated beam on the face of the Koesters prisms; results from clocking errors and misalignments of the SSA and SSB assemblies with respect to the Koesters prisms.
breathing (thermal breathing)	Change in telescope focus possibly resulting from temperature changes incurred as HST crossed the day/night terminator during each orbit.
check star	Targets observed more than once per POS mode visit; used as positional references to detect and allow for the removal of the apparent motion of the FOV during the visit.
CoarseTrack	Search algorithm used by the Fine Guidance Electronics which compares the counts from all four PMTs to continuously update the estimate of the target's photocenter.
COSTAR	Corrective Optics Space Telescope Axial Replacement; set of corrective optics installed in the 1993 HST servicing mission to correct the FOC, FOS, and GHRs for the spherically aberrated wavefront due to the misformed HST primary mirror. COSTAR does not correct the wavefront as seen by the FGS.
de-jittering	The process of correcting a POS mode observation for the effects of spacecraft jitter and oscillations by establishing a fixed, though arbitrary reference frame determined by the x, y centroids of guide stars observed with the guiding FGSs and compensating for motions of those guide stars during post-observation processing.
dominant guider	The FGS used to control the HST's translational attitude during an observation.
drift	Relative motions between FGS 3 and FGSs 1 and 2; thought to be a result of thermal effects.
F583W	FGS "Clear" filter, effective central wavelength of 5830 Å, with a bandpass of 1500 Å.
F5ND	FGS neutral-density filter; attenuates by 5 magnitudes.

FGE	Fine Guidance Electronics, on-board microprocessors which control the FGSs during the search for, acquisition of, and Position mode tracking of the target.
FGS	Fine Guidance Sensors, term used to describe one of the three white light Koesters prism (shearing) interferometers aboard HST.
FES	Fine Error Signal.
FESTIME	Fine error averaging time; time over which PMT data are averaged for computation of the Fine Error Signal.
FGS X,Y detector coordinates	Coordinate system defined for each FGS originating from the telescope's optical axis (the V1 bore sight); easily maps to the HST V1,V2,V3 coordinate system.
field dependency	Variations of measured quantities of the Transfer Function (i.e., morphology and modulation) as a function of location in the FOV.
FineLock (FL)	Stage of target acquisition in which the star selectors are moved to continuously zero the FES via a closed loop feedback between the position of the IFOV and PMT counts.
FITS	Flexible Image Transport System; the standard astronomical data interchange and archival format.
fold flat mirror (FF3)	Non-adjustable mirror assembly employed by FGS2 and FGS3 to redirect the light emergent from the star selector and filter wheel assemblies onto the faces of the Koesters prisms.
FOV	Field of view, for an individual FGS is approximately a quarter annulus with inner and outer radii of 10.2 and 14.0 arcminutes respectively. The total field of view is sometimes referred to as the FGS <i>pickle</i> .
GEIS	Generic Edited Information Set; HST file format, similar in many ways to the FITS format standard; data consists of a header file and a binary data file with multiple data groups.
GO	General Observer.
GTO	Guaranteed Time Observer.
guide star	A star acquired in FineLock by the FGS and used by the HST pointing control system to make continuous corrections to the telescope's pointing; used to eliminate translational and rotational drift of the telescope during observations.
HIPPARCOS	High-Precision Parallax Collecting Satellite; European Space Agency satellite launched in 1989 to determine astrometric position and parallax measurements of bright stars to an accuracy of 1 milliarcsecond and 2 milliarcseconds/year respectively.
HST	Hubble Space Telescope.
IFOV	Instantaneous Field of View, the roughly 5" × 5" aperture located by the positions of the two star selectors for FGS observations.

IRAF	Image Reduction and Analysis Facility, the suite of analysis tools developed by NOAO to process general astronomical data.
Koesters prism	Prism at the heart of FGS interferometer; constructed of two halves of fused silica and joined along a surface coated to act as a dielectric beam splitter.
LTSTAB	Long Term Stability Monitoring; program of short POS mode observations of an astrometric field made in the F583W filter to monitor the long term stability of the OFAD and plate scale calibration; usually repeated monthly or bi-monthly.
M35	Open cluster in Gemini (RA 06 ^h 08.9 ^m , Dec +24° 20'; $m_V \sim 5.3$) from which several stars are used in <i>LTSTAB</i> observations.
NEA	Noise Equivalent Angle.
NOAO	National Optical Astronomy Observatories.
n u l l (interferometric null)	Position in IFOV corresponding to the zero-point crossing of the transfer function for a given interferometric axis.
OFAD	Optical Field Angle Distortion, distortion incurred as a result of the combined effects of the FGS/OTA optical train and errors in SSA and SSB encoder values; alters the measured relative angular separations of stars distributed across the FGS pickle from their true angular separations.
ORIENT angle	Angle measured from North (through East) to the HST U3 axis. This angle definition is used in proposals and should not be confused with roll angle. (See “roll angle”).
OTA	Optical Telescope Assembly.
parallax	Angular displacement in the apparent position of a celestial body when observed from separated points.
PI	Principle Investigator.
pickle	The total field of view (FOV) of a given FGS, roughly 69 square arcminutes in (angular) area.
pick-off mirror	Pickle-shaped plane mirror used to deflect light from the HST Optical Telescope Assembly (OTA) to the FGS; defines the field of view (FOV) of a given FGS.
pitch	Rotation of HST in the V1,V3 plane.
plate scale	Magnification of the combined OTA and FGS optical system.
PMT	Photo-Multiplier Tube.
Position (POS) mode	FGS mode in which a star is observed in FineLock; used to measure the parallax, proper motion, or reflex motion of a given target or targets.

POS TARG coordinate system	FGS coordinate system originating from the center of the FGS field of view, with the Y-axis positive in the radial direction from the FGS center and the X-axis rotated 90 degrees counter-clockwise to the A-axis.
Proper Motion	Apparent angular motion of a star on the celestial sphere over time.
PUPIL	A 2/3 pupil stop used to block the portion of the wavefront originating from the outer 1/3 of the HST primary mirror, reducing the deleterious effects of spherical aberration.
roll	Rotation of HST along the V1 axis.
roll angle	Angle measured from North (through East) to the HST V3 axis. This angle definition is relative to the V3 axis as projected on the sky and should not be confused with the orient angle. (See "ORIENT angle").
RPS2	A graphical software system for designing HST observing programs. It has been replaced by the Astronomer's Proposal Tool (APT)
SAA	South Atlantic Anomaly; lower extension of the Van Allen radiation belts lying in a region above South America and the South Atlantic Ocean; no HST scientific or calibration observations are possible during spacecraft passages through the highest SAA contours.
S-Curve	The FGS's interferometric fringe from a point source (also, see Transfer Function).
SM3	1999 HST Servicing Mission.
SMOV	Servicing Mission Orbital Verification.
S/N	Signal-to-noise ratio.
Spiral Search	Search algorithm during which the star selectors command the IFOV in an outward spiral search around a target's expected position.
Spoiler	A star nearby the intended target inadvertently acquired by the FGS.
SSA	Star Selector A Assembly; a two-mirror and five element optical corrector group used to correct for optical aberrations induced by the OTA and aspheric pickoff mirror; along with the SSB, defines and locates the IFOV aperture.
SSB	Star Selector B Assembly; a four-mirror optical group used to pilot the collimated beam through the filter assembly and onto the polarizing beamsplitter; along with the SSA, defines and locates the IFOV aperture.
STAT	Space Telescope Astrometry Science Team.
step-size	Angular distance covered by the IFOV during one photon integration period (FESTIME); default step-size is 1.0 mas.
strfits	STSDAS routine to convert FITS files to GEIS images, STSDAS tables or text files.
STScI	Space Telescope Science Institute.

STSDAS	Space telescope Science Data Analysis System, the set of data analysis and calibration routines used to process HST data; based on the IRAF set of analysis tools produced by National Optical Astronomy Observatories (NOAO).
sub-dominant (roll) guider	The FGS used to maintain control of HST's rotation about the V1 axis during an observation.
SV	Science Verification, the process of taking observations used for HST instrument calibration and verification of science capabilities.
tilt	Angle of wavefront at face of Koesters prism.
Transfer Function (TF)	The difference in counts of the two PMTs for a given interferometric axis, normalized by the sum of those counts, versus the tilt angle of the wavefront at the entrance face of the Koesters prism.
Transfer (TRANS) mode	FGS observing mode used primarily to measure the angular separations and relative magnitudes of multiple stars or the angular size of extended targets.
U1,U2,U3 Orient Reference Frame	Coordinate system fixed in the HST focal plane as projected onto the sky; U1 corresponds to the V1 axis, while U2 and U3 correspond to the negative directions of V2 and V3 respectively.
Upgren69	FGS standard reference star (RA $00^{\text{h}} 37^{\text{m}} 51.9^{\text{s}}$, Dec $+84^{\circ} 57' 47.8''$; $m_V \sim 9.58$; B-V = 0.49) used to monitor the interferometric response of the FGS over time.
URL	Universal Resource Locator (or Link); the unique address used to define the "location" of a WWW-based document.
V1,V2,V3 reference frame	Fixed telescope coordinate system, with the V1 axis lying along the optical axis, V2 parallel to the solar-array rotation axis, and V3 perpendicular to the solar-array axis.
vehicular jitter	Variations in the HST pointing measured by the FGS's tracking of guide stars; thought due to mechanical or thermal transients over the course of the orbit.
WalkDown (WalkDown to FineLock)	Target acquisition mode in which the IFOV is moved toward target photocenter in equal steps along x,y until FineLock is achieved.
yaw	Rotation of HST within the V1,V2 plane.
zero-point crossing	Point at which the difference in PMT counts along a given interferometer axis is zero; ideally, this crossing should occur at interferometric null.